SEISMIC PERFORMANCE ASSESSMENT OF ALL-MASONRY INFILLED FRAMES USING FINITE ELEMENT STUDY

by

Soraya Roosta

Submitted in partial fulfilment of the requirements
for the degree of Doctor of Philosophy

at

Dalhousie University
Halifax, Nova Scotia
August 2022

I dedicate this dissertation to

My husband, Ali, who has always believed in me and supported me.

My loving parents, Parivash and Bahman, and my caring siblings who have been a source of encouragement for me throughout my life.

TABLE OF CONTENTS

LIST OF TABLES

LIST OF FIGURES

ABSTRACT

This research study presents the seismic performance assessment of a newly proposed masonry infilled frame system, referred to as all-masonry infilled frames, under in-plane seismic loading conditions. Unlike conventional masonry infilled frames where reinforced concrete or steel is often used as the bounding frame material, the bounding frame of all-masonry infilled frames is made of masonry units. A literature review revealed that there are limited systematic studies on seismic behaviour and performance evaluation of masonry infilled frames in general. There are no design provisions available in the North American masonry design standards addressing the seismic design of masonry infilled frames. This study was motivated to fill the research gap in seismic behaviour and performance evaluation of masonry infilled frames. A numerical study using finite element modeling and supplemented by experimental testing was the main strategy adopted in the study. The physical specimens were tested to 1) experimentally evaluate the behaviour and strength of all-masonry infilled frames under loading conditions that can be achieved with the laboratory capabilities; and 2) provide results for validation of the finite element model. The numerical study began with the development of a finite element macro-model capable of incorporating properties of masonry infilled frames using OpenSees. The model was verified under both monotonic pushover and quasi-static cyclic analyses. Subsequently, the model was used in a finite element study to conduct the seismic performance assessment of all-masonry infilled frames covering a range of design parameters.

The experimental results showed that all-masonry infilled frames exhibited similar behaviour in terms of stiffness and strength as their infilled RC frame counterparts. However, differences in terms of ultimate failure mode were observed. While the infill corner crushing was the predominant failure mode for the infilled RC frames, diagonal cracking extending into the boundary columns was the governing failure for all-masonry infilled frames. The post-ultimate behaviour of all-masonry infilled frames was sustained with higher displacement ductility than their infilled RC frame counterparts.

The developed model showed that its novelty from existing models was its consideration of infill shear behaviour. While diagonal struts were used to represent the compressive behaviour of the infill, the shear behaviour of mortar joints was captured by a shear spring, configured in a serial manner with the struts. The compressive constitutive law assigned to the struts and the shear behaviour assigned to the shear spring were defined based on material properties observed in the auxiliary tests on masonry prisms. The verification showed that the proposed multi-strut-spring model simulated the in-plane response adequately for both static and cyclic loading conditions.

The seismic performance assessment of all-masonry infilled frames was conducted using Incremental Dynamic Analysis (IDA) technique. Eight all-masonry infilled frame archetypes with different design parameters were analysed under 22 pairs of strong ground motion records. The seismic performance of all archetypes was presented in terms of IDA curves, pushover curves, and fragility curves for three levels of performance limit states. Seismic response modification factors were also determined for all archetypes. The results showed that the all-masonry infilled frames attained a seismic modification factor, R, comparable to the SFRS category of moderately ductile to ductile masonry shear walls as defined in the Canadian masonry design standard CSA S304-14.

LIST OF ABBREVIATIONS AND SYMBOLS USED

Abbreviation

ASCE	American Society of Civil Engineers
BF-AM	Bare Frame - All-Masonry
BF-RC	Bare Frame - Reinforced Concrete
CSA	Canadian Standard Association
CMU	Concrete masonry unit
DM	Damage Measure
DSFM	Disturbed Stress Field Model
FEMA	Federal Emergency Management Agency
IDA	Incremental Dynamic Analysis
IF-AM	Infilled Frame - All-Masonry
IF-RC	Infilled Frame - Reinforced Concrete
IF-AM-wide	Infilled Frame - All-Masonry with infill aspect ratio of 0.5
IF-AM-tall	Infilled Frame - All-Masonry with infill aspect ratio of 1.3
IF-AM-BB	Infilled Frame - All-Masonry with Bond Beams
IF-AM-BJ	Infilled Frame - All-Masonry with Bed Joints
IF-AM-80b	Infilled Frame - All-Masonry with 80kN total load on Beam
IF-AM-80c	Infilled Frame - All-Masonry with 80kN total load on Columns
IF-AM-160c	Infilled Frame - All-Masonry with 160kN total load on Columns
IF-AM-TG-C	Infilled Frame - All-Masonry with Top Gap under Cyclic loading
IF-AM-SG-C	Infilled Frame - All-Masonry with Side Gaps under Cyclic loading
IF-RC-TG-C	Infilled Frame - Reinforced Concrete with Top Gap under Cyclic loading
IF-RC-SG-C	Infilled Frame - Reinforced Concrete with Side Gaps under Cyclic loading

IM	Intensity Measure
LVDT	Linear Variable Differential Transformer
NBCC	National Building Code of Canada
RC	Reinforced concrete
SFRS	Seismic Force Resisting System
TMS	The Masonry Society

Symbols

c	Mortar cohesiveness factor
C_d	Displacement amplification factor
E_0	Young's moduli of masonry in the directions parallel to bed joints
E_{90}	Young's moduli of masonry in the directions normal to bed joints
$E_{m-\theta}$	Young's moduli of masonry in the directions θ to bed joints
E_m	Elastic modulus of the infill prisms
E_c	Elastic modulus of concrete
f'_{bf}	Maximum compressive strength of boundary CMUs
f'_{bi}	Maximum compressive strength of infill CMUs
f'_m	Maximum compressive strength of masonry
f'_{mt}	Maximum compressive strength of mortar
f'_{m-0}	Compressive strength of masonry parallel to bed joints
f'_{m-90}	Compressive strength of masonry normal to bed joints
$f'_{m-\theta}$	Compressive strength of masonry for angle θ to the bed joints
f'_{block}	Maximum compressive strength of block
f_t	Concrete tensile strength
f_y	Yield strength of reinforcing bars
f_u	Ultimate strength of reinforcing bars
f_{mu}	Masonry ultimate compressive strength
G	Shear modulus
H	Story height

h	Masonry infill height
I_b	Moment of inertia of the beams
I_c	Moment of inertia of the columns
I_{ce}	Equivalent moment of inertia of the transformed section
k_{ini}	Initial stiffness
k_{cr}	Secant cracking stiffness
l	Length of the masonry panel
P_f	Failure load
P_u	Ultimate load
R	Response modification factor
R_d	Ductility reduction factors
S_a	Spectral acceleration
$\hat{S}_{CT}$	Median collapse intensity
SD	Standard deviation
t	Thickness of the masonry infill
V_e	Elastic lateral strength demand
V_{max}	Maximum lateral strength
w	The width of the equivalent strut
λ_1	Relative stiffness of infill and bounding frame
θ	Slope of the strut with respect to the horizontal axis
δ_y	Yield displacement
δ_{max}	Displacement corresponding to the maximum strength
Ω_o	Overstrength factors
ϕ	Internal friction angle
ϕ_i	Initial friction angle
ϕ_r	Residual friction angle
φ	Dilatancy angle
τ_0	Initial shear bond strength of mortar joints
τ_m	Maximum shear bond strength
τ_r	Residual shear strength

τ_u	Ultimate shear strength of mortar bed joints
μ	Friction coefficient between sliding surfaces
σ_n	Compressive stress perpendicular to mortar bed joints
α_h	Column-infill contact length
α_l	Beam-infill contact length
ν_{0-90}	Poisson's ratio of masonry defined as the ratio of the strain in the direction normal to the bed joints to the strain in the direction parallel to the bed joints
ε_0	Strain at maximum strength
ε_{mu}	Strain at ultimate strength
γ_m	Shear unit displacement at maximum stress
γ_r	Residual shear unit displacement
γ_u	Shear unit displacement at ultimate strength

ACKNOWLEDGEMENTS

I would like to express my deepest gratitude to my supervisor, Dr. Yi Liu, for her generous support and guidance, without whom I could not have undertaken my Ph.D. journey.

Many thanks to my supervisory committee members, Dr. Gordon Fenton and Dr. Kyle Tousignant, and my external examiner, Dr. Svetlana Brzev, for taking the time to review my dissertation, attending my defense, and providing knowledge and expertise.

I would also like to thank my colleagues, Seyedali Hosseini and Saber Foroushani, and laboratory technicians, Mr. Jordan Maerz and Mr. Jesse Keane, for their valuable assistance and collaboration with the experimental projects.

Lastly, I wish to acknowledge the Natural Sciences and Engineering Research Council of Canada (NSERC) and Abdol Majid Bader Graduate Scholarship for providing financial support, and the Canadian Concrete Masonry Producers Association (CCMPA) for their kind assistance and providing the mason and materials.

CHAPTER 1 INTRODUCTION

1.1 General

The masonry infilled frame is a type of construction widely used around the world. It consists of a frame structure, conventionally made of reinforced concrete (RC) or steel materials, and a masonry panel built within, referred to as masonry infills. Masonry infills can be made of a variety of masonry materials, and clay bricks and concrete masonry blocks are two primarily used infill materials around the world. A typical masonry infilled RC frame example is shown in Figure 1.1. Due to the readily availability of masonry materials, masonry infills are a popular form of construction often used as either partitions to separate spaces in a building or cladding to complete a building envelope. Previous research showed that when built in tight contact with the boundary frame, the masonry infill can significantly increase the stiffness and strength of the infilled system under lateral loading. When dynamic loading is concerned, the infills were also shown to be beneficial to the ductility and energy dissipation of the infilled system, even after significant cracking. In seismic regions, accurate evaluation of influence of masonry infills on the seismic properties of the frame structure is crucial for a safe design. Despite a considerable amount of research showing the benefit of masonry infills, the industry practice has been to treat infills as non-structural elements and design frames for gravity and lateral loading. This disconnect is mainly attributed to two factors. One is that the research findings

obtained thus far have not been effectively translated into comprehensive design guidelines. A literature review revealed that the design guidelines contained in various masonry design standards (CSA S304-14, 2014; Eurocode 6, 2009; TMS 402/602, 2016) for masonry infills provides only basic treatment of strictly "standard" infills. For infills with openings, interfacial gaps, and combined vertical loading etc., the guidelines are few to none. When it comes to seismic loading, the standards are nearly silent. The complexity of the problem has often been attributed to the lack of comprehensive guidelines as it is difficult to quantify the exact extent of the infill-to-frame interaction for various combinations of infill and frame materials and geometries. The second factor is a practical one. For conventional masonry infilled RC or steel frames, the construction involves the coordination of two trades. The concrete or steel frame is constructed first and masonry infills are then constructed separately. Since the masonry infills are considered non-structural, they are often designed by architects whereas the frame design is usually carried out by structural engineers.

This study was then motivated to investigate the behaviour and capacity of masonry infilled frames with a focus on their seismic characteristics under a framework of seismic performance assessment. A new all-masonry infilled frames where both the boundary frame and infills are made of masonry block units was used as the vehicle for this investigation.

Figure 1.1 Typical example of masonry infilled RC frames (Charleson, 2008)

1.2 All-Masonry Infilled Frames

The all-masonry infilled frames were first proposed and experimentally studied at Dalhousie University (Foroushani, 2019). The all-masonry infilled frame is conceptually similar to a masonry infilled RC frame with the difference being that the bounding frame is also made of masonry. A schematic view of all-masonry infilled frames is shown in Figure 1.2. Masonry reinforced columns and tied beams form the masonry frame while the masonry infill can be constructed in the same manner as in the conventional infilled RC frames. As constructed with one material at the same time, this form of infilled frames eliminates the need to coordinate with concrete or steel trades as in the case of steel or RC frames and thus accelerates the construction process. In addition, simultaneous construction of the frame and infill makes it easier to include vertical reinforcement in the infill as well as provide alternative forms of interfacial connection such as mechanical anchorage between the frame and infill, as opposed to simple mortar bedding. While sharing some similarities with masonry infilled RC frames, unique behavioural

characteristics can be expected due to different configuration and associated construction details for the all-masonry infilled frame system, which justifies further investigation.

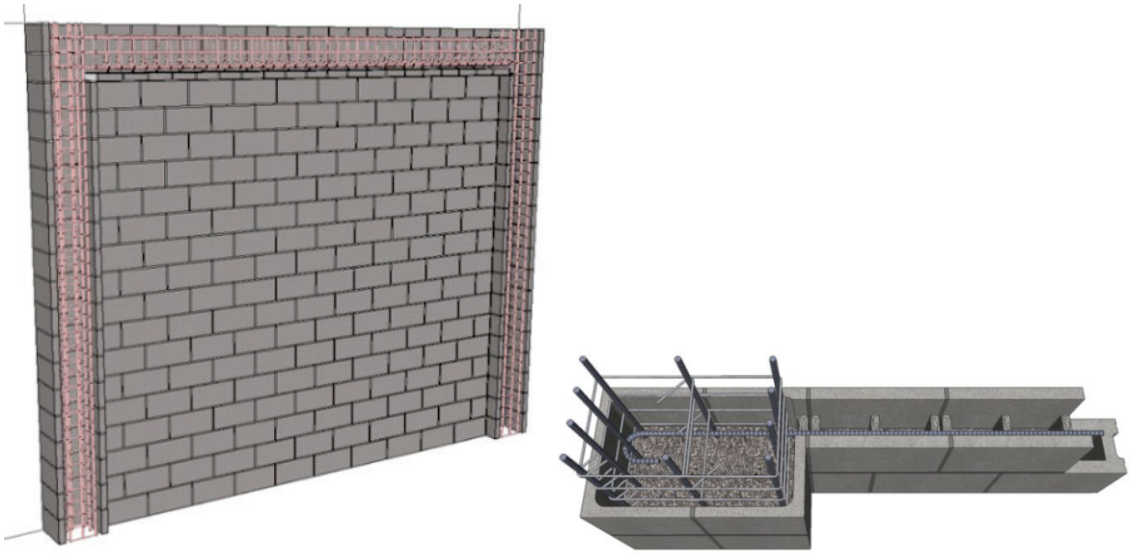

Figure 1.2 A schematic view of all-masonry infilled frames

1.3 Methodology and Objectives of the Research

This research is part of an ongoing experimental and numerical research program being conducted at Dalhousie University on masonry infilled frames. Under this framework, studies have been conducted in the same research group on masonry infilled RC frames subjected to in-plane lateral loading (Foroushani, 2019; Hosseini, 2020; Steeves, 2017). The objective of this research study is to expand the investigation to the all-masonry infilled frame systems as proposed and evaluate their structural performance in the context of seismic performance.

The methodology adopted in this study focused on the numerical study using a finite element model and supplemented with experimental investigations. In the first phase, a macro-model was developed to simulate both static and seismic behaviour of masonry infilled frames of either RC or masonry boundary frames. The developed model was intended to be able to capture the frame failure (development of plastic hinges in the frame beam-column elements) as well as masonry infill failure including sliding shear failure and compression failure. The model was encoded in OpenSees software since OpenSees provides nonlinear static and dynamic analyses capabilities. Concurrent with the finite element work, an experimental program was conducted on all-masonry infilled frames subjected to lateral loading by the same research group. The results of the experimental study as well as those obtained from literature were used to verify the finite element model.

In the second phase, the verified model was used in the seismic performance assessment of all-masonry infilled frames. Seismic assessment focused on the fragility curves and seismic design parameter evaluation of the all-masonry infilled frames. The Incremental Dynamic Analysis (IDA) process (Vamvatsikos & Cornell, 2002a) and methodology was followed.

The detailed objectives of this research include:

1. Develop a finite element model for all-masonry infilled frames that is simple to implement for practical design and also capable of simulating seismic behaviour.
2. Validate the model using the experimental results. The goal is to validate the model at both element and structural levels with sensitivity analyses on a range of input parameters. The resulting model is to be easily implemented for the analysis of all-masonry infilled frames and masonry infilled RC frames in general by others.

3. Assess seismic performance: specifically estimate the collapse risk of the proposed system, including both nonlinear static pushover and incremental dynamic analyses on a series of all-masonry infilled frame archetypes with different design parameters.
4. Compute seismic response modification factors, including the overstrength factors, Ω_o, ductility reduction factors, R_d, response modification factor, R, for all-masonry infilled frame archetypes.

1.4 Thesis Outline

This document is organized according to the "paper" format. The first chapter introduces the subject and objectives of this research. The second chapter provides a detailed literature review on the general behaviour of masonry infill, different numerical modeling approaches, and seismic assessment analyses. Chapter 3 to 5 consist of three papers. Chapter 3 includes a published paper on the experimental investigation of all-masonry infilled frames under static and quasi-static lateral loading. Chapter 4 includes a published paper on the development of a muti-strut-spring model for evaluating the masonry infill contribution in the design of masonry infilled frames using a practical and rational approach. Chapter 5 is to be submitted as a paper on the seismic performance assessment and fragility of all-masonry infilled frames using incremental dynamic analysis (IDA). Lastly, a summary of this research, conclusions drawn from findings of the study, and recommendations for future studies are presented in Chapter 6.

CHAPTER 2 LITERATURE REVIEW

2.1 Introduction

Since all-masonry infilled frames are new and little information is available besides the research conducted at Dalhousie University, the following literature review focused on the existing research of its counterpart, i.e., masonry infilled RC frames under lateral loading. It is believed that similarities between the two render the discussion on the fundamentals in general behaviour and research findings valid.

2.2 General Behaviour

The in-plane lateral behaviour of masonry infilled frames has been studied by many researchers during the past decades. Both experimental testing and numerical studies conducted have shown that masonry infills significantly contribute to the global response of frame structure, including its lateral strength, drift, and energy dissipation (Al-Chaar et al., 2002; Anil & Altin, 2007; Guerrero et al., 2014; Liu & Soon, 2012; Martins et al., 2017; Mehrabi et al., 1996). Much effort has also been made to develop a simple and rational modeling approach and accurately consider the infill effect on the overall behaviour of the bounding frame system. To that end, the "diagonal strut method" has been developed and established as the most commonly used approach. Polyakov (1956) and Holmes (1961) were among the first to propose the strut concept. They observed that

at relatively low level of lateral force, the infill and frame acted together to provide shear resistance to deformation. As load increased, the infill began to form diagonal cracks connecting loaded corners, and as cracking developed and the frame further deformed, two contact regions, in the diagonal direction, were created, thus acting as a strut. The infill-strut concept is schematically shown in Figure 2.1. Based on this concept, the infilled frame can then be treated as an equivalent braced frame. Once the strut width is known, a simple frame analysis can be performed to calculate the frame stiffness and strength.

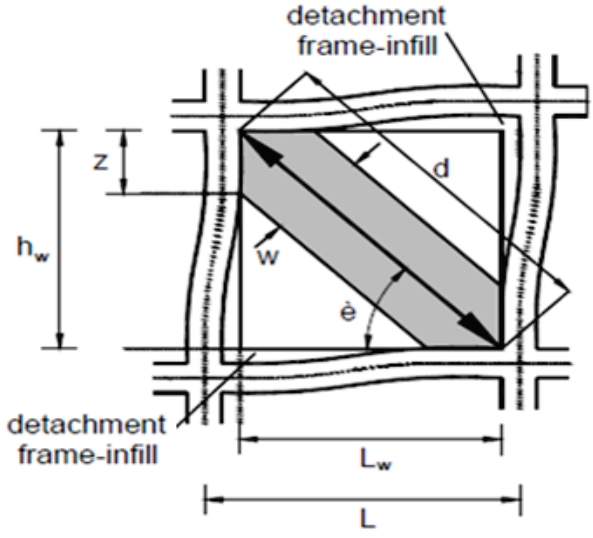

Figure 2.1 Equivalent diagonal strut model concept (Asteris et al., 2011)

Due to its simplicity, this general approach has been adopted in both the Canadian and American masonry design standards (CSA S304-14, TMS 402/602, ASCE/SEI 41-17, FEMA 306) for the design of masonry infills. However, different strut width equations have been adopted in these standards based on different analytical models proposed by researchers (Dolšek & Fajfar, 2008; Liberatore & Decanini, 2011; Panagiotakos & Fardis,

1996; Paulay & Priestley, 1992; Saneinejad & Hobbs, 1995). It is no surprise that strut widths calculated using different equations were found in disparity with one another and the infill strength calculated based on these strut width values did not always compare well with the experimental results. None of the equations was found to be universally applicable to masonry infilled frames of varying material and geometric properties. Therefore, more research is required to better understand and quantify the infill-frame interaction as affected by material and geometric characteristics of both the infill and frame.

In terms of the failure modes, experimental observation identified five possible failure modes: 1) diagonal compression failure; 2) corner crushing of infills; 3) sliding shear failure of mortar joints; 4) diagonal tension cracking; 5) frame failure. These failure modes are shown in Figure 2.2. For masonry infills and frames of typical geometry and materials, corner crushing and sliding shear have been recognized as the most common failure modes. It should be pointed out that in most cases, the failure is initiated by diagonal tension cracking (Figure 2.2 d) but the system continues to resist additional load until one of the other four failure modes mentioned above occurs. Therefore, diagonal tension cracking is treated as a serviceability limit state in this study, as opposed to an ultimate limit state as in most studies.

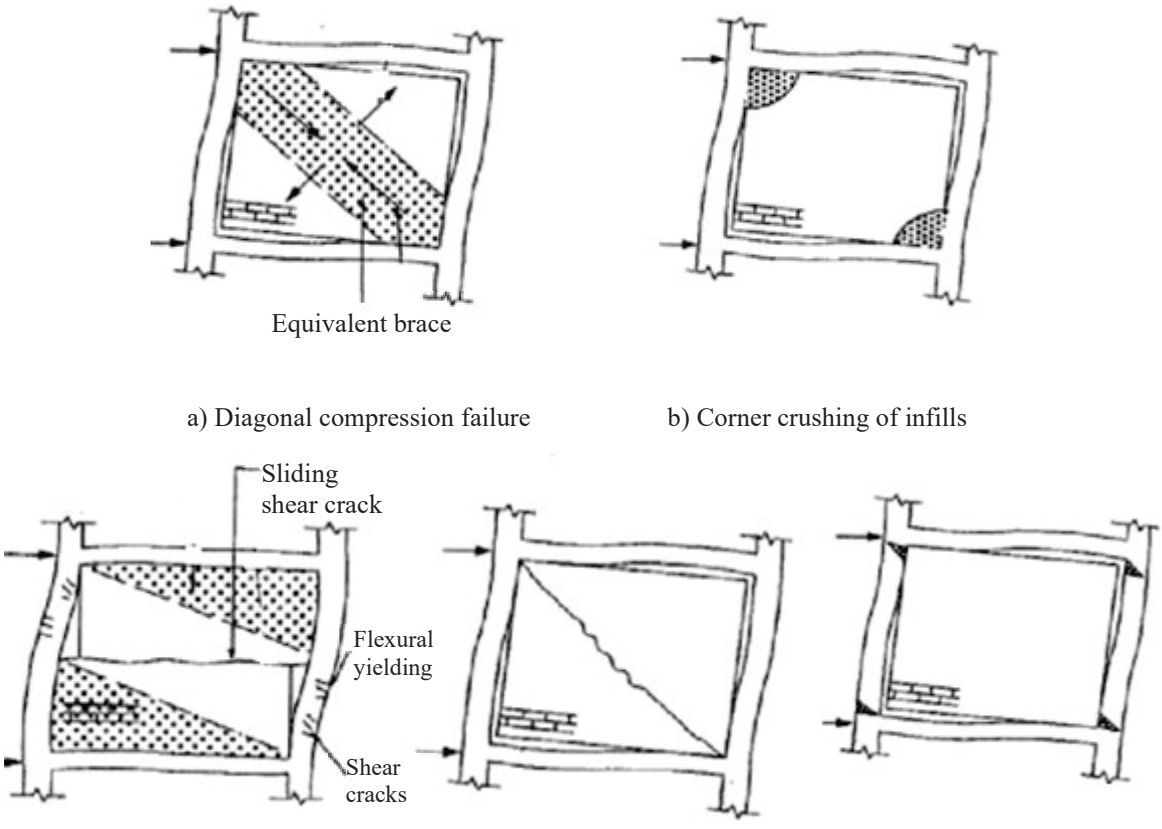

a) Diagonal compression failure b) Corner crushing of infills

c) Sliding shear failure of mortar joints d) Diagonal tension cracking e) Frame failure

Figure 2.2 Failure modes of masonry infilled frames (El-Dakhakhni et al., 2003)

2.3 Effect of Several Important Parameters

The failure mode under which a masonry infilled frame fails is influenced by several factors such as frame and infill materials, infill geometry and relative stiffness of bounding frame and masonry infills. The following section provides brief discussions of effect of several parameters relevant to this study.

While the compressive behaviour of infill is relatively well understood , its shear behaviour has not been thoroughly investigated and thus left out of the strut model. The shear resistance of mortar bed joints is a combination of two mechanisms, i.e., mortar bond strength and friction resistance between joint surfaces. Experimental studies (Armaanidis, 1998; Hansen, 1999; Van der Pluijm, 1993) showed that the presence of normal compressive stress increased mortar shear strength. In some studies, effects of normal compressive stress along with uplift expansion normal to the mortar joint, which is called dilatancy, were considered. (Armaanidis, 1998) expressed shear strength along limestone weak discontinuities with a combination of internal friction angle (ϕ) and dilatancy angle (φ) as shown in Eq (2.1).

$$\tau_m = \tau_0 + \sigma_n \, tan\,(\phi + \varphi) \tag{2.1}$$

Moreover, it was also observed that the effect of dilatancy when mortar joint is under high compression can be ignored (Gabor et al., 2006). Therefore, shear strength formulation when moderate compression stresses exist can be simplified as the Mohr-Coulomb criterion indicated in Eq (2.2) (Lourenço et al., 2004).

$$\tau_{\mathrm{m}} = \tau_0 + \mu\, \sigma_n \tag{2.2}$$

where τ_0 is the initial shear bond strength of mortar joints, μ is the friction coefficient between sliding surfaces, and σ_n is the compressive stress perpendicular to mortar bed joints.

A wide range of values for τ_0 and μ have been experimentally evaluated by many researchers (Andreotti et al., 2018; Augenti & Parisi, 2011; Paulay & Priestley, 1992). The measured values for friction coefficient ranged from 0.6 to 1.0 and contradictory results on factors that affect this coefficient has been reported. Approximate formulations were proposed by Paulay and Priestley (1992) to calculate shear bond strength based on masonry compressive strength (f'_m) as shown in Eq (2.3). However, these types of formulations and the one adopted in CSA S304-14, Eq (2.4), are very conservative and in most cases far from the real value of mortar shear bond strength.

$$\tau_0 = 0.03\, f'_m \tag{2.3}$$

$$\tau_0 = 0.16\, \sqrt{f'_m} \tag{2.4}$$

In addition to shear bond strength and friction resistance, strains corresponding to maximum bond strength and residual friction resistance including stiffness and post debonding behaviour are critical factors in determining a constitutive law for bed joint sliding response and capturing stiffness and strength of the infill.

Mortar and unit properties and surfaces bond strength are also identified as important factors in determining the shear strength of mortar joints. Several studies (Chaimoon & Attard, 2009; Hansen, 1999; Rahman & Ueda, 2014) considered the effect of mortar compressive strength on shear strengths including parameters such as cohesion and friction angle. Their findings are summarized in Table 2.1. In some tests, maximum and ultimate shear strengths were increased with increasing mortar compressive strength. These correlations were established based on tests conducted on masonry prisms with solid clay

blocks. To the best of the author's knowledge, there is no technical information as such on the shear behaviour of mortar joints with concrete hollow blocks.

Table 2.1 Effect of mortar compressive strength on shear strength of mortar joints

Author's name and Test method	f'_{mt} (MPa)	f'_{block} (MPa)	σ_n (MPa)	τ_m (MPa)	τ_u (MPa)	c (MPa)	ϕ_i	ϕ_r
Hansen (1999) Couplet test with solid clay bricks	3.8	32.0	0.1	0.7	0.08	0.68	23.9	40.1
			0.2	0.79	0.17			
			0.5	0.89	0.42			
	11.5	26.0	0.1	1.2	0.06	1.2	17.2	41.7
			0.2	1.29	0.21			
			0.5	1.34	0.43			
	19.0	25.0	0.1	1.11	0.13	1.08	17.5	45.4
			0.2	1.05	0.23			
			0.5	1.21	0.49			
Chaimoon and Attard (2009) Couplet test with solid clay bricks and frog marks	7.3	11.1	0.2	0.7	0.28	0.43	30.4	38.9
			0.4	0.82	0.4			
			0.8	1.02	0.66			
	16.8	11.1	0.2	0.3	0.24	0.18	39.8	40.3
			0.4	0.67	0.37			
			0.8	0.87	0.64			
Rahman and Ueda (2014) Triplet test with solid clay bricks	10.0	17.0	0.25	0.33	0.25	0.12	60.8	49.4
			0.5	0.78	0.56			
			1.00	1.68	1.13			
			1.25	2.01	1.50			
			1.50	2.28	1.61			
	12.5	17.0	0.25	0.47	0.35	0.19	56.3	56.3
			0.5	0.97	0.74			
			1.00	1.87	1.48			
			1.25	2.11	1.68			
			1.50	2.30	1.77			
	20.0	17.0	0.25	0.67	0.46	0.16	65.6	56.8
			0.5	1.32	0.8			
			1.00	2.34	1.6			
			1.25	2.62	1.78			
			1.50	2.85	1.89			
	28.5	17.0	0.25	0.84	0.42	0.23	69.4	61.5
			0.5	1.6	0.94			
			1.00	2.94	1.88			
			1.25	3.5	2.25			

Experimental and numerical studies on masonry infilled frames with different infill aspect ratios showed the significant effect of this factor on the strength, stiffness, and the

type of failure modes observed in these studies. The influence of the infill aspect ratio (height (h)-to-length (l)) was numerically studied using Abaqus by Chandel and Sreevalli (2019). They showed that the lower the infill aspect ratio, the higher the resistance to lateral load for brick infilled RC frames. It was also experimentally observed in studies by Flanagan and Bennett (1999) and Mehrabi et al. (1996) that the infill stiffness and ultimate capacity decreased as the infill *h/l* increases. Infills with low aspect ratio tended to fail under shear modes, while for infills with higher aspect ratios, flexural behaviour is the dominant mode which leads to toe crushing in masonry infilled frames.

In studying the interaction between the infill and its bounding frame, the infill to frame stiffness ratio plays an important role. To characterize the relative infill to frame stiffness, Stafford-Smith and Carter (1969) suggested the following equation.

$$\lambda_1 H = H\left(\frac{E_m t \sin 2\theta}{4E_c I_c h}\right)^{1/4} \tag{2.5}$$

where H is the frame height, E_m and E_C are the infill masonry and column moduli of elasticity, respectively, t is the infill thickness, θ is the angle of infill diagonal to the horizontal axis, I_c is the moment of inertia of the columns, and h is the infill height. Studies conducted by Mainstone (1971) and Stafford-Smith and Carter (1969a) showed the effect of infill to frame stiffness ratio on infill-frame contact lengths and consequently on the equivalent strut width. As illustrated in Figure 2.3, as the relative infill to frame stiffness ($\lambda_1 H$) increased, the ratio of strut width to length (*a/d*) has decreased (Al-Chaar, 2002). This suggests that a strong infill combined with a weak frame resulted in a weaker strut action.

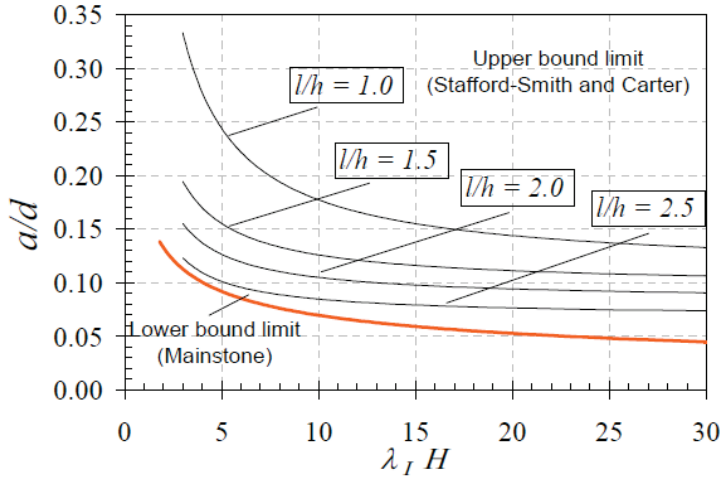

Figure 2.3 Effect of infill-to-frame stiffness ratio on strut width (Al-Chaar, 2002)

In the case where the infilled frame is also subjected to vertical load when the lateral load is applied, it is generally recognized in the Canadian masonry design standard CSA S304-14 that the vertical load is beneficial to the lateral strength of the infill. However, there are no specific design guidelines to determine the effect of the vertical load and no specification is provided with respect to the manner of application of the vertical load, i.e., through the frame column or through the frame beam, to warrant the benefit.

2.4 Numerical Modelling

In the past two decades, with the advancement of computer technology and software, numerical modeling using finite element method (FEM) has become increasingly accepted as an effective tool for the simulation of masonry structures including masonry infilled frames. The commercial software ABAQUS, ANSYS, and open-source software OpenSees have been often used programs for modeling.

As numerical modeling is one of the focus points of this research, the following sections provide a summary of the finite element modeling techniques currently used in the field. Since masonry is not a homogenous and isotropic material, simulating cracking patterns and post-ultimate behaviour of masonry structures under different loading conditions has been a modeling challenge. The current modeling techniques can be divided into three categories depending on the level of detail desired for the masonry components (units, mortar and their interaction), and associated processing time and effort. They are micro-, meso- and macro-modeling which varies from being the most detailed to the most simplified technique (Tarque et al., 2015).

2.4.1 Micro-modeling

In the micro-modeling approach, the constituents of masonry, i.e., units and mortar joints, are simulated with their respective properties separately. By doing so, the aim of the micro-modeling approach is to capture all failure mechanisms in either masonry units or mortar joints or both, including joint tensile cracking or slipping, tension cracks in units, and masonry crushing (Figure 2.4). Different levels of simplification have been employed under the framework of micro-modeling approach to make the model more computationally efficient. A so-called "Simplified Micro-Modeling" proposed by Lotfi and Shing (1994) used a zero-thickness cohesive interface model to replace the physical mortar joints. Attard et al. (2007) and Stavridis and Shing (2010) proposed a continuum brick element and used interface line elements between continuum elements to simulate the behaviour of mortar joints (Figure 2.5). Stavridis and Shing (2010) used rectangular continuum elements, while Attard et al. (2007) used triangular continuum elements. The drawback of this continuum approach is that it is not capable of recognizing the difference

between the failure in brick-mortar interface and failure in mortar material itself and thus cannot cover different aspects of brick and mortar interactions.

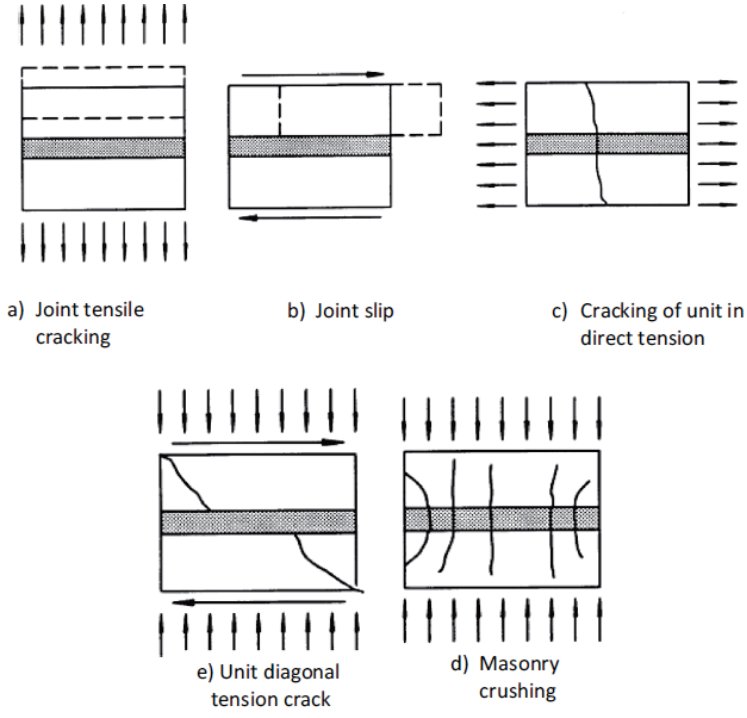

Figure 2.4 Possible failure mechanisms in masonry (Lourenço & Rots, 1997)

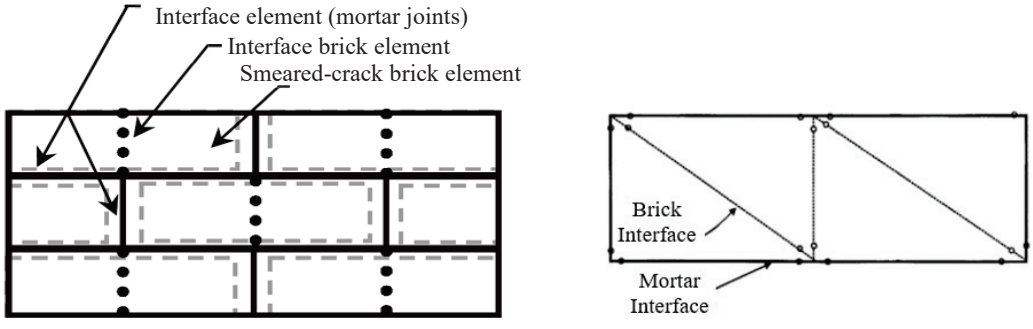

a) Stavridis and Shing (2010) b) Attard et al. (2007)

Figure 2.5 Finite-element discretization of masonry infill

2.4.2 Meso-modeling

In the meso-modeling approach, masonry units, mortar, and their interface are treated together as a continuum, so it is also called a one phase material model (Noh et al., 2017). There are different material models for modeling the continuum including the homogenization technique, the smeared crack approach, and the disturbed stress field model (DSFM). In the homogenization technique, the basic idea is to introduce average quantities for stress and strain in masonry elements based on the properties of individual components. A comprehensive review of this method is available in Lourenço et al. (2007). The smeared crack approach, which was originally developed for the analysis of reinforced concrete, assumes the cracked material as a continuum orthotropic material, with the axes of orthotropy being considered parallel to the direction of the crack. Smeared crack approach can be further subdivided into a variety of models such as the fixed crack model (Rashid, 1968), the multiple fixed crack model (de Borst & Nauta, 1985), and the rotating crack model (Cope et al., 1980). The difference between these methods lies in the orientation of smeared crack which can be kept constant, changed in multiple steps, or changed in a continuous manner. Lotfi and Shing (1991) applied the fixed and rotating smeared crack approach to masonry shear wall panels. It was found that although the flexural response of masonry shear walls can be accurately captured by the smeared crack model, shear fractures such as diagonal cracking cannot be reasonably predicted. The rotating smeared crack approach showed more load degradation in the post-peak behaviour than the fixed crack model (Lotfi & Shing, 1991). The DSFM model developed by Vecchio (2000, 2001) for reinforced concrete, was formulated by Facconi et al. (2014) for unreinforced masonry. In this method, local shear stress and shear slip of mortar joints are

added to the average microscopic behaviour of masonry. The main advantage of DSFM method over conventional smeared crack models is its ability to combine the average macroscopic representation of the material behaviour with the local shear stress and shear slip response of mortar joints. However, this approach significantly increases the computational cost.

2.4.3 Macro-modeling

2.4.3.1 Single-strut model

While micro-modeling and meso-modeling techniques are considered effective in providing detailed failure and cracking patterns and localized behaviour, they are computationally costly and not easy to be adopted for practical use. The need for a practical approach with less modeling complexity and high computational efficiency leads to the development of macro-modeling techniques. This modeling approach has shown to be sufficiently accurate in capturing the global response of the system. The "diagonal strut method" adopted in CSA S304 and TMS 402/602 is essentially a single strut macro-model.

Since the inception of this method, much research has focused on the determination of strut width which can best estimate the stiffness and strength of the infilled frame (Asteris et al., 2011; Tarque et al., 2015). Several existing diagonal strut models adopted in various standards are summarized in Table 2.2 and the failure modes considered for each model are also indicated. As mentioned previously, while all are based on the single diagonal strut concept, these models provide different formulations for strut width as shown in Table 2.2. Several studies (Chen, 2016; Liu & Soon, 2012; Manesh, 2013; Sepasdar, 2017) compared test results of masonry infilled RC and steel frames with

adopted formulations in codes and suggested that the diagonal strut methods proposed by the referenced standards do not adequately predict the failure modes and strength.

Table 2.2 Failure mechanisms incorporated in available analytical single diagonal strut models of various standards

	Diagonal compression failure	Corner crushing	Sliding shear failure	Diagonal tension cracking	Strut width
CSA S304	Yes	Yes	Yes	Yes	$w = \frac{\pi}{2}\sqrt[4]{\frac{4E_f\left(\frac{\sqrt{I_c h}}{4}+\sqrt{I_b l}\right)^2}{E_m t\sin(2\theta)}} \le \frac{\sqrt{h^2+l^2}}{4}$
TMS 402/602	No	Yes	Yes	No	$w = \frac{0.3}{\cos(\theta)}\sqrt[4]{\frac{4E_f I_c h}{E_m t\sin(2\theta)}}$
FEMA 306	Yes	Yes	Yes	Yes	$w = 0.175\left(\frac{4E_f I_c h}{E_m t\, sin(2\theta)}\right)^{0.1}\frac{\sqrt{h^2+l^2}}{h^{0.4}}$
ASCE 41-17	Yes	No	Yes	No	$w = \frac{\sqrt{h^2+l^2}}{E_m t\cos^2(\theta)}\left(\frac{1}{\frac{h^3}{3E_m I_{ce}}+\frac{h}{0.4\,E_m\,tl}}-\frac{6E_f I_c}{h^3}\right)$

2.4.3.2 Multiple-strut model

While the single-strut method remains the most accepted approach, several studies (Buonopane & White, 1999a; Saneinejad & Hobbs, 1995; Thiruvengadam, 1985) suggested that one diagonal strut cannot adequately capture the shear force and bending moment in frame members. The multiple-strut concept was then proposed by some researchers (Burton & Deierlein, 2014; Chrysostomou et al., 2002; Crisafulli & Carr, 2007; El-Dakhakhni et al., 2003; Syrmakezis & Vratsanou, 1986) and some of these multi-strut models are shown in Figure 2.6. El-Dakhakhni et al. (2003) proposed a three-strut model based on the nonlinear analysis of steel framed masonry infills. The masonry panel is represented by three struts while two of them are off-diagonal and connected to the beam and columns at the end of the contact lengths. However, this model was found to

overestimate the strength and ductility of infilled steel frames. Crisafulli and Carr (2007) developed a model composed of two parallel struts and a shear spring to account for diagonal tension and sliding shear failure of the infill; however, the parallel configuration of shear spring and struts does not allow system to fail when either of sliding or compression failure happens. The multi-strut model proposed by Burton and Deierlein (2014) is a compression-only dual-strut model with elastic frame members for struts and zero-length spring elements implemented at the end of frame members to capture the loss in the axial load carrying capacity due to column shear failure. None of these models considered the sliding shear failure of mortar joints which was experimentally observed to be one of the major failure modes of masonry infilled frames.

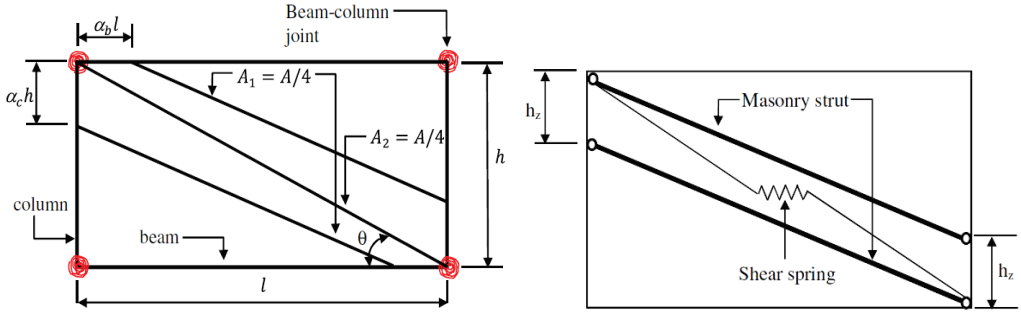

a) El-Dakhakhni et al. (2003) b) Crisafulli and Carr (2007)

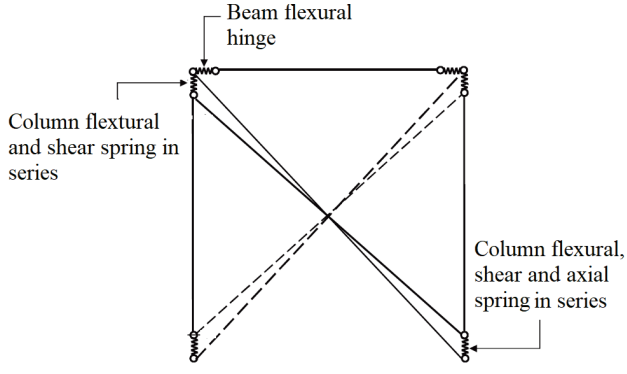

c) Burton and Deierlein (2014)

Figure 2.6 Multiple diagonal strut models

2.5 Seismic Analysis

Earthquakes are among the major causes of extensive damage and losses of structures across the world. Buildings with masonry infill walls are a common type of structures built in seismic regions. While the masonry infills are generally considered non-structural elements in the seismic design process, their impact on the overall strength, stiffness, and other seismic characteristics of the infilled structure can not be ignored.

2.5.1 Experimental studies

While most existing experimental studies were conducted using static pushover tests, there are a few dealing with quasi-static cyclic loading and shake table tests (Bertero & Brokken, 1983; Klingner et al., 1996; Klingner & Bertero, 1977; Mehrabi et al., 1996). In comparison to monotonic loading, quasi-static cyclic loading can simulate the seismic behaviour of the structure and evaluate certain seismic performance features of the structures such as energy dissipation, loading and unloading strength and stiffness deterioration, and ductility. The quasi-static loading is a testing procedure in which the structure is loaded and unloaded very slowly to generate a hysteretic response. Available experimental studies on cyclic behaviour of masonry infilled frames showed that masonry infilled frames can sustain substantial lateral loads at considerable inter-storey drifts and many hysteretic loops before major damages.

2.5.2 Numerical studies-Incremental dynamic analysis

Incremental dynamic analysis (IDA) involves performing a large number of nonlinear time history dynamic analyses under ground motion accelerations which are incrementally

intensified at multiple levels. Therefore, IDA is a powerful and comprehensive tool to estimate the seismic demand and capacity of structures in comparison to nonlinear static procedures (Bhatt & Bento, 2012). Despite being a computationally expensive analysing method, nonlinear dynamic analysis procedures have been recommended to be used by various design standards. One of the important aspects of dynamic analysis is the choice of ground motions since the structural responses are considerably affected by ground motion characteristics. To provide more reliable results and to account for the uncertainty of earthquake records, it is reasonable to increase the number of selected records. In most studies in the literature, a set of earthquake records were selected from the PEER NGA-West2 database and used in the analyses. The results of IDA were presented in terms of intensity measure (IM) versus damage measure (DM) produced based on various levels of ground motion intensity for each selected record. Maximum inter-storey drift is a common selection for DM, as it relates well with dynamic instability and structural performance limit states. For IM selection, the first mode spectral acceleration, S_a, has been widely used in the literature to represent the intensity of ground motions used in the IDA (Vamvatsikos & Cornell, 2002a).

2.5.3 Numerical study software

OpenSees has been used to model masonry infilled frames under cyclic and seismic loadings in previous research (Burton & Deierlein, 2014; Furtado et al., 2015; Hashemi & Mosalam, 2007; Kadysiewski & Mosalam, 2008; Noh et al., 2017). Kadysiewski and Mosalam (2008) showed that utilizing beam-column elements with fibre sections led to satisfactory results for both static pushover and dynamic analyses of URM infilled RC frames. They proposed a single diagonal strut model for masonry infills with two diagonal

beam-column elements joined at the midpoint of the diagonal where a lumped mass was placed to model out of plane behaviour. This model was also added to the library of OpenSees; however, since it implements the single diagonal strut model, it cannot capture the frame and infill interaction. Burton and Deierlein (2014) modeled dual compression struts in OpenSees to consider the effect of infill-frame interaction on the shear failure of columns. The drawback of their model is that they did not incorporate sliding shear failure of masonry infills and the model was calibrated with a specific set of test results and thus did not have generality. Noh et al. (2017) compared some material models available in OpenSees, including Concrete01 material, Hysteretic material, and Pinching4 material applied to the single diagonal strut model to model the strength degradation, and loading and unloading behaviour of RC frames with URM infill walls. It was found that the Pinching4 material is the most accurate material model while the Concrete01 material is a good compromise between simplicity and accuracy to simulate the cyclic response of the infill. In this study, different types of elements including Zero-Length Elements, Truss Elements, and Nonlinear Beam-Column Elements along with a range of constitutive models for concrete masonry and reinforcing bars were employed to simulate all possible failure mechanisms of all-masonry infilled frames.

2.6 Summary

In this chapter, a literature review on the general behaviour of masonry infilled frames, effect of several parameters, existing modeling techniques, and seismic analysis on masonry infilled frames was presented. This literature review is intended to serve as a general review of the topic. More detailed literature review is provided in each following

"paper" chapter that is deemed relevant and specific to the topic covered in each paper. In general, the behaviour of masonry infilled frames, regardless of the boundary frame materials, is complex as it is affected by many factors of geometric, material, and loading characteristics of the system. While some advancement in understanding of the behaviour has been made, the research gap in the seismic analysis is identified. More information is needed to connect the research findings of benefit of using masonry infilled frames with industry design practice.

CHAPTER 3 BEHAVIOR OF CONCRETE MASONRY INFILLS BOUNDED BY MASONRY FRAMES SUBJECTED TO IN-PLANE LATERAL LOADING - EXPERIMENTAL STUDY

Soraya Roosta, Yi Liu

Published in Engineering Structures Journal, Volume 247, 15 November 2021, 113153

https://doi.org/10.1016/j.engstruct.2021.113153

3.1 Abstract

This paper presents an experimental study on the in-plane behavior of a masonry infilled frame system, referred to as all-masonry infilled frames. This infilled frame system is one where both the infill and the bounding frame are built with one material, i.e., masonry units. In this study, masonry columns and beams were constructed from custom-made masonry boundary element units and fully grouted and reinforced, whereas the infill panel was constructed with half-scale standard 200 mm concrete masonry units and was ungrouted. The objective of the study is to investigate the effects of several design parameters on the behavior of this type of infilled frame and assess its performance against its infilled RC frame counterparts. A total of fifteen specimens were tested in this study, including 11 all-masonry infilled frame specimens and four RC framed specimens. The results showed that all-masonry infilled frame and its RC frame counterpart exhibited similar behavior in terms of stiffness and strength. While the RC framed infill showed

pronounced corner crushing at failure, the masonry framed infill failed by severe diagonal cracking extending into the boundary columns. The all-masonry infilled frames also showed a better ability to sustain the ultimate load as displacement increased and the post-ultimate behavior was more ductile than their RC frame counterparts.

Keywords: Masonry infills, Masonry frames, RC frames, In-plane lateral loads, Cyclic loading, Failure pattern, Experimental study

3.2 Introduction

In modern construction, masonry infilled frames often refer to either steel or reinforced concrete (RC) structural frames with masonry walls built within. A distinction may be drawn between infilled RC frame systems and confined masonry (CM) systems. In the case of infilled frame systems, masonry infills are built after the cast and hardening of RC frames, whereas in CM systems, the RC frame elements are cast after the masonry construction. In the CM system, the interaction between the confining elements and the masonry panel allows a CM wall system to be considered as a composite wall, behaving as a whole under lateral loading up to large deformation levels (Gouveia & Lourenço, 2007; Jäger & Schöps, 2009). On the other hand, the infill can be generally divided into "non-participating" and "participating" (TMS 402/602, 2016) depending on whether its interaction with the bounding frame is enabled. For "non-participating infills", the infill needs to be adequately isolated from the bounding frame commonly through the use of movement joints to avoid infill-to-frame interaction. These infills are considered non-loadbearing in design. For the participating infill, the infill is constructed in a tight fit with the bounding frame, and its contribution in load sharing with the bounding frame needs to

be considered in the design of the system. This study deals with the behaviour of the infilled frame systems with "participating infills" under lateral loading.

Previous research (Al-Chaar, 2002; Cavaleri & Di Trapani, 2014; Dawe & Seah, 1989; Holmes, 1961; Mander et al., 1993; Mehrabi et al., 1996; Papia et al., 2003) has shown that the “participating infill” inevitably affects the behavior of infilled frame system when subjected to in-plane loading. Properly designed infills contribute significantly to the lateral stiffness, strength, and ductility of the frame system. Cyclic loading tests, although relatively limited, also showed a significant energy dissipation capability of infilled frames even after cracking (Drysdale & Hamid, 2005; Mehrabi et al., 1996; Moghaddam, 2004). On the other hand, poorly designed masonry infill walls have been reported to cause large damages to frames in recent destructive earthquakes (Kaplan et al., 2010; Liel & Lynch, 2012; Sorrentino et al., 2019; Yön et al., 2019). Anić et al. (2020) reported that the failures from inertial forces commonly occur with infills having less connections with their bounding frames. The damage can be prevalent for infilled frames subjected to out-of-plane ground motion. Research in recent years investigated the effects of variables beyond simple infill situations, for example, infill openings, infill-to-frame gaps, and axial load presence, on the in-plane behavior of masonry infilled frames (Campione et al., 2015; Chen & Liu, 2016; Kakaletsis & Karayannis, 2008; Liu & Soon, 2012). However, the benefit of masonry infill walls, as demonstrated in various studies, has not been fully realized in industry practice where masonry infills are still often treated as non-structural elements and their effect on the system stiffness and strength is therefore ignored. In North America, the design of “participating infills” is governed by masonry design standards CSA S304-14 in Canada and TMS 402/602 in the US. Both are based on

the “diagonal strut method”. This method treats the entire infill as a compression strut in the diagonal direction connecting loaded corners. Once the strut width is known and the thickness is assumed to be the same as the infill, the infilled frame is transformed into an equivalent braced frame. A simple frame analysis can then be performed to determine the system stiffness and strength. However, due to a wide range of combinations of material and geometric properties of both the bounding frame and the infill wall, both standards contain only provisions for “regular” infills and they were calibrated with a limited number of specimens. For those “irregular” infills, such as infills with openings, infills with interfacial gaps with the frame, or infills with different bounding materials other than RC or steel, no explicit design guidelines are provided in the standards. The lack of design information for more complex but realistic infill situations contributed to the disconnect between the research findings and the industry practice.

This paper proposes an all-masonry infilled frame system where the bounding frame is also constructed from masonry units. In this case, masonry reinforced columns and tied beams form the masonry frame, and the masonry infill wall can be constructed in the same manner as in the conventional infilled RC frames. From both construction and design perspectives, all-masonry infilled frames are advantageous as design for the frame and infill can be carried out by structural engineers. The construction for the frame and infill can occur at the same time, thus eliminating the need to coordinate with concrete or steel trades as in the case of steel or RC frames. In addition, simultaneous construction of the frame and infill makes it easier to provide alternative forms of interfacial connection where mechanical anchorage between the frame and infill may be implemented as opposed to simple mortar bedding. It should be pointed out that while sharing some resemblance, the

all-masonry infilled frame system as proposed herein is different from the so-called Wide-Spaced Reinforced Masonry (WSRM) walls. The WSRM wall is essentially a type of masonry shear wall with vertical reinforcement spaced at a large distance (800 to 2000 mm) (Haider & Dhanasekar, 2004). Its lateral resistance is mainly derived from the flexural behaviour of the entire wall acting as one unit. On the other hand, the all-masonry infilled frame system is constructed to have two distinctive components, i.e., the frame and the infill. There is no block interlocking at alternate courses between the two as would be in a typical construction of a masonry wall. The masonry columns are formed with much larger masonry units (referred to as boundary elements) (Abo El Ezz et al., 2015; Banting & El-Dakhakhni, 2012; Kingsley et al., 2014) where the grouting and reinforcement is concentrated. The infill is left unreinforced. For this system, its lateral resistance is derived from the compressive strength of the infill through strut action and the flexural behaviour of the frame to a lesser extent.

It is recognized that while sharing some similarities with masonry infilled RC frames, the all-masonry infilled frame system is essentially a unique system with potentially different behavioral characteristics. This paper presents the results of an experimental study where all-masonry infilled frame specimens and masonry infilled RC frame counterparts were tested under in-plane loading to failure. The load vs. displacement response, failure mode, ultimate strength, and post-ultimate behavior of specimens are presented and discussed. The performance of all-masonry infilled frames as affected by several design parameters, as well as its comparison with masonry infilled RC frames, are presented and discussed.

3.3 Experimental Program

A total of fifteen specimens categorized into six groups was tested. Table 3.1 summarizes the details of design parameters for each specimen. In groups 1, 2, and 6, masonry infilled RC frame counterparts were tested alongside the all-masonry infilled frames for comparison. Groups 1 to 5 specimens were subjected to monotonic lateral loading to failure, whereas Group 6 specimens were tested under cyclic loading. The all-masonry infilled specimens are labeled as IF-AM and the masonry infilled RC frame counterparts are labeled as IF-RC.

Table 3.1 Summary of specimens

Group	Spec. ID	Infill aspect ratio	Vertical loading	Infill reinf.	Window opening	Frame-infill gap	In-plane loading
1	BF-AM BF-RC	0.73	-	-	-	-	Monotonic
2	IF-AM IF-RC	0.73	-	-	-	-	Monotonic
3	IF-AM-wide IF-AM-tall	0.5 1.3	-	-	-	-	Monotonic
4	IF-AM-BB IF-AM-BJ	0.73	-	Bond beams Bed joint reinf.	-	-	Monotonic
5	IF-AM-80b IF-AM-80c IF-AM-160c	0.73	80 kN on beam 80 kN on columns 160 kN on columns	-	-	-	Monotonic
6	IF-AM-TG-C IF-AM-SG-C IF-RC-TG-C IF-RC-SG-C	0.73	-	-	17%	Top gap, 12 mm Side gaps, 6 mm each side Top gap, 12 mm Side gaps, 6 mm each side	Cyclic

3.3.1 Test specimens

The geometry and dimensions, and frame reinforcement details of the masonry frame and RC frame were kept the same between IF-AM and IF-RC specimens. All masonry infills were constructed with custom-made half-scale 200 mm standard concrete masonry units (CMUs) laid in a running bond. Scaled CMUs for infill walls has been commonly used in experimental studies (Liu & Soon, 2012; Mehrabi et al., 1996; Mosalam et al., 1997). The masonry columns and beam were formed with custom-made C shaped boundary element units with a 190 x 190 mm cross-section, and they were fully grouted and reinforced. The masonry beam was constructed as a bond beam and tied into columns to form the frame. Similarly, the RC frame member cross-section also measured 190 x 190 mm. For both types of frames, the columns and beam were reinforced with 4-10M longitudinal rebars and 10M stirrups at 100 mm center-to-center spacing. The cover of longitudinal reinforcement in masonry frame was 45 mm to accommodate the geometry of the block and this cover distance was also used in the RC frame members to be consistent. The reinforcement detail, including size, spacing, the arrangement of longitudinal bars and stirrups, was first determined for the RC frame in accordance with the Canadian concrete design code (CSA A23-3, 2014) assuming it is at the bottom story of a four-story reinforced concrete commercial building. The same detail was then used for other specimens (including AM specimens) for consistency. A detailed depiction of frame cross-sections and reinforcement is shown in Figure 3.1.

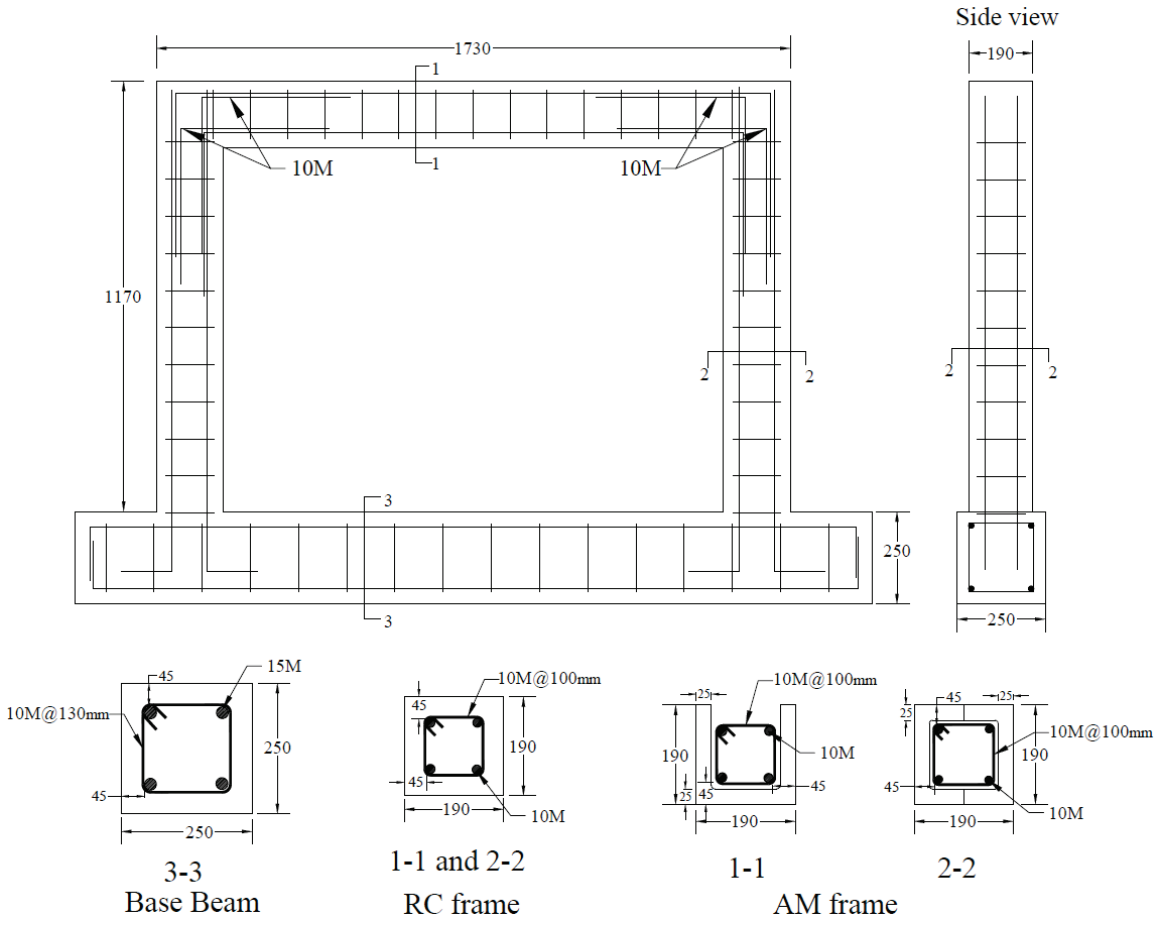

Figure 3.1 Reinforcement details of specimen frames (unit: mm)

Supplement to Table 3.1, Figure 3.2 shows the essential details of specimens (using IF-AM specimens to illustrate). Group 1 specimens consisted of two bare frames of masonry or RC frame. Group 2 specimens consisted of two infilled frame specimens with masonry or RC bounding frame as defined previously. Groups 3, 4, and 5 specimens had all-masonry infilled frame specimens tested to study effects of infill aspect ratio, infill horizontal reinforcement, and presence of vertical load, respectively. Two aspect ratios of 0.5 and 1.3, representing a wide and a tall infill panel, were used in Group 3 specimens. Group 4 specimens were constructed with different forms of infill horizontal

reinforcement. Specimen IF-AM-BB had two bond beams constructed at the third and eighth courses of the infill. They were horizontally grouted and reinforced with a 10M rebar placed at the center of infill blocks, extending into the columns with a 90-degree bent leg (Figure 3.2 (e)). Specimen IF-AM-BJ had 5 mm ladder-type joint reinforcement at every other mortar bed joint, and they were extended into the column and grouted with the column reinforcement (Figure 3.2 (f)). Group 5 specimens were tested under a constant vertical load, while the lateral load was gradually increased to the failure of the specimen.

The vertical load was applied through either frame columns or the frame beam with the magnitude as indicated. Group 6 specimens were tested under cyclic loading, including both infill opening and infill-frame interfacial gaps. While a 17% central window opening was implemented for all specimens in this group, a 12 mm gap between the infill and the frame top beam was used for TG (top gap) specimens and a 6 mm gap between the infill and the frame columns was used for SG (side gap) specimens. As mentioned earlier, "participating" infills are built in a tight fit with the bounding frame. However, due to the wall shrinkage and workmanship defects, the interfacial gap is difficult to eliminate. Previous studies showed that infill-to-frame interaction can still occur with interfacial gaps but to a lesser extent. In this study, the gaps were introduced at the designated interface by adjusting the mortar thickness along the height or width of the infill during construction.

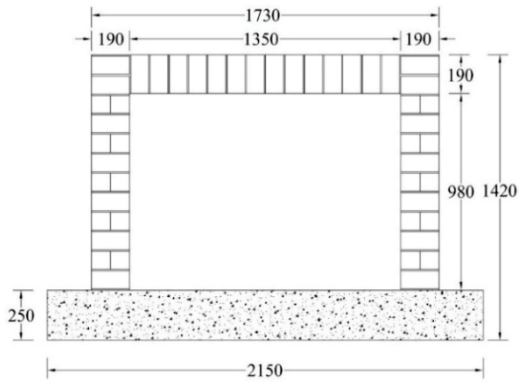

a) Group 1 specimens

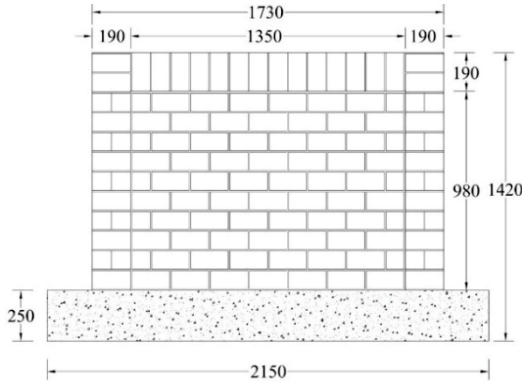

b) Groups 2 and 5 specimens

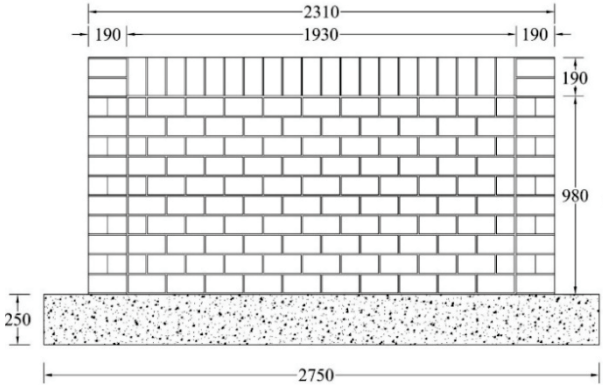

c) Group 3 (IF-AM-wide)

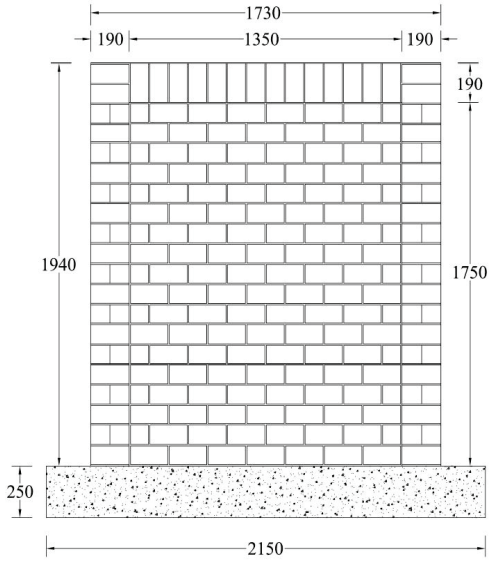

d) Group 3 (IF-AM-tall)

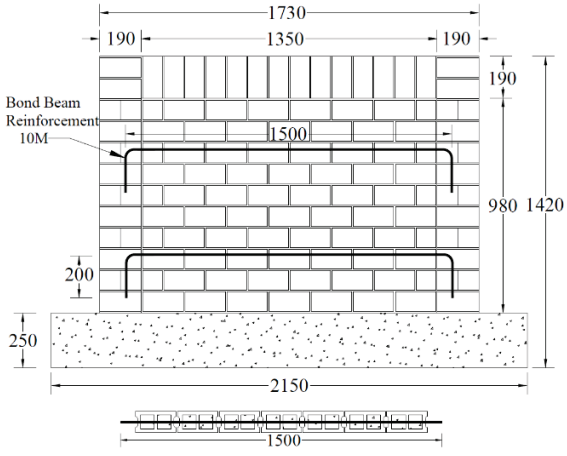

e) Group 4 (IF-AM-BB)

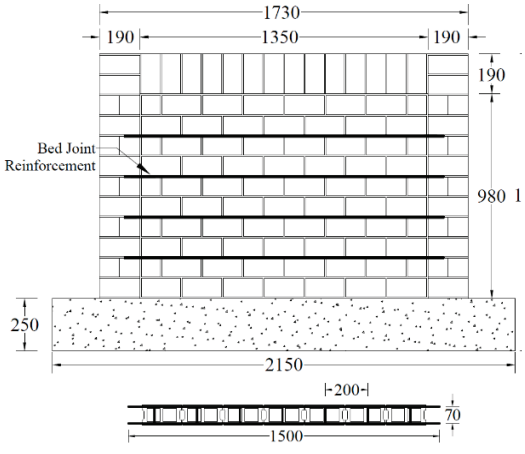

f) Group 4 (IF-AM-BJ)

Figure 3.2 Geometric and design details of specimens (unit: mm) – cont'd

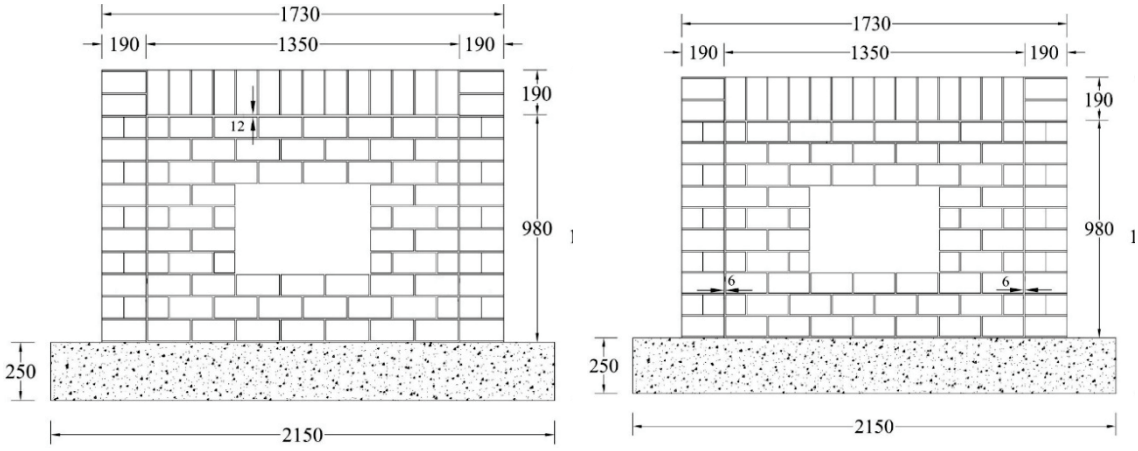

g) Group 6 specimens (IF-AM-TG-C) h) Group 6 specimens (IF-AM-SG-C)

Figure 3.2 Geometric and design details of specimens (unit: mm)

3.3.2 Test setup

Figure 3.3 shows a schematic view of the lateral loading setup. A hydraulic actuator reacting against an independent frame, was used to apply the lateral load at the top beam level of the bounding frame. A steel plate was placed between the load cell and the frame to ensure a uniform distribution of the concentrated load. The base beam of the frame was secured to the strong floor with two W-shape steel beams through 40 mm high strength threaded rods. To further prevent any lateral movement, the base beam was braced against the column of the reaction frame using a hydraulic jack on each end. For cyclic loading, the push and pull actions at the top beam of the specimen were realized using a threaded rod extending beyond the full length of the top beam. The rod was positioned at the beam center and was grouted in with the steel caging when constructing the top beam. The rod was then cut to length and securely anchored to the beam and the loading head of the actuator to facilitate the push and pull actions.

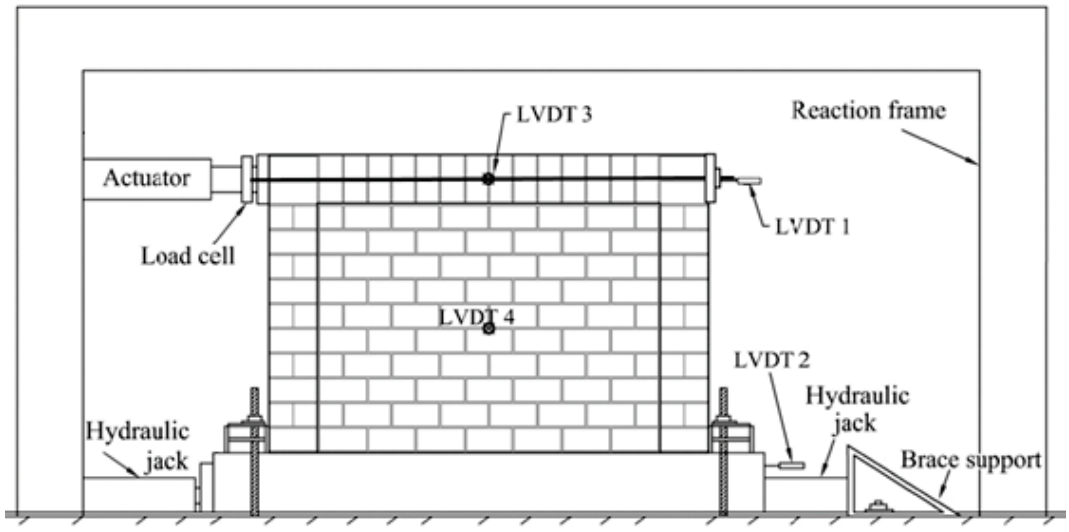

Figure 3.3 Experimental test setup for lateral loading

For Group 5 specimens under combined vertical and lateral loading, the vertical load was applied either through the frame columns or through the frame top beam at its one-third points, as shown in Figure 3.4. The vertical load was applied using a hydraulic actuator through a W-shape steel spreader beam. A pivot was installed between the actuator and the spreader beam at the loading point to accommodate the potential rotation of the spreader beam in the vertical direction. To facilitate the relative movement between the spreader beam and the specimen when the in-plane loading was applied, the spreader beam was rested on an assembly of rollers at two loading locations.

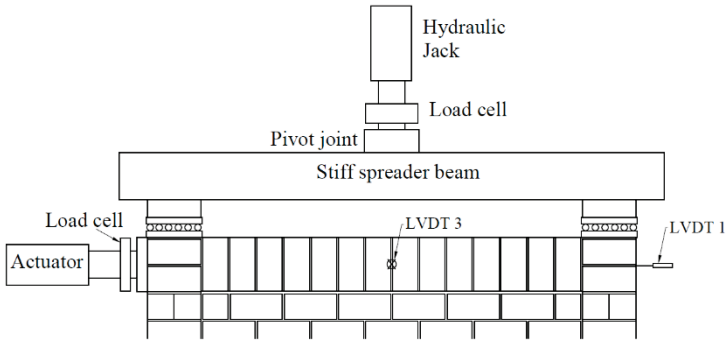

a) IF-AM-80c and IF-AM-160c

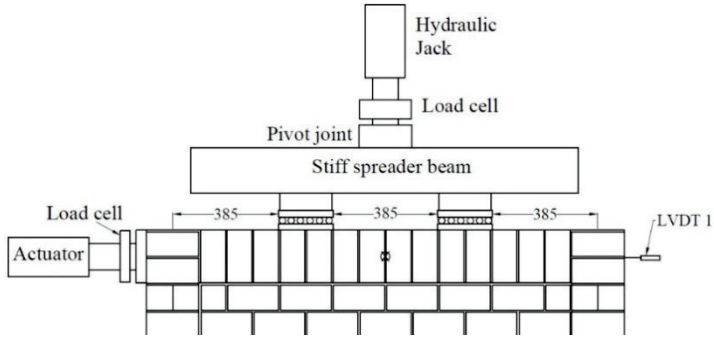

b) IF-AM-80b

Figure 3.4 Vertical loading setup

For Group 6 specimens, the cyclic load was applied in a quasi-static manner with a loading protocol according to ATC 24 (1992a). A same protocol has been used for the loading procedure of concrete masonry infill RC frames in several experimental programs by others (Al-Nimry et al., 2014; El-Dakhakhni, 2002; Mosalam, 1996). The protocol consists of consecutive cycles with increasing displacement amplitudes with three or two cycles for each amplitude. The applied loading history is shown in Figure 3.5. The displacement amplitude of the first six elastic cycles were $0.5\delta_y$ and $0.75\delta_y$, where δ_y is the yield displacement of the specimen. Subsequent cycles had an amplitude of δ_y, $2\delta_y$, and $3\delta_y$ with three cycles each. If failure has not occurred by the end of these cycles, two

cycles at magnitudes of $4\delta_y$, $5\delta_y$, and $6\delta_y$ each were applied to the specimen until failure. Tomazevic et al. (1996) showed this type of cyclic loading procedure is adequate in capturing seismic behavior of masonry walls.

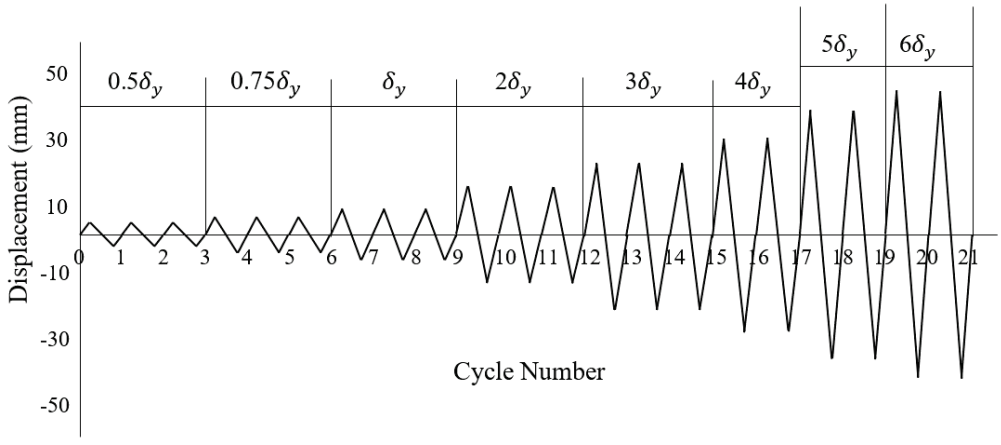

Figure 3.5 Loading protocol for quasi-static cyclic loading according to ATC 24 (ATC-24, 1992b)

The instrumentation of the tests is shown in Figure 3.3. For all infilled specimens, two linear variable differential transformers (LVDTs 1 and 2) were placed at the centerlines of the top beam and base beam to measure the lateral displacement of the specimen. Two LVDTs (LVDT 3 and 4) were used to monitor possible out-of-plane displacements at the center point of the infill panel and the top beam.

3.3.3 Fabrication of specimens

All infill walls were constructed with Type S mortar to the standard of practice by an experienced mason in a well-controlled laboratory environment with an ambient temperature variation ranging from 15 to 25 °C. For RC framed specimens, the RC frames

were cast with ready-mix concrete and cured for at least 28 days before the construction of the masonry infill wall directly inside them. For all-masonry infilled specimens, the concrete base beam was first constructed with the column rebar mounted in place and cured for at least 28 days. The infill and masonry columns were constructed at the same time, course by course. Mortar was employed on both bed joints and head joints at each course. At the top beam level, once the beam units were laid in place and the reinforcement "cage" was positioned inside the beam units, the columns and beam were grouted simultaneously, and grout was vibrated and compacted as best as possible to reduce air pockets. For specimen IF-AM-BB with two bond beams built inside the infill, the bond beam course was also fully grouted horizontally. For specimens with openings, the course directly above the opening was grouted horizontally per the standard of practice. Except for these horizontally grouted cases, the infills of all specimens were ungrouted vertically. All infill walls were moisture-cured for seven days followed by air curing. The testing was commenced approximately 40 days after the air curing of the specimens.

3.3.4 Test procedure

Before each test, the specimen was positioned in the test frame and was aligned properly in both in-plane and out-of-plane directions. The base beam was then secured to the strong floor. The LVDTs were mounted at their designated locations and all readings were checked to make sure that they functioned properly before the test began. The monotonic lateral loading was applied gradually in the displacement-control mode with a rate of 0.02 mm per second until the failure of the specimens. For specimens under combined vertical and lateral load, the vertical load was applied first to the specified level and held constant while the lateral load was applied until the failure. The cyclic loading rate was adjusted to

0.05 mm per second to control the duration of a test to be within a reasonable time frame. The failure was deemed to have occurred when the specimen showed an irreversible decrease in the load to more than 20% of the specimen ultimate strength. An electronic data acquisition system was used to monitor and record loads and LVDT readings with an interval of 0.1 seconds for each test.

3.3.5 Material properties

The material properties of CMUs, mortar, grout, masonry prisms, concrete, and reinforcing steel were determined experimentally. The Canadian masonry standard CSA S304-14 Annex D was used for testing CMUs, mortar, and masonry prisms whereas ASTM C39/C39M (1999) was used for testing concrete cylinders. For each property, a minimum of five samples was constructed and tested with the specimen. A summary of the average and standard deviation of compressive strengths of the materials for each specimen is presented in Table 3.2. It is seen that the masonry prism strength was markedly greater for boundary frames than that of masonry infills with similar strengths of CMUs. This is associated with the difference in prism construction and their failure modes in the two cases. As illustrated in Figure 3.6, for both the boundary frame and infill, five-high masonry prisms were constructed, mimicking their in-situ conditions. The boundary frame prisms were grouted and the infill prisms were ungrouted. The failure mode of the infill prisms exhibited typical vertical cracking through faceshells whereas the boundary frame prisms sustained faceshell spalling but with the grouted core acting as a solid column resisting additional compression. Hence, the boundary frame masonry strength was greater than that of masonry infills. As for reinforcement, three coupons of each of the 10M and the ladder reinforcement were tested for tensile strength as per ASTM E8/E8M-16 (2016).

Average yield stress of 446 MPa and 390 MPa, and ultimate strength of 665 MPa and 455 MPa, were obtained for 10M and 5M ladder reinforcement, respectively.

Table 3.2 Summary of compressive strengths for test specimens

Group	Spec. ID	Boundary frame			Masonry infill		
		Masonry prism f'_m±SD (MPa)	Boundary CMUs f'_{bf}±SD (MPa)	Concrete cylinder f'_c ±SD (MPa)	Infill prism f'_m±SD (MPa)	Infill CMUs f'_{bi}±SD (MPa)	Mortar f'_{mt}±SD (MPa)
1	BF-AM	30.6±3.1	17.9±2.1	-	-		
	BF-RC	-		42.3±2.9			
2	IF-AM	30.6±3.1	17.9±2.1	-	16.1±1.1	17.9±2.8	16.9±2.4
	IF-RC	-	-	42.3±2.9	17.1±2.0	22.0±1.1	21.0±1.9
3	IF-AM-wide IF-AM-tall	30.6±3.1	17.9±2.1	-	16.1±1.1	17.9±2.8	16.9±2.4
4	IF-AM-BB IF-AM-BJ	30.6±3.1	17.9±2.1	-	16.1±1.1	17.9±2.8	16.9±2.4
5	IF-AM-80b IF-AM-80c IF-AM-160c	33.8±3.4	19.8±2.4	-	20.7±1.7	18.9±1.8	17.5±1.4
6	IF-AM-TG-C IF-AM-SG-C	33.8±3.4	19.8±2.4	-	20.7±1.7	18.9±1.8	17.5±1.4
	IF-RC-TG-C IF-RC-SG-C	-	-	42.3±2.9	16.7±2.2	22.0±1.1	21.5±2.6

a) Masonry prism for infills b) Masonry prism from boundary frames

Figure 3.6 Masonry prisms and failure modes

3.4 Results and Discussion

3.4.1 Group 1: bare frames

The lateral load vs. displacement curves of bare frames are shown in Figure 3.7, together with the load and displacement results observed at the first cracking, the ultimate load, and the final failure. The initial stiffness, k_{ini}, and secant cracking stiffness, k_{cr}, were determined and also shown. The first significant crack was often marked by a noticeable stiffness decrease or a load drop (with an immediate load recovering thereafter) on the rising branch of the response curve. The secant cracking stiffness is then defined as the slope of the line connecting the point where the first significant crack was observed to the origin. The ultimate load, P_u, is defined as the maximum load attained by the specimen, and the failure load, P_f, represents the final failure load when either the load dropped more than 20% of P_u or the test was discontinued. These definitions are also used in the following discussions for other specimens.

It can be seen that the general behavior of these two bare frames is similar throughout the loading history. For the ultimate lateral load, specimen BF-RC attained a slightly higher value (58.0 kN) than specimen BF-AM (56.5 kN). While the AM frame had a markedly lower compressive strength than the RC frame (f'_m vs. f'_c), the difference in the ultimate load was nearly negligible and both reached 34 mm displacement or 3.1% drift at ultimate point. Noting that both frames had the same reinforcement, it suggests that the yielding of the steel reinforcement played a governing role in the failure as opposed to the masonry or concrete strength. The initial stiffness of specimen BF-RC is higher than specimen BF-AM (16.8 vs. 6.8 kN/mm) whereas their cracking stiffness is similar. This is

believed to be attributed to the fact that different from the monolithic nature of RC frames, the AM frame is an assemblage of masonry units, mortar, and grout which results in a more inherently flexible frame system at the initial stage of deformation. Once the assemblage is engaged as a whole, its behavior tracks that of an RC frame. The experimental cracking patterns of both specimens were similar showing flexural cracks developing along the column height and beam length with more concentration at the bottom of columns and at the beam-column joints where high flexural moments were induced.

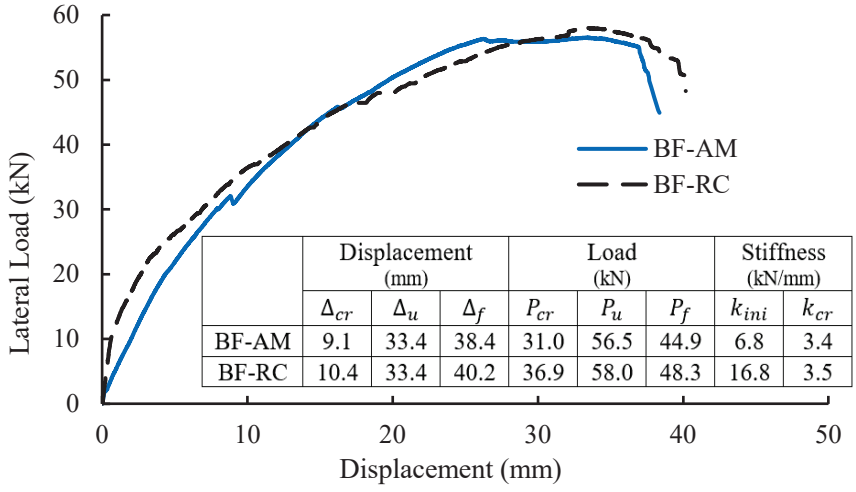

	Displacement (mm)			Load (kN)			Stiffness (kN/mm)	
	Δ_{cr}	Δ_u	Δ_f	P_{cr}	P_u	P_f	k_{ini}	k_{cr}
BF-AM	9.1	33.4	38.4	31.0	56.5	44.9	6.8	3.4
BF-RC	10.4	33.4	40.2	36.9	58.0	48.3	16.8	3.5

Figure 3.7 Load vs. displacement curves of Group 1 specimens – bare frames

3.4.2 Group 2: control infilled frame specimens

The overall behavior of Group 2 specimens is shown in Figure 3.8(a). In order to compare the behavior of masonry infills bounded by two different frames, a normalization process was performed to the overall response curves. First, the load carried by the frame was

subtracted from the overall behavior curves using the results of Group 1 specimens. The resulted curves were then normalized by dividing the lateral strength by the square root of their respective masonry compressive strengths (f'_m) of the infill as determined from the prism tests. This is a method commonly used to normalize shear strength in masonry shear walls of different strengths (Shing et al., 1989; Voon & Ingham, 2006). The normalized load vs. displacement responses of masonry infills are shown in Figure 3.8(b). Where the infilled system is concerned, specimen IF-AM yielded a 6% higher ultimate load than specimen IF-RC. The initial and cracking stiffnesses of the two infilled specimens were in the same range and in both cases, they were much greater than the stiffness of the bare frame specimens. It is thus reasonable to deduce that the infill governs the stiffness of the infilled system and the effect of frames on overall stiffness is insignificant. Where the masonry infill is concerned (Figure 3.8(b)), specimen IF-AM infill sustained a 15% higher ultimate load than specimen IF-RC infill. After the first significant crack, the former continued to resist additional load without a marked stiffness reduction while the latter showed a more evident softening. Further, the normalized loads sustained at 1%, 2%, and 2.5% story drift levels were also determined and shown in Figure 3.8(b). These are allowable story drifts for post-disaster buildings, schools, and all other buildings specified by the National Building Code of Canada [46]. It shows that specimen IF-AM sustained greater loads at all drift levels than specimen IF-RC. Specially noted is that the former was more capable of maintaining the capacity (or a large portion of) over a large displacement while specimen IF-RC had a pronounced load drop immediately after the ultimate load.

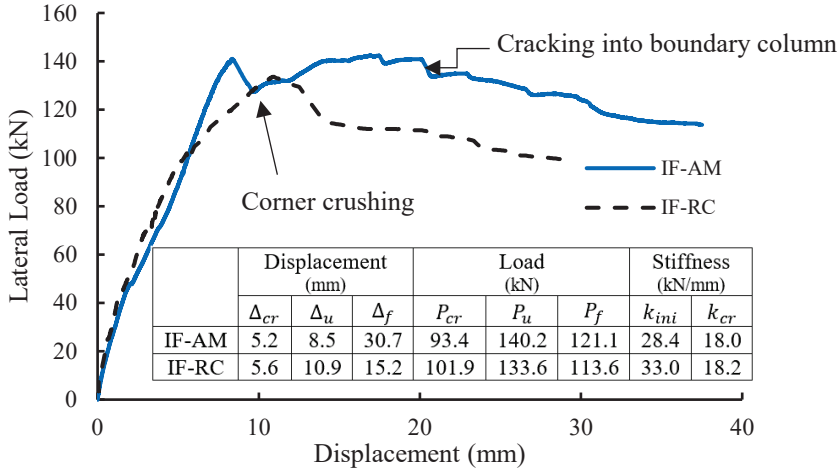

	Displacement (mm)			Load (kN)			Stiffness (kN/mm)	
	Δ_{cr}	Δ_u	Δ_f	P_{cr}	P_u	P_f	k_{ini}	k_{cr}
IF-AM	5.2	8.5	30.7	93.4	140.2	121.1	28.4	18.0
IF-RC	5.6	10.9	15.2	101.9	133.6	113.6	33.0	18.2

a) Overall curves of infilled frame specimens

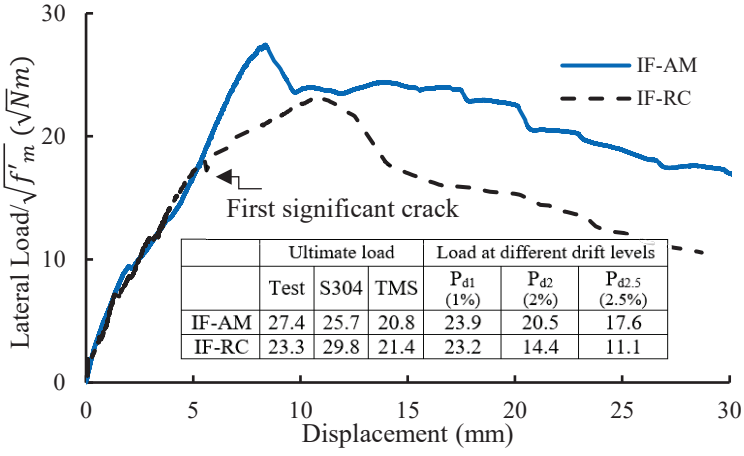

	Ultimate load			Load at different drift levels		
	Test	S304	TMS	P_{d1} (1%)	P_{d2} (2%)	$P_{d2.5}$ (2.5%)
IF-AM	27.4	25.7	20.8	23.9	20.5	17.6
IF-RC	23.3	29.8	21.4	23.2	14.4	11.1

b) Normalized curves of infills

Figure 3.8 Load vs. displacement curves of Group 2 specimens - regular infilled frames

The failure modes of the two specimens are compared in Figure 3.9 and the occurrence of the failure in both specimens was indicated in Figure 3.8(a). Both specimens developed some form of diagonal cracking in the infill leading up to the final failure. Specimen IF-AM failed when the diagonal cracks extended into the corner of the right boundary column. Specimen IF-RC showed corner crushing at the right bottom corner of the infill. As for the frame, both specimens developed similar cracks at the beam-column region where the load was applied and some flexural cracks through the height of the left

boundary columns. The corner crushing vs. extensive cracking into boundary columns is the most distinctive difference in the failure of the two specimens. It suggests that corner crushing is brittle in nature, resulting in the infill loss of capacity to carry additional load immediately thereafter. The development of cracking into the boundary column is a more ductile failure where the infill can still sustain a large portion of the capacity over displacement. The all-masonry infilled frame construction facilitates the latter failure mode.

To provide some insights into the efficacy of current design equations in estimating the capacity of "regular" infills, the analytical ultimate load of both specimens was calculated using equations in CSA S304-14 and TMS 402/602, respectively. As neither standard contains design equations for failure characterized by cracking into the boundary column, corner crushing failure was assumed to govern the strength in both cases for ease of comparison. The normalized ultimate loads are shown in Figure 3.8(b). Overall, the analytical values are in a similar range to the experimental results. However, it is noted that contrary to the test results, both standards predict a higher infill ultimate load for specimen IF-RC than IF-AM. This underscores that the corner crushing used for RC framed infills may not be accurate for predicting the strength of all-masonry framed infills. The failure mode of the latter needs to be studied further with more testing.

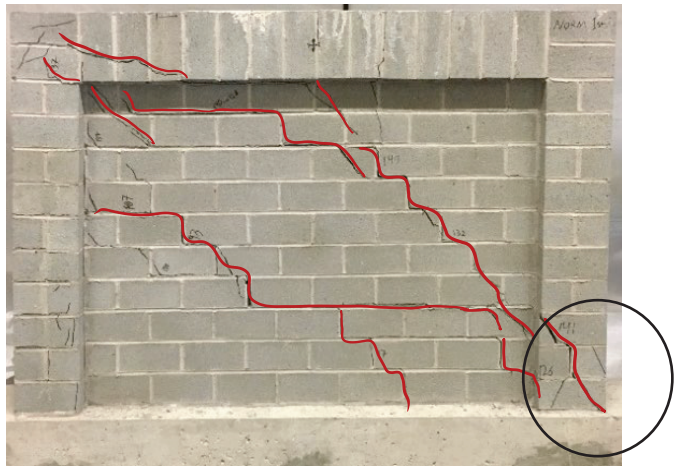

a) IF-AM

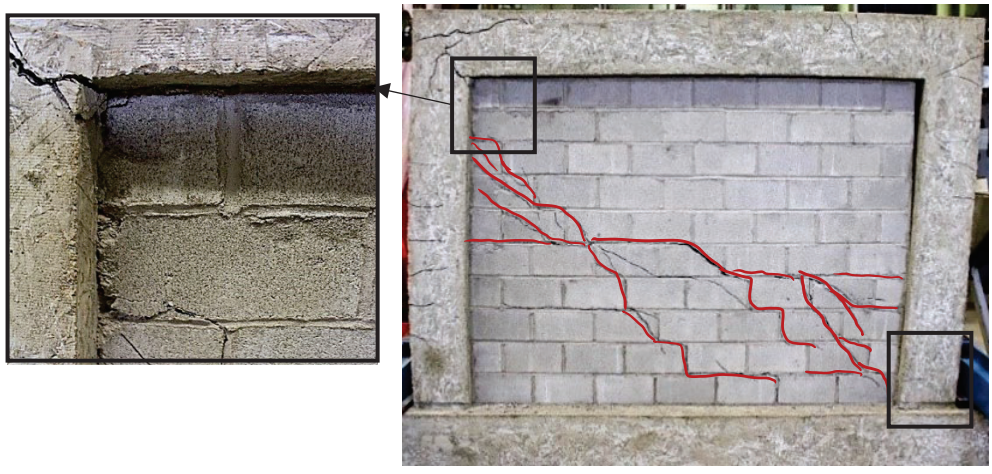

b) IF-RC

Figure 3.9 Failure pattern of Group 2 specimens

3.4.3 Group 3: effect of aspect ratio

The overall behavior of Group 3 specimens is compared in Figure 3.10 together with the control specimen IF-AM for the aspect ratio study. It is evident that as the aspect ratio increased from 0.5 to 1.3 (as the wall becomes slender), stiffness decreased, and flexibility increased. Specifically, the initial and cracking stiffness of specimen IF-AM-tall was about 25 and 33% that of specimen IF-AM-wide and the former reached the ultimate load at a greater displacement than the latter (21.2 vs. 7.9 mm). However, the two specimens

attained similar ultimate loads with about 5% difference. The control specimen (IF-AM) with an aspect ratio of 0.73 attained the lowest capacity of the group, about 30% lower than specimen IF-AM-wide.

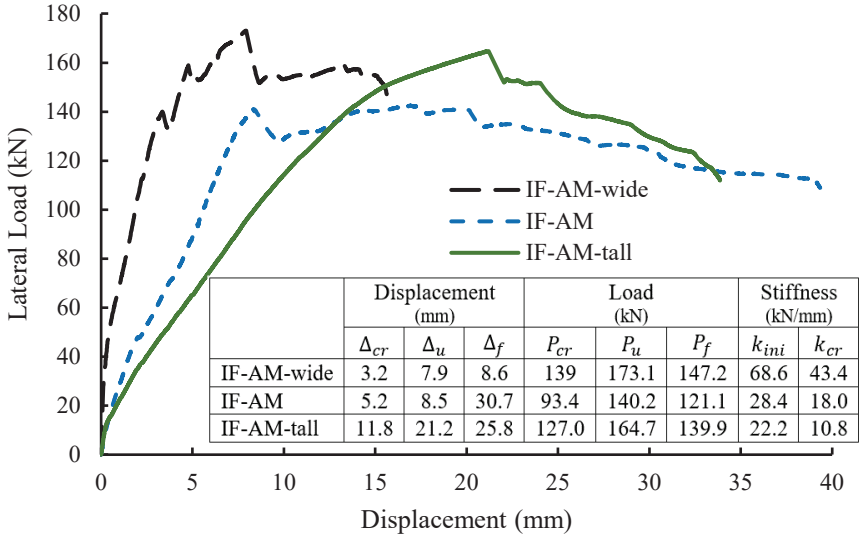

	Displacement (mm)			Load (kN)			Stiffness (kN/mm)	
	Δ_{cr}	Δ_u	Δ_f	P_{cr}	P_u	P_f	k_{ini}	k_{cr}
IF-AM-wide	3.2	7.9	8.6	139	173.1	147.2	68.6	43.4
IF-AM	5.2	8.5	30.7	93.4	140.2	121.1	28.4	18.0
IF-AM-tall	11.8	21.2	25.8	127.0	164.7	139.9	22.2	10.8

Figure 3.10 Load vs. displacement curves of Group 3 specimens with different aspect ratios

The failure patterns presented in Figure 3.11 show that for both specimens, diagonal cracking in the direction connecting loaded corners was the predominant failure mode and there was no evident corner crushing observed. Based on the diagonal strut method as specified in CSA S304-14, the strut widths were determined to be 837 mm for specimen IF-AM-wide, 764 mm for specimen IF-AM-tall, and 745 mm for specimen IF-AM. It is also recognized that due to the anisotropic property of masonry, the masonry strength of struts developed in these three specimens might be different as the angle of their diagonal struts with respect to bed joints is different (52, 27, and 35 degrees, respectively). While the exact correlation between the angle of compression and masonry strength is not known,

some studies suggested that masonry compressive strength parallel to bed joints is equal to 0.7 of that perpendicular to bed joints. For other angles of compression in between, a factor between 0.7 and 1.0 may be used for the estimate (Seah, 1998). The above discussion suggests that the wide specimen has a greater strut width but a lower masonry strength than the tall specimen. The combining effect of both factors may explain the similar ultimate loads of the two specimens from a qualitative sense. It also suggests that while the aspect ratio has a direct impact on the stiffness and flexibility, the diagonal strut geometry and dimension play a more determining role on the ultimate load of the infilled system if the failure is governed by diagonal compression failure of infills.

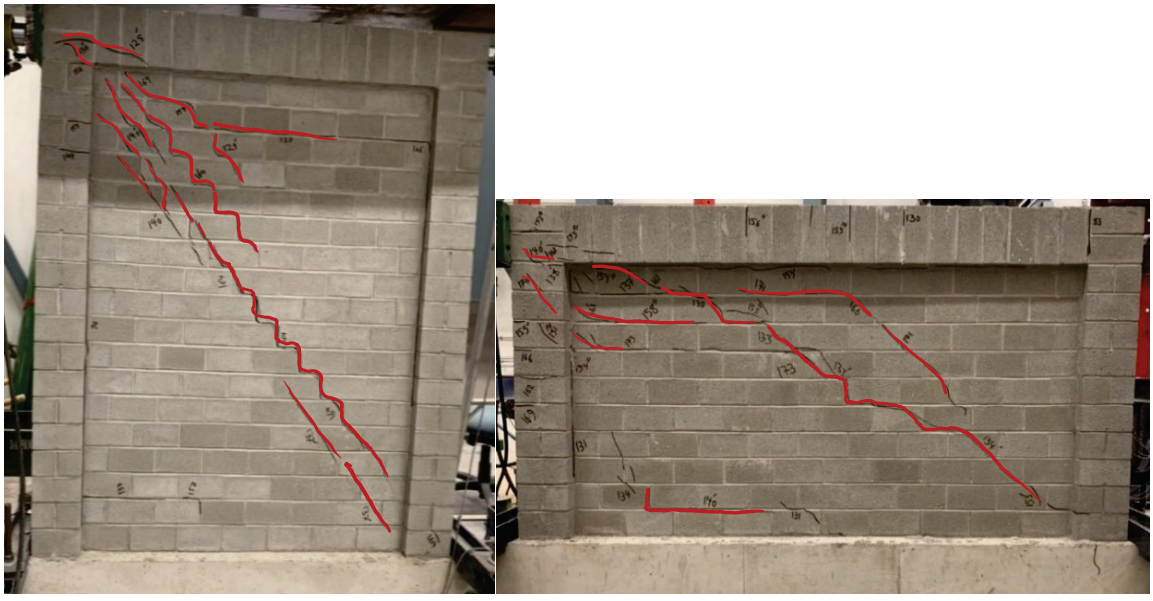

a) IF-AM-tall b) IF-AM-wide

Figure 3.11 Failure pattern of Group 3 specimens with different aspect ratios

3.4.4 Group 4: effect of infill horizontal reinforcement

The effect of infill horizontal reinforcement is studied in Group 4 specimens. Figure 3.12 compares the lateral load vs. displacement curves for specimens IF-AM, IF-AM-BB, and IF-AM-BJ. It can be seen that adding horizontal reinforcement in the form of either bond beams with reinforcement ratio of 0.0022 mm/mm or bed joint reinforcement with reinforcement ratio of 0.0019 mm/mm resulted in a marked increase in the stiffness of the rising portion of the response curve of specimens. In terms of strength, the horizontal reinforcement also resulted in an increase in ultimate loads and the magnitude of this increase was 4.2 and 6.8% for specimens IF-AM-BB and IF-AM-BJ, respectively. Specimens IF-AM-BB and IF-AM-BJ reached their ultimate loads at greater displacements than the control specimen. A comparison between specimens IF-AM-BB and IF-AM-BJ suggests that a more distributed reinforcement scheme (IF-AM-BJ) performed better than a concentrated one (IF-AM-BB) in achieving both higher capacity and overall ductility.

Failure patterns of specimens IF-AM-BB and IF-AM-BJ are shown in Figure 3.13. One distinctive characteristic of the failure for these specimens was the pronounced shear sliding cracks through mortar joints. Cracks in the general diagonal direction were also developed between the shear sliding cracks. As loading increased, the sliding cracks extended through the mortar joints till their entire length and diagonal cracks widened. In the case of specimen IF-AM-BB, the first significant crack was a sliding shear crack that occurred at the fourth-course mortar joint (one course above the bond beam) at a load of around 75 kN, which corresponded to the “kink” point on the load vs. displacement curve (Figure 3.12) of the specimen. The specimen continued to resist load and the second sliding

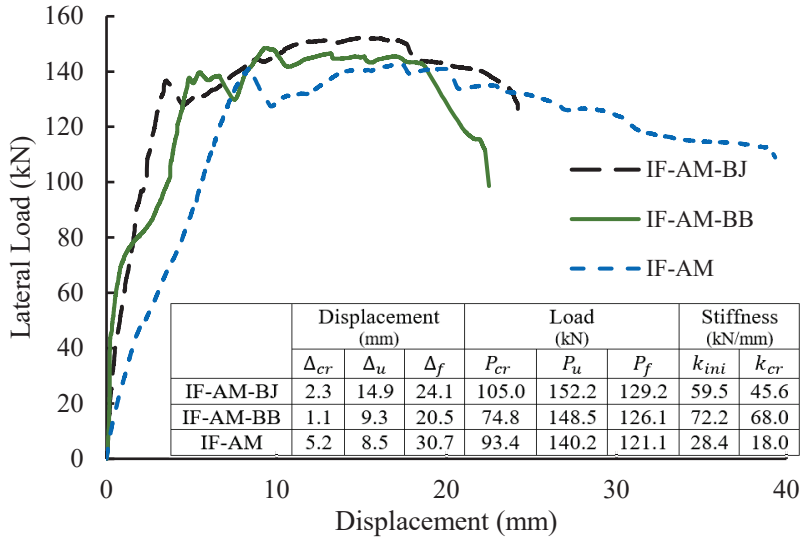

	Displacement (mm)			Load (kN)			Stiffness (kN/mm)	
	Δ_{cr}	Δ_u	Δ_f	P_{cr}	P_u	P_f	k_{ini}	k_{cr}
IF-AM-BJ	2.3	14.9	24.1	105.0	152.2	129.2	59.5	45.6
IF-AM-BB	1.1	9.3	20.5	74.8	148.5	126.1	72.2	68.0
IF-AM	5.2	8.5	30.7	93.4	140.2	121.1	28.4	18.0

Figure 3.12 Load vs. displacement curves of Group 4 specimens with horizontal reinforcement

crack occurred at around 140 kN in the ninth-course bed joint (one course above the bond beam). Along with diagonal cracks, these cracks extended into the columns at failure. In the case of specimen IF-AM-BJ, the sliding cracks occurred at each course having the bed joint reinforcement and a combination of bed joint sliding cracks and diagonal cracks in between the sliding cracks was also observed at failure. The development of these cracks through the width of the joints corresponded to the large deformation experienced by the specimen at failure. The implementation of infill horizontal reinforcement changed the cracking pattern from predominately diagonal cracking to shear sliding, rendering horizontal reinforcement diminished benefit in adding strength. This explains an insignificant increase in capacity as a result of adding horizontal reinforcement. It is interesting to note that similar behavior of shear sliding was reported in several studies on seismic behavior of masonry infills with sliding joints where concentration of damage was

observed and an increase in energy dissipation through sliding was reported (Morandi et al., 2018).

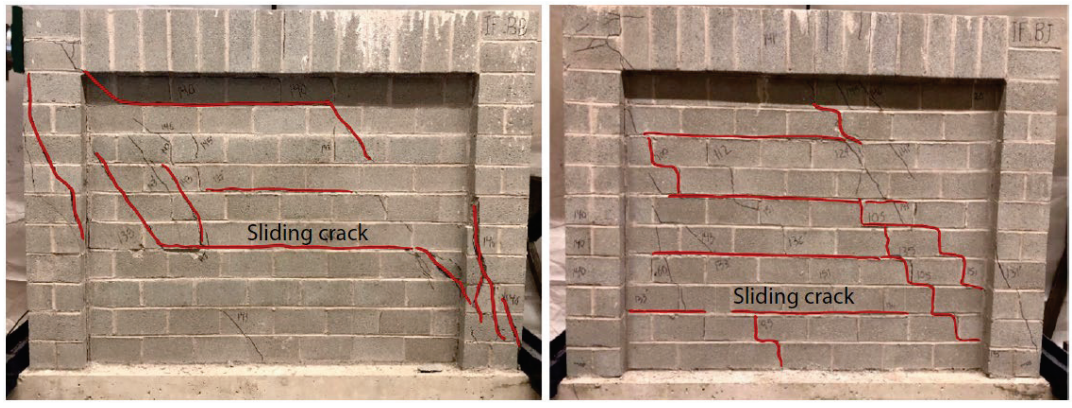

a) IF-AM-BB b) IF-AM-BJ

Figure 3.13 Failure pattern of Group 4 specimens with infill horizontal reinforcement

3.4.5 Group 5: effect of vertical load

The effect of vertical loading is shown in Figure 3.14 where the lateral load vs. displacement curves of Group 5 specimens are compared along with the control specimen IF-AM. It can be seen that both the magnitude of vertical load and its application methods affect the stiffness and strength of the infilled specimen. When applied through the columns, a total vertical load of 80 kN increased the lateral capacity of the specimen by 15% when compared with the control specimen. When the total load increased from 80 to 160 kN, the lateral capacity increased by about 80%. When the total load of 80 kN was applied through the top beam, specimen IF-AM-80b attained about 21% greater lateral capacity and failed at lesser displacement than specimen IF-AM-80c (with 80 kN applied through frame columns).

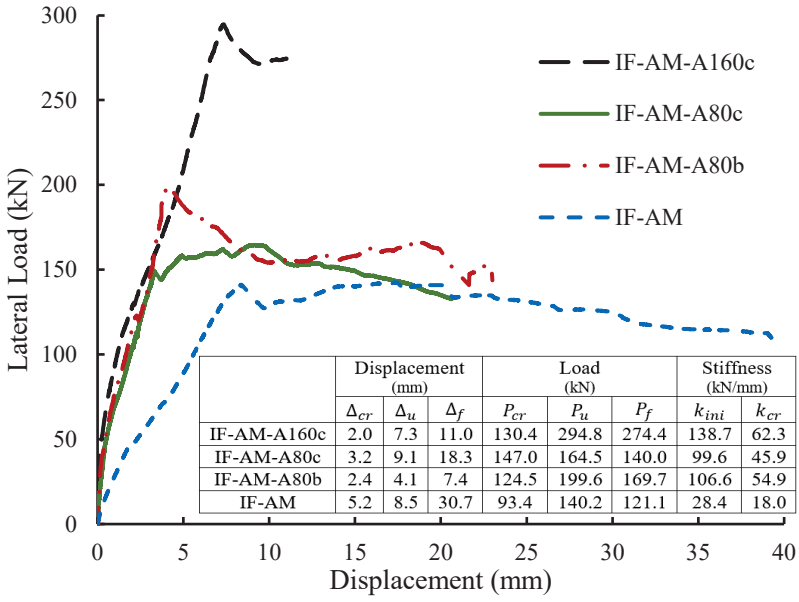

	Displacement (mm)			Load (kN)			Stiffness (kN/mm)	
	Δ_{cr}	Δ_u	Δ_f	P_{cr}	P_u	P_f	k_{ini}	k_{cr}
IF-AM-A160c	2.0	7.3	11.0	130.4	294.8	274.4	138.7	62.3
IF-AM-A80c	3.2	9.1	18.3	147.0	164.5	140.0	99.6	45.9
IF-AM-A80b	2.4	4.1	7.4	124.5	199.6	169.7	106.6	54.9
IF-AM	5.2	8.5	30.7	93.4	140.2	121.1	28.4	18.0

Figure 3.14 Load vs. displacement curves of Group 5 specimens with vertical loads

The failure modes of all vertically loaded specimens shown in Figure 3.15 indicate that all three specimens failed by diagonal cracking extending into the boundary column region. The failure of specimen IF-AM-80b was sudden without the development of visible diagonal cracks before failure, which is also reflected on the response curve where a significant load drop was observed after the ultimate load. Specimens IF-AM-80c and IF-AM-160c attained more extensive diagonal cracking at failure. While the presence of vertical load resulted in an increase in the lateral capacity of the infilled frame, the main mechanism for the capacity increase is believed to be different depending on the vertical load application. The vertical load applied through columns essentially increases the stiffness of the frame, which results in greater contact areas between the frame and the infill based on the diagonal strut concept. This subsequently results in a greater strut width and thus increased strength in the infill. On the other hand, when applied through the frame

beam, the vertical load is transferred directly to the infill, resulting in additional compressive forces on the infill, which in turn increases the infill shear strength and delays the diagonal cracking. The comparison suggests that the increase in shear strength of the infill results in a greater lateral capacity increase for the infilled system but at the expense of a more brittle failure.

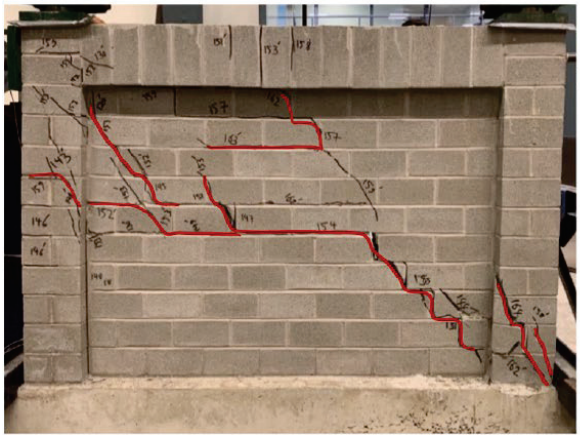

a) IF-AM-80c

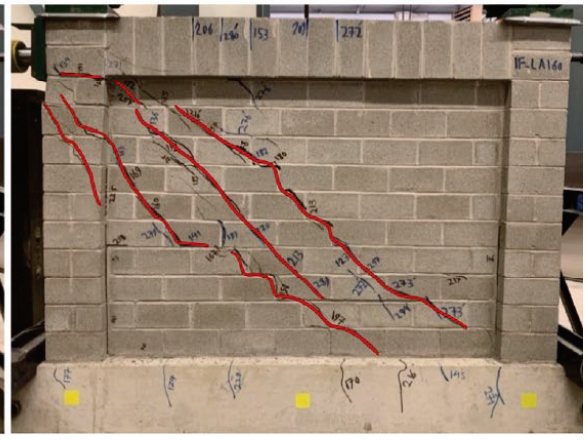

b) IF-AM-160c

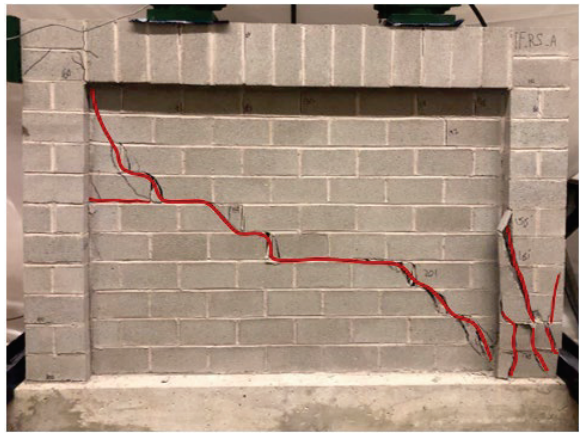

c) IF-AM-80b

Figure 3.15 Failure pattern of Group 5 specimens with vertical loads

3.4.6 Group 6: cyclic loading

Group 6 specimens were tested to study the seismic performance characteristics of all-masonry infilled frames versus masonry infilled RC frames through quasi-static cyclic loading.

3.4.6.1 Failure pattern

Figure 3.16 illustrates the experimental failure mode of Group 6 specimens. They share

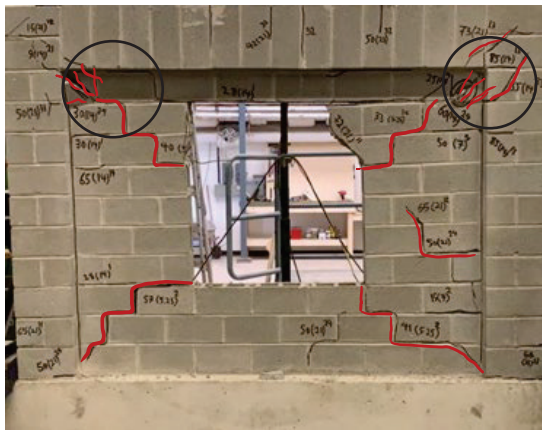

a) IF-AM-SG-C

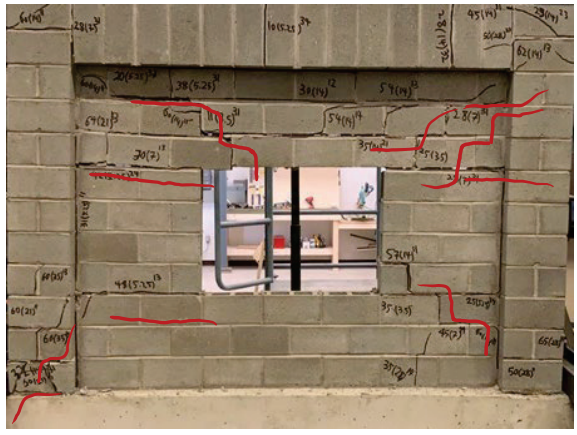

b) IF-AM-TG-C

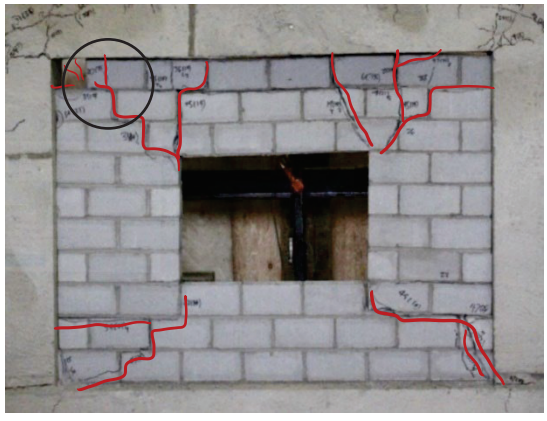

c) IF-RC-SG-C

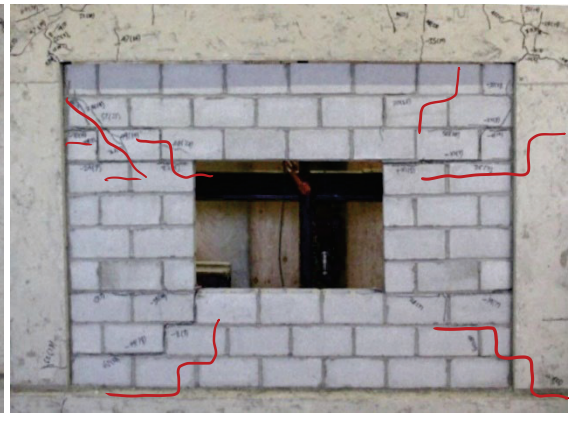

d) IF-RC-TG-C

Figure 3.16 Failure pattern of Group 6 specimens under cyclic loading

marked similarities where diagonal cracking extending from the opening corners to infill corners. Specimens with side gaps showed some corner crushing (in circles) in both bounding frames. Top-gapped specimens did not show evident corner crushing.

3.4.6.1 Hysteric response

The lateral load vs. displacement hysteric responses of all four specimens are shown in Figure 3.17 where positive loads and displacements represent pulling action and negative values are for pushing action. Overall, both sets of specimens showed a similar behavior in terms of hysteretic pinching characteristics.

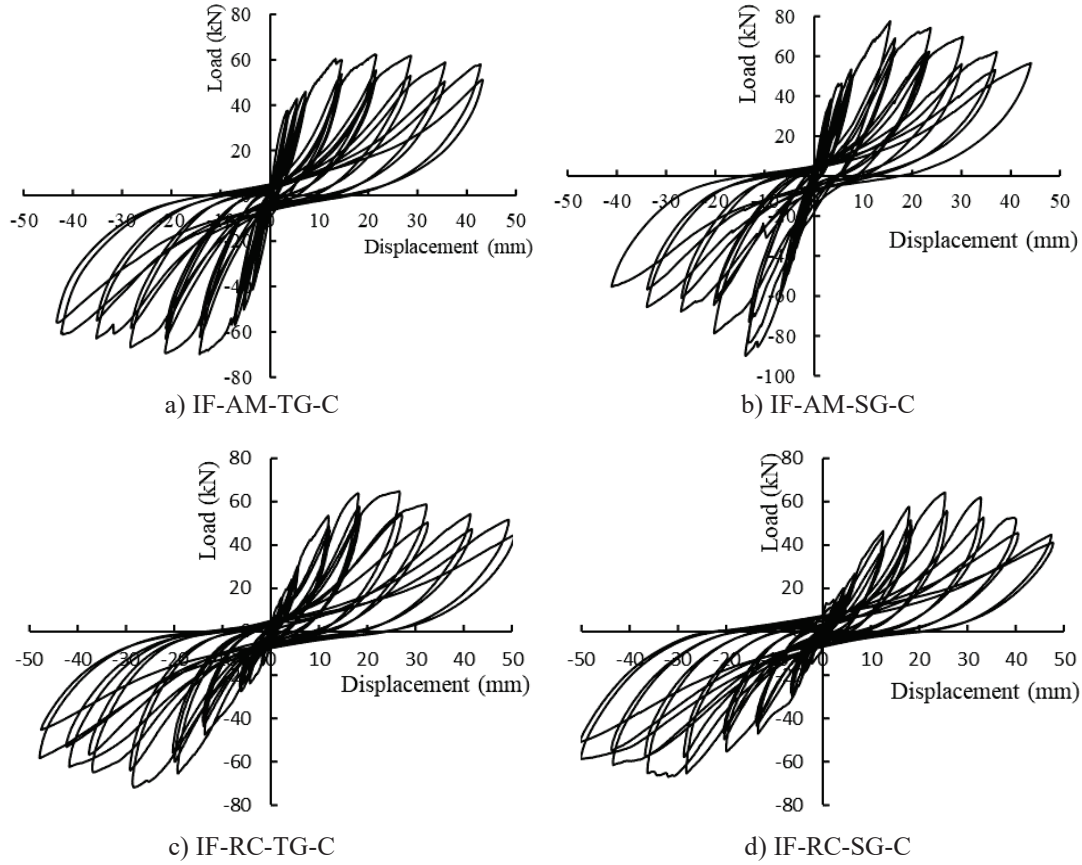

a) IF-AM-TG-C b) IF-AM-SG-C

c) IF-RC-TG-C d) IF-RC-SG-C

Figure 3.17 Lateral load vs. displacement hysteric responses

A summary of key results collected from the hysteric curves, including cracking, ultimate, failure loads, and their corresponding displacements in the pulling and pushing actions as well as the drift at ultimate load, is presented in Table 3.3. The specimens resisted drifts in the range of 1.29~2.92%. This is in line with experimental results of cyclically loaded masonry infilled RC frames reported by others (Cavaleri & Di Trapani, 2014; Jiang et al., 2015). For the RC framed specimens, the gap location did not have a significant effect on either the crack or ultimate loads. For the all-masonry infilled frames, specimen IF-AM-SG-C (side gap) attained higher ultimate loads by 24% and 30% than specimen IF-AM-TG-C (top gap) in the pulling and pushing actions, respectively.

Table 3.3 Cracking, ultimate, and failure load and displacement from hysteric curves

Specimen ID	P_{cr} (kN)	Δ_{cr} (mm)	P_u (kN)	Δ_u (mm)	P_f (kN)	Δ_f (mm)	Ultimate Drift %
IF-AM-TG-C	35.0	2.9	62.3	21.6	58.0	42.1	2.0
	-24.0	-1.4	-69.4	-21.2	-61.2	-42.0	1.97
IF-AM-SG-C	40.0	3.9	77.5	15.5	62.0	37.3	1.44
	-33.0	-3.3	-90.0	-13.9	-67.0	-29.5	1.29
IF-RC-TG-C	19.4	3.4	64.8	28.2	55.1	39.9	2.62
	-19.3	-2.7	-71.8	-26.8	-62.4	-41.7	2.49
IF-RC-SG-C	31.8	8.3	64.2	27.3	54.6	38.5	2.54
	-25.1	-4.4	-66.9	-31.4	61.5	-43.5	2.92

3.4.6.2 Backbone curves

Since the program did not test bare frames under cyclic loading, the following assumption was made for the normalization of backbone curves of these specimens. It was assumed that based on the comparison of Group 1 specimens under monotonic loading, the cyclic behavior of bare frames of two materials would also be similar. For infilled frames, the stiffness and strength are mainly contributed from the infill. Thus, the backbone curves

were normalized by dividing the lateral strength of the specimen by the square root of its masonry infill strength f'_m, and the normalized curves are shown in Figure 3.18. A summary of initial and secant stiffnesses at the first significant crack and at ultimate are also listed. In this case, the initial stiffness k_{ini} is defined as the slope of the tangent of the initial linear portion (up to 5% of the ultimate load level) of the first cycle of the load vs. displacement curve. This method was also used in the studies by Mosalam (1996b) and Al-Nimry et al. (2014) for masonry infilled frames. The secant cracking stiffness $k_{cr\ sec}$ and the secant ultimate stiffness $k_{u\ sec}$ are defined as the slope of the line connecting two cracking or ultimate points of respective cycles (in pulling and pushing actions) where cracking point (P_{cr} and Δ_{cr}) and ultimate point (P_u and Δ_u) were obtained.

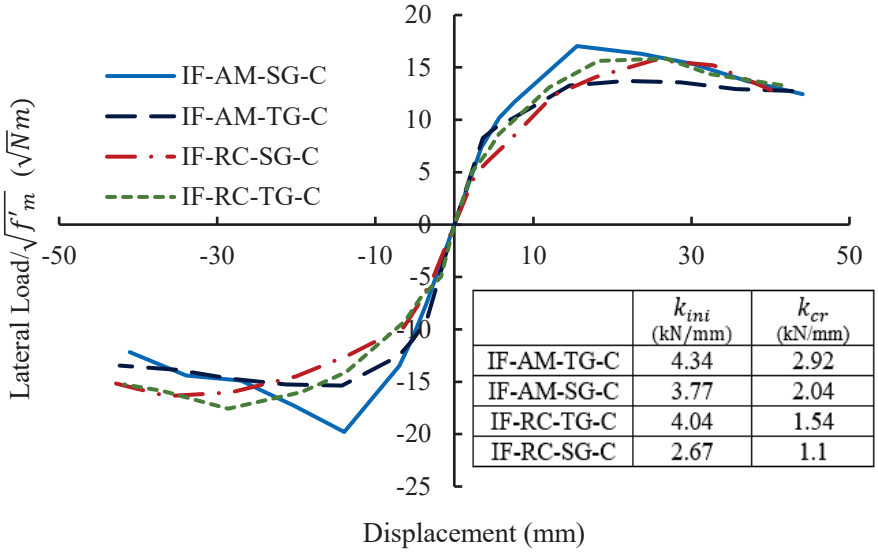

	k_{ini} (kN/mm)	k_{cr} (kN/mm)
IF-AM-TG-C	4.34	2.92
IF-AM-SG-C	3.77	2.04
IF-RC-TG-C	4.04	1.54
IF-RC-SG-C	2.67	1.1

Figure 3.18 Normalized backbone curves of Group 6 specimens

It can be seen that, in general, the behavior of two sets of specimens is comparable under cyclic loading. The all-masonry infilled frame specimens attained slightly higher

stiffness in both initial and cracking stiffness and higher ultimate loads than RC frame specimens. This, however, needs to be further verified with a more thorough normalization process where the bare frame response from different materials can be accounted for. It is believed that the general observation of similar behavior and performance of specimens with two bounding frames is valid. Moreover, for both sets of specimens, side gaps resulted in lower initial and cracking stiffnesses than the top gaps. This is attributed to the fact that more deformation is required to close the side gaps at the column-infill interface before the infill is engaged in load sharing. In terms of the strength, for the all-masonry infilled frame specimens, the top gap showed a more detrimental effect where the top-gapped specimen had a lower lateral strength than the side-gapped specimen. For the infilled RC frame specimens, however, the strength difference between the two specimens was negligible.

3.4.6.3 Ductility

Under seismic loading conditions, ductility of a lateral load resisting structural system is an important factor to indicate the system's ability to undergo large deformations while maintaining most of their load-carrying capacity. Different methods have been used by researchers to determine ductility (Minaie et al., 2010; Rizaee et al., 2020; Shendkar et al., 2021; Soltanzadeh et al., 2018). In this study, a tri-linear method suggested by ASCE 41-17 (2017a) was adopted for ductility calculation. In this method, the actual force-displacement curve is replaced by an idealized tri-linear curve defined by P_y, P_u, and P_f as shown in Figure 3.19 . On the idealized curve, P_u corresponds to the ultimate strength (peak point) whereas P_f corresponds to the point where 20% of the ultimate strength is lost or the last point of loading on the actual force-displacement curve. The first line segment

connects the origin to a point on the actual force-displacement curve at a load equal to 60% of the yield point P_y. The yield point of the system, P_y, can be found through an iterative process considering that the area between the actual and idealized curves is equal. The ductility ratio is calculated as the ratio of the final displacement, Δ_f, to the yield displacement, Δ_y.

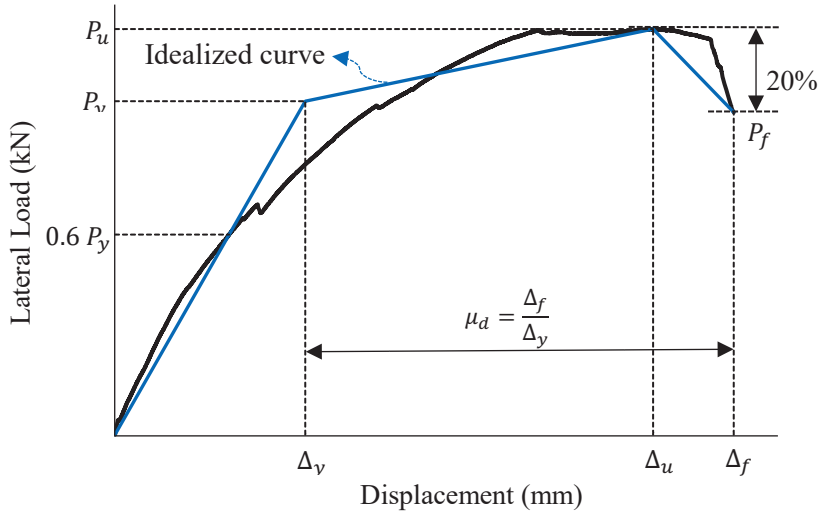

Figure 3.19 Idealized force-displacement curve

Table 3.4 summarizes the ductility factor of Group 6 specimens based on the normalized backbone curves. Overall, all specimens attained ductility ratios well above 1.0, ranging from 3.8 to 8.6. Ductility values in a similar range (5 to 10) have been reported by other researchers on infilled RC frames with different types of masonry infills including clay brick infill, concrete block infill, calcarenite stone infill which were mostly failed by diagonal and stepped cracks in the infill wall (Cavaleri & Di Trapani, 2014; Jiang et al., 2015). In the current National Building Code of Canada (NBCC, 2015), the ductility ratio

of masonry infilled frames, regardless of the bounding frame materials, is assigned to be 1.0 for design. The table shows that both AM and RC infilled frames are capable of attaining more ductility than what is specified in the design. For both sets of systems under cyclic loading, specimens with side gaps had lower ductility than specimens with top gaps. The all-masonry infilled frame specimens showed an overall greater ductility than their infilled RC frame counterparts.

Table 3.4 Summary of ductility factors of Group 6 specimens

Specimen ID	P_y ($\sqrt{N}m$)	P_u ($\sqrt{N}m$)	P_f ($\sqrt{N}m$)	Δ_y (mm)	Δ_u (mm)	Δ_f (mm)	μ_d
IF-AM-SG-C	13.0	17.0	13.6	6.2	15.5	37.3	6.0
	-10.7	-19.8	-15.8	-5.0	-13.9	-24.4	4.9
IF-AM-TG-C	11.4	13.7	12.7	5.0	21.6	42.8	8.6
	-13.0	-15.4	-13.4	-4.9	-14.2	-42.3	8.6
IF-RC-SG-C	12.5	15.7	12.8	10.5	25.4	40.1	3.8
	-12.4	-16.4	-15.1	-7.3	-36.4	-43.4	5.9
IF-RC-TG-C	11.5	15.8	13.3	6.9	26.8	41.4	6.0
	-11.4	-17.6	-15.3	-6.8	-28.6	-41.7	6.2

3.4.6.4 Energy dissipation

Energy dissipation capacity is another factor that indicates the efficiency of the system under seismic and cyclic lateral loading. Energy dissipation of each loading cycle (E_c) is equal to the area under the load-displacement curve of that cycle. For each drift ratio, the sum of all cycle areas from the beginning of loading and before that drift is termed as cumulative energy dissipation. This factor is calculated for Group 6 specimens under cyclic loading and plotted in Figure 3.20. It shows that prior to cracking, the cumulative energy dissipated by all specimens is almost negligible. As applied displacement increases,

the dissipated energy increases, and the difference between the AM and RC sets of specimens increases. At the ultimate load and till the final failure, the all-masonry infilled frame specimens show markedly greater energy dissipation than the infilled RC frame specimens. Within each set of specimens, there is no significant difference in energy dissipation observed between the top-gapped and side-gapped specimens.

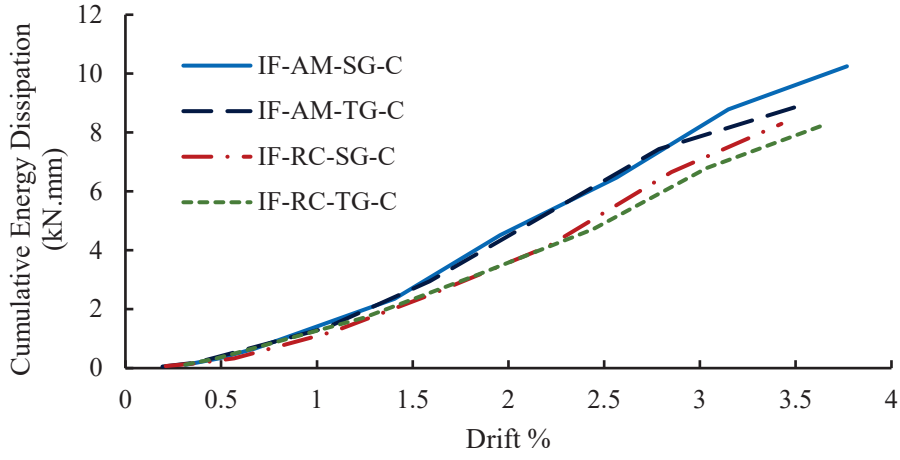

Figure 3.20 Cumulative energy dissipation of specimens under cyclic loading

3.5 Conclusions

An experimental program aimed to investigate the performance of all-masonry infilled frames under lateral loading was conducted. The uniqueness of this type of infilled frame is that the bounding frame is also constructed with masonry units. Parameters considered included infill aspect ratio, presence of vertical load, infill-to-frame interfacial gap, and loading conditions. The results were also used as appropriate to compare with the masonry infilled RC frame counterparts. The following conclusions were drawn from this study.

For the all-masonry infilled frame specimens, as the infill aspect ratio increased, the infilled system stiffness decreased, and flexibility increased. The failure modes were predominately diagonal cracking which indicates that the diagonal strut concept applies. The ultimate load was found to be dependent on the effective strut width and length as opposed to just an aspect ratio. Adding horizontal reinforcement in the infill, whether in the form of joint reinforcement or bond beam, increased both initial and cracking stiffness of the infilled system significantly. In terms of strength, the increase was also observed but more on a moderate level. In terms of failure mode, infill reinforcement was shown to change the diagonal cracking to shear sliding at courses where the reinforcement was present, resulting in greater displacement before reaching the ultimate and more ductile post-ultimate behavior. Overall, a distributed reinforcement scheme (bed joint reinforcement) performed better than a concentrated reinforcement scheme (bond beam) in terms of increasing the strength and ductility. The combined vertical and lateral load study showed that the presence of vertical load increased the system's initial and cracking stiffnesses and lateral strength but reduced its ductility. The extent of this effect was dependent on the method of vertical load application. For a given vertical load, when applied through the frame beam as opposed to columns, the increase in lateral strength was greater but with a higher reduction in ductility.

For comparison with the RC framed specimens, the general behavior of all-masonry infilled frames is similar to their infilled RC frame counterparts under both monotonic and cyclic loading. The difference between these two types of systems was in the experimentally observed failure mode. While both types of infilled frames sustained pronounced diagonal cracking within the infill prior to failure, the final failure of infilled

RC frames was predominantly by corner crushing, whereas the all-masonry infilled frames failed by diagonal cracking extending into the boundary columns. Under cyclic loading, the all-masonry infilled frames were found to attain greater ductility, energy dissipation and ultimate load than the RC framed specimens with the same design parameters. Overall, both infilled frame systems showed significantly greater ductility at ultimate than what is specified for masonry infilled frames in the design practice. While it is recommended that more testing be conducted to further verify these findings, the results in this study suggest that the all-masonry infilled frames are as effective as masonry infilled RC frames when resisting lateral loads.

3.6 Acknowledgments

The authors wish to recognize the contribution of financial assistance provided by the Natural Sciences and Engineering Research Council of Canada (NSERC), and kind assistance from the Canadian Concrete Masonry Producers Association in providing the mason and materials.

CHAPTER 4 DEVELOPMENT OF A MACRO-MODEL FOR CONCRETE MASONRY INFILLED FRAMES

Soraya Roosta, Yi Liu

Published in Engineering Structures Journal, Volume 257, 15 April 2022, 114075

https://doi.org/10.1016/j.engstruct.2022.114075

4.1 Abstract

Masonry walls, when built to infill a frame structure, have been shown to have a significant effect on the strength, stiffness, and seismic properties of the frame structure. The accurate consideration of this effect is crucial in lateral behavior analysis of the infilled frame structures, especially under the seismic loading condition. This study proposes a new macro-model in an effort to developing a practical and rational approach for evaluating the masonry infill contribution in the design of masonry infilled frames. This model accounts for the compressive and shear behavior of the masonry infill as well as the infill effect on the bounding frame. Compressive behavior was represented through compressive struts located in the diagonal direction connecting loaded corners of the infill. Two sets of three struts were used to replace the top and bottom half of the masonry infill. The shear behavior of the infill was captured through a shear spring connecting the two sets of struts at the center of the infill. The struts and shear spring were configured in a serial manner such that both compressive and shear sliding failure can be predicted. The constitutive

laws assigned to the struts and spring were based on consideration of orthotropic properties of masonry and experimental observations. This model was verified against the test results of masonry infilled masonry frames obtained in this study and of masonry infilled RC frames reported in the literature. Both monotonic pushover and quasi-static cyclic analyses were considered in the model verification. The results showed that the proposed model is capable of simulating the in-plane response of infilled frames of both masonry and RC and in both loading conditions adequately.

Keywords: Masonry infilled frames, In-plane lateral loads, Seismic loading, Macro-model, Shear sliding failure, Compressive strut

4.2 Introduction

Steel or reinforced concrete (RC) frames infilled with masonry wall panels are commonly used in modern building construction. The resulting system is often referred to as the infilled frame. It is well documented that the masonry infill tends to interact with the bounding frame and thus significantly changes the stiffness, strength, and failure mode of the frame structure (Al-Chaar et al., 2002; Dawe & Seah, 1989; Fiore, Netti, et al., 2012; Mehrabi et al., 1996; Papia et al., 2003; Uva et al., 2012). An accurate representation of the effect of infills on the frame structure is crucial in lateral behavior analysis where the stiffness of the system drives the distribution of the lateral load. The evaluation of the infill effect is, however, complex, as it depends on the interaction of two-component materials (infill and its bounding frame) which typically have different material properties and behavior characteristics. Further analytical complexities may be introduced due to material nonlinearity resulted from the cracking and crushing of the masonry infill, and cracking

and yielding of rebars in the case of RC bounding frame and yielding of steel sections in the case of steel bounding frame. The development of a simple and rational analytical model that can adequately capture the effect of the infill has attracted much research interest over the past six decades. To that end, two main categories of modeling techniques have been developed for the analysis of infilled frames, i.e., micro-modeling and macro-modeling. The micro-modeling technique models individual blocks and mortar using their respective constitutive relationship with the focus of capturing the localized stress and failure patterns, and the macro-modeling technique uses simplified models to consider the infill effect based on a physical understanding of the overall system behavior. In the latter case, the infill can be treated as a continuum or discrete elements with a defined stress-strain relationship. In general, the micro-modeling is often used when the objective of the analysis is to provide detailed stress and behavior at a localized level, and the latter is considered effective in simulating the global response and a more practical approach, especially in seismic analysis of infilled frames. The use of macro-models in seismic analysis of infilled frames is well documented in the literature (Fiore, Porco, et al., 2012; Kareem & Pantò, 2019; Panagiotakos & Fardis, 1996; Pantò et al., 2017).

The “diagonal strut method” is a typical example of macro-models. Originally proposed by Polyakov (1956) and Holmes (1961), the method replaces the entire infill panel with a diagonal strut connecting loaded corners, essentially simulating a masonry infilled frame as a braced frame structure. Since its inception, much research has been dedicated to developing the strut geometry, in particular, strut width, to adequately predict the lateral strength and stiffness observed in the experimental studies (Cavaleri & Papia, 2003; Decanini & Fantin, 1986; Flanagan & Bennett, 1999; Mainstone, 1971; Paulay &

Priestley, 1992; Stafford Smith & Carter, 1969). This general approach also formed the basis for the design of masonry infills in both the Canadian and American masonry design standards (ASCE/SEI 41-17, 2017; CSA S304-14, 2014; FEMA 306, 1998; TMS 402/602, 2016), albeit with different equations for strut width calculation. Recognizing the challenge of using strut width alone as a parameter to represent the complex mechanical behavior of the infill-frame system, much research in recent years has been dedicated to refining the single-strut method by developing strut axial force-displacement constitutive models (Cavaleri & Di Trapani, 2014; De Risi et al., 2018; Di Trapani, 2021; Di Trapani et al., 2018; Dolšek & Fajfar, 2008; Liberatore & Decanini, 2011). One limitation of this approach is that the development of constitutive models relied on extensive calibration with experimental results from the system strength and behavior. It was shown that when evaluated against a database of results with varying infill-frame materials and geometries, different constitutive models produced a wide range of prediction error (Liberatore et al., 2018). Further, in terms of the infill effect on the bounding frame, several studies (Buonopane & White, 1999b; Saneinejad & Hobbs, 1995; Thiruvengadam, 1985) suggested that one diagonal strut cannot adequately capture the shear force and bending moment induced in frame members. Cavaleri and Di Trapani (2015) proposed an equation to express the local shear forces acting on beam and column ends as a fraction of the axial load experienced by the equivalent strut in the single-strut framework. Some other studies proposed a multi-strut concept where the infill is replaced with multiple compressive struts connected at different contact points of the frame member to account for shear and moment action in the frame (Burton & Deierlein, 2014; Crisafulli & Carr, 2007; El-Dakhakhni et al., 2003).

This study presents the development and implementation of a new macro-model for simulating the in-plane behavior of masonry infilled RC frames. Using a multi-strut-spring configuration, this model accounts for sliding shear failure, strut compression failure, and frame infill interaction failure. In addition to masonry infilled RC frames, a new type of masonry infilled frames where both the infill and the bounding frame are made of masonry blocks, was also used to validate the proposed model in the paper. The comparison with experimental results demonstrated the model's capability of predicting the stiffness, strength, and post-ultimate response of masonry infilled frames over a wide range of material and geometric parameters and under lateral monotonic as well as cyclic loading. This model is intended to provide an accurate and simple analysis tool that can be used in industrial practice for analysing and designing masonry infilled systems using common commercial structural design programs.

4.3 Existing Multi-Strut Models

Several existing multi-strut models and their limitations in simulating the structural response of the infilled systems were studied first. El-Dakhakhni et al. (2003) proposed a three-strut model for masonry infilled steel frames where the masonry panel is represented by three struts with a configuration as shown in Figure 4.1. While this model may better capture the corner crushing mode than the single-strut model by including the infill effect over the contact length of frame beams and columns, it does not consider the shear behavior of the infill within the three struts and thus cannot directly simulate the shear failure of the infill panel.

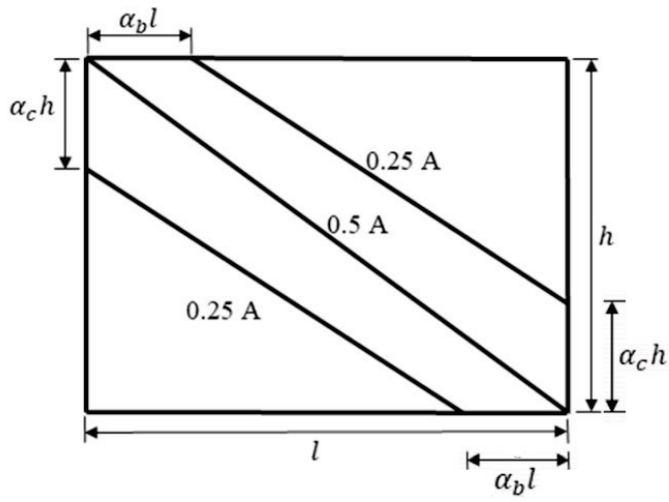

Figure 4.1 Multi-strut model proposed by El-Dakhakhni et al. (2003)

Crisafulli and Carr (2007) developed a model composed of two parallel struts and a shear spring to account for diagonal tension and sliding shear failure of the infill, as shown in Figure 4.2. In this model, the shear sliding and the horizontal component of strut axial displacements were assumed to be equal, and the total stiffness of the infill was the sum of shear spring stiffness and strut stiffness. The shear spring stiffness was taken as 50 to 75 percent of strut stiffness where the magnitude of the fraction was calibrated with the test results of their specimens. As the shear spring and struts were configured in a parallel manner, this model implies that shear spring failure does not govern the failure of the infill.

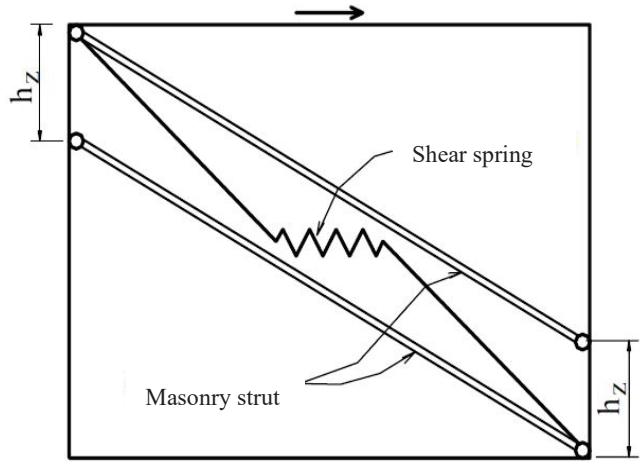

Figure 4.2 Multi-strut model proposed by Crisafulli and Carr (2007)

Burton and Deierlein (2014) proposed a dual-strut model with two struts and zero-length spring elements implemented at the end of elastically defined frame members as shown in Figure 4.3. The spring elements were to capture flexural plasticity, shear degradation, and the loss in the axial load carrying capacity of the beam and columns. The struts were assigned a trilinear force vs. displacement curve which was obtained from calibration to hysteretic responses of three cyclic tests on masonry infilled frames conducted by Blackard et al. (2009). However, no shear behavior of the masonry infills and frame-infill contact lengths were explicitly considered in this model.

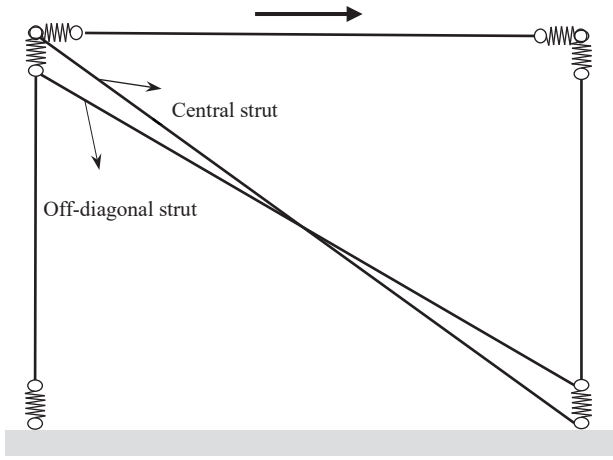

Figure 4.3 Multi-strut model proposed by Burton and Deierlein (2014)

It can be seen that in the existing multi-strut models, more attention was given to simulating corner crushing failure of the infill and the internal forces in the frame members. Shear behavior of mortar bed joints was less considered. Even when the shear behavior was considered as in the Crisafulli and Carr's model, the manner it was considered may not accurately reflect the degradation of infill stiffness due to shear controlled failure. Based on these observations, a multi-strut-spring model using a combination of strut and shear spring was developed in this paper to capture the shear behavior and shear failure of the masonry infill panel.

4.4 Proposed Model

An accurate analytical model needs to consider all potential failure modes of the masonry infilled frames. The existing studies (El-Dakhakhni, 2002; Ghosh & Amde, 2002; Wood, 1978) have identified the common failure modes of masonry infilled frames as the

following: 1) frame failure caused by high moments at plastic hinges or shear failure of frame members in the region of contact lengths; 2) compression failure of masonry either at loaded corners (corner crushing) or at the center of infill panel due to out of plane instability; and 3) mortar bed joint debonding which can be stepwise (diagonal cracking) or a thorough bed joint crack through the length of infill (shear sliding). It is pointed out that while diagonal cracking connecting loaded corners of the masonry infill is sometimes recognized as a governing failure mode (CSA S304-14, 2014), a large amount of experimental evidence shows that the infill often continues to resist additional load after diagonal cracking, albeit at a reduced stiffness. Thus in this study, diagonal cracking is not considered as a failure mode and the other three failure modes mentioned above are the points of focus of the model. The existing models described in Section 2 employed the multi-strut to consider the compression failure of the infill and the frame failure. This methodology has shown reasonable success and hence is adopted herein. The focus of this study is then to improve the modeling of shear behavior of the mortar joints. Both Canadian masonry design standard CSA S304 (2014) and American masonry design standard TMS 402/602 (2016) consider that shear failure of the mortar bed joints can govern the behavior and failure of the infilled frame. This model assumes that the infill panel in-plane horizontal displacement (Δ_{inf}) is the sum of displacement at mortar bed joints (Δ_j) and the horizontal component of diagonal compression displacement of masonry (Δ_c). Unlike the Crisafulli and Carr's model where compressive struts and shear spring were configured in a parallel manner where Δ_j and Δ_c were assumed equal, this model proposes that compressive struts and shear spring act in a serial manner and failure of either of them causes failure of the infill panel.

As shown in Figure 4.4, the model proposed in this study consists of a shear spring in the middle region of infill and two groups of equivalent strut elements. The strut elements are intended to transfer loads to the frame beams and columns as well as to the beam-column joints. The transfer points on beams and columns are assumed to be at the center of the respective contact lengths α_l and α_h. The shear spring is to model shear behavior and shear failure along mortar joints. This is intended to represent better the shear and moment effect exerted by the infill on the bounding frame than a single strut. While this approach captures the shear demand on the columns, it does not simulate the column base failure due to shear. For cyclic loading, the same strut configuration can be used in the other direction (shown in dotted lines).

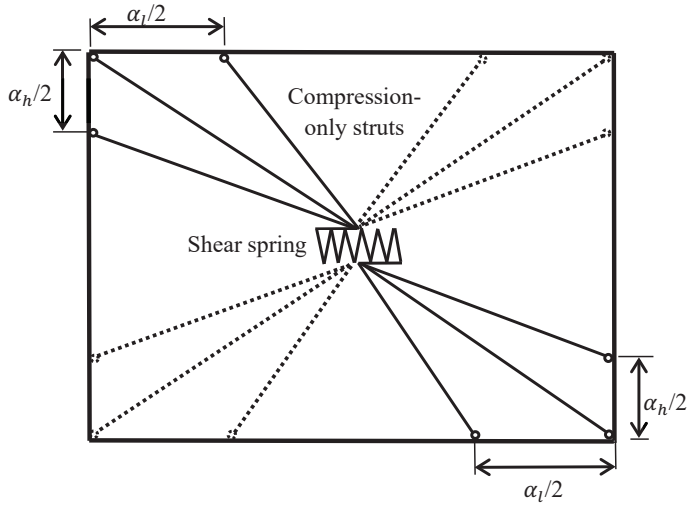

Figure 4.4 Proposed strut-model configuration

4.5 Numerical Modeling

In this study, the proposed model was developed and implemented in OpenSees software platform for both nonlinear static pushover and cyclic analyses of infilled RC frames. OpenSees was selected because it offers a large number of modeling classes ranging from linear elastic to nonlinear hysteretic material models. Its capability in modeling cyclic loading behavior of masonry infilled frames was reported in various studies (Burton & Deierlein, 2014; Furtado et al., 2015; Hashemi & Mosalam, 2007; Kadysiewski & Mosalam, 2008; Noh et al., 2017).

4.5.1 Modeling of masonry infill panel

4.5.1.1 Modeling of compressive struts

To establish the appropriate strut geometry, it was assumed that the total area of the three struts representing either the top or the bottom half panel is equivalent to that of the single diagonal strut subjected to uniform compression. The area division among the struts followed the same principle as proposed by El-Dakhakhni et al. (2003) where 50% of the total area was assigned to the center diagonal and 25% of the total area was assigned to each of the off-center diagonals. Each off-center diagonal was assigned to be located at the center of the contact lengths along either beams or columns (Figure 4.4). The strut configuration was the same for the bottom half panel, resulting in a total of six struts connected and coupled at the centre point of the infill panel. All struts were modeled as compression-only truss elements with pinned connections. Further, assuming the struts have the same thickness as the infill panel, the total width of struts was proposed to be equivalent to the strut width considered in the single diagonal strut method. The strut width

equation specified in CSA S304-14 as expressed in Eq. (4-1) was adopted. Originally developed by Stafford Smith and Carter (1969), this equation, or some form of it, has been commonly used for determining the effective strut width where uniform compressive stress can be assumed.

$$w = 0.5\sqrt{{\alpha_h}^2 + {\alpha_l}^2} \tag{4.1}$$

where α_h and α_l are the infill to column and beam contact lengths, respectively, and are computed according to Eq. (4-2) and Eq. (4-3).

$$\alpha_h = \frac{\pi}{2}\sqrt[4]{\frac{4E_f I_c h}{E_m t\ sin 2\theta}} \tag{4.2}$$

$$\alpha_l = \pi\sqrt[4]{\frac{4E_f I_b l}{E_m t\ sin 2\theta}} \tag{4.3}$$

where E_f and E_m are elastic moduli of the frame and infill materials, respectively; t, l, and h are thickness, length, and height of masonry infill panel, respectively; I_c and I_b are column and beam moment of inertia; and θ is the angle between infill diagonal and horizontal direction.

For the material model of the struts, special attention was paid to consider the effect of loading directions on the masonry material properties. Hamid and Drysdale (1980) showed that masonry has varied compressive properties as the direction of loading with respect to bed joints changes. El-Dakhakhni et al. (2003) suggested that the Young's modulus, E_θ, of the panel in the direction loaded with angle θ to the bed joints, can be

determined based on the following equation using orthotropic plate analysis proposed by Shames and Cozzarelli (1992).

$$E_\theta = \frac{1}{\frac{1}{E_0}cos^4\theta + \left[-\frac{2\nu_{0-90}}{E_0} + \frac{1}{G}\right]cos^2\theta sin^2\theta + \frac{1}{E_{90}}sin^4\theta} \quad (4.4)$$

where E_0 and E_{90} are the Young's moduli in the directions parallel and normal to the bed joints, respectively; ν_{0-90} is the Poisson's ratio defined as the ratio of the strain in the direction normal to the bed joints to the strain in the direction parallel to the bed joints; and G is the shear modulus.

In a standard test, the compressive strength and modulus of elasticity of masonry are obtained in the direction perpendicular to bed joints (f'_{m-90}, E_{90}). Seah (1998) suggested that the compressive strength of masonry parallel to bed joints (f'_{m-0}) is equal to $0.7\, f'_{m-90}$. There is an established relationship between Young's modulus and compressive strength in various standards. For example, CSA S304-14 specifies that $E_{90} = 850 f'_{m-90}$. The same factor may be used to relate f'_{m-0} to E_0. Adopting the above assumptions, masonry compressive strength and its corresponding modulus of elasticity ($f'_{m-\theta}, E_{m-\theta}$) for different angle θ to the bed joints can be determined.

For the material constitutive relationship of struts, the Kent-Scott-Park material model (Scott et al., 1982) available in OpenSees for concrete material was adopted and is shown in Figure 4.5. In this study, the secant stiffness at the ultimate load was assumed to be equal to half of the initial stiffness as suggested by Saneinejad and Hobbs (1995). This material model was assigned to each strut with the maximum stresses modified based on

the corresponding $f'_{m-\theta}$. The unloading and reloading stiffness degradation model proposed by Karsan and Jirsa (1969) was adopted in Concrete01 material to model its hysteretic stress-strain relation. Concrete01 material has been shown as an accurate material model in simulating the cyclic response of infills (Noh et al., 2017).

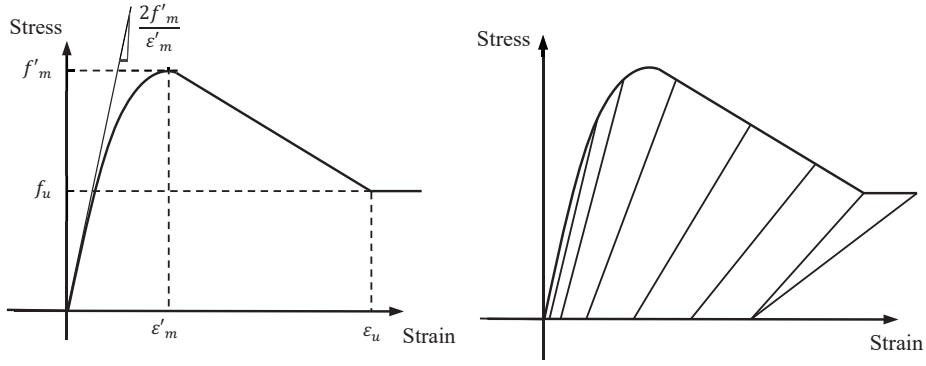

a) Material properties b) Hysteretic model

Figure 4.5 Constitutive model of Concrete01 material for strut members

4.5.1.2 Modeling of shear spring

The shear spring was modeled as a zero-length element, placed between the top and bottom struts where the connected nodes were coupled in vertical and rotational degrees of freedom. The shear resistance of mortar bed joints was assumed to be a combination of two mechanisms, i.e., mortar bond strength and friction resistance between joint surfaces. Thus, the maximum bond strength and residual friction resistance post debonding are critical parameters in determining an accurate material model. The literature contains some studies on shear behavior of solid clay bricks but little information for concrete masonry units. To develop the shear behavior model, a series of shear tests on masonry triplets were

conducted in this study. To account for the effect of compressive stress on the shear behavior, these triplets were subjected to pre-compression ranging from 0.2, 0.6, to 1 MPa as per the specification EN1052-3 (2007) (Figure 4.6 a). The average experimental shear stress vs. unit displacement responses are plotted in Figure 4.6 (b). It shows that the shear resistance is dependent on the pre-compressive stresses, exhibiting a distinctive three-phase behavior for all the levels of pre-compression.

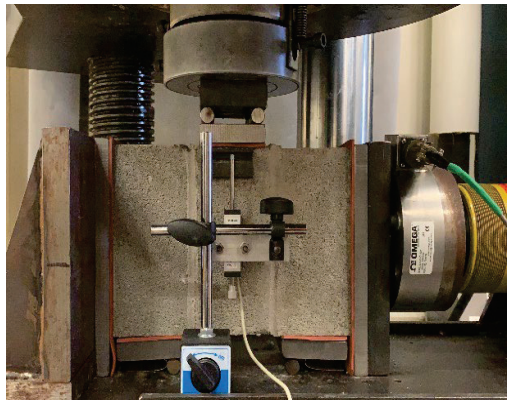

a) Triplet test setup

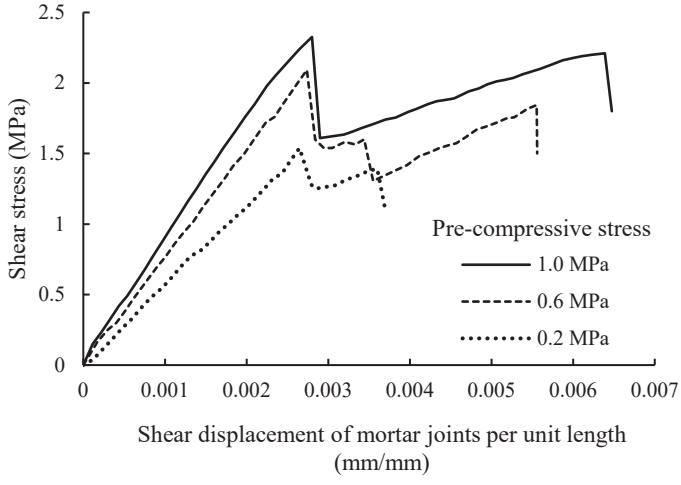

b) Average experimental results

Figure 4.6 Shear triplet tests on concrete masonry units

Based on this experimental observation, the general material constitutive model for the spring was proposed and is shown in Figure 4.7. The salient features of the model include: 1) the first phase of linear behavior up to the maximum bond strength (τ_m) which is followed by a load drop (approximately 15% of the maximum bond strength) indicating the failure of bond; 2) the second phase of shear strength increase to the ultimate shear strength of mortar bed joints (τ_u), which corresponds to additional strength gained through interlocking between mortar and sliding surfaces; and 3) the final phase of shear strength reduction to its residual strength (τ_r), which is the friction resistance between sliding surfaces.

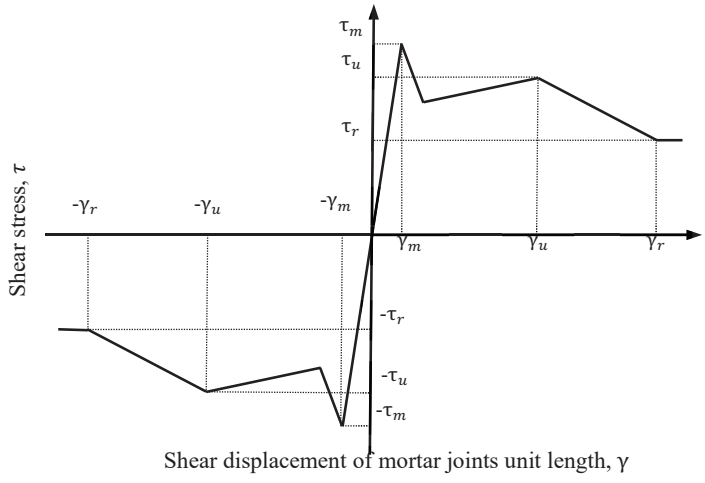

Figure 4.7 Shear stress-displacement constitutive model for sliding shear behavior of masonry

The correlation of shear strength and normal compressive stress was also observed in other experimental studies (Armaanidis, 1998; Hansen, 1999; Van der Pluijm, 1993). Lourenço et al. (2004) suggested that shear strength formulation when moderate compression stresses exist can be simplified as the Mohr-Coulomb criterion as expressed in Eq. (4.5).

$$\tau_m = \tau_0 + \mu\sigma_n \quad (4.5)$$

where τ_0 is the initial shear bond strength of mortar joints, σ_n is the compressive stress perpendicular to mortar bed joints, and μ is the friction coefficient between sliding surfaces. A wide range of values of μ, from 0.6 to 1.0, have been reported mainly from clay brick triplet tests (Andreotti et al., 2018; Augenti & Parisi, 2011; Paulay & Priestley, 1992).

A regression analysis on the triplet test results obtained in this study on concrete masonry blocks showed the following relationship providing the best fit for the experimental data.

$$\tau_m = 0.77\sigma_n + 1.48 \quad (4.6)$$

$$\tau_u = 1.32\sigma_n + 1.05 \quad (4.7)$$

$$\frac{\tau_u}{\tau_m} = 0.28\sigma_n + 0.78 \quad (4.8)$$

The residual strength τ_r was assumed to be 50% of the shear strength, τ_m, in this model. In addition to shear strengths, the unit displacements corresponding to maximum bond strength and residual friction resistance are critical factors in describing bed joint sliding response. Again, with little information on these values in the literature, triplet test results obtained in this study were mainly relied upon for the determination of these values. The unit displacement corresponding to the maximum strength, γ_m, ranged from 0.002 to 0.003, and that corresponding to the ultimate strength, γ_u, ranged from 0.005 to 0.009.

The unit displacement corresponding to residual strength, γ_r, was assumed to range from 0.01 to 0.03. It is worth mentioning that as seen in Figure 4.6 , the unit displacement at maximum shear stress, γ_m, was not sensitive to the change in pre-compression while γ_u(at the ultimate strength) varies markedly with the level of pre-compression, and the lower the pre-compression, the higher the unit displacement.

The shear constitutive model acting in both directions as shown in Figure 4.7 was assigned to the zero-length element using the Pinching4 material of OpenSees. The Pinching4 material is defined as a uniaxial material with a pinched load-deformation response and strength and stiffness degradation under cyclic loading.

4.5.2 Modeling of bounding frame

The bounding frame was modeled with the nonlinear beam-column element in OpenSees. This element assigns a fibre section to frame members and defines each fibre by its specific uniaxial material model. In the case of RC frames, the concrete and reinforcement can be modeled separately with their respective material models as shown in Figure 4.8. To account for the increase of concrete strength due to the confinement effect by transverse reinforcement, the constitutive relationship of the middle portion of the concrete confined by transverse steel can be adjusted based on the formulation proposed by Braga et al. (2006).

Among concrete material models in OpenSees, Concrete02 material was selected and used in this study. As shown in Figure 4.8(a), this model includes tensile behavior and gradual stiffness degradation. The advantages of Concrete02 material are that post-peak parameters such as ultimate strain and stress can be defined by users and the tensile

behavior was simply defined with just two parameters including peak tensile strength and tension softening stiffness. The steel reinforcement was modeled with isotropic strain hardening behavior using Steel02 material proposed by Filippou et al. (1983) as shown in Figure 4.8(b). This material model is widely implemented in modeling steel reinforcement in concrete and masonry structures because of its simplicity and accuracy in its formulation.

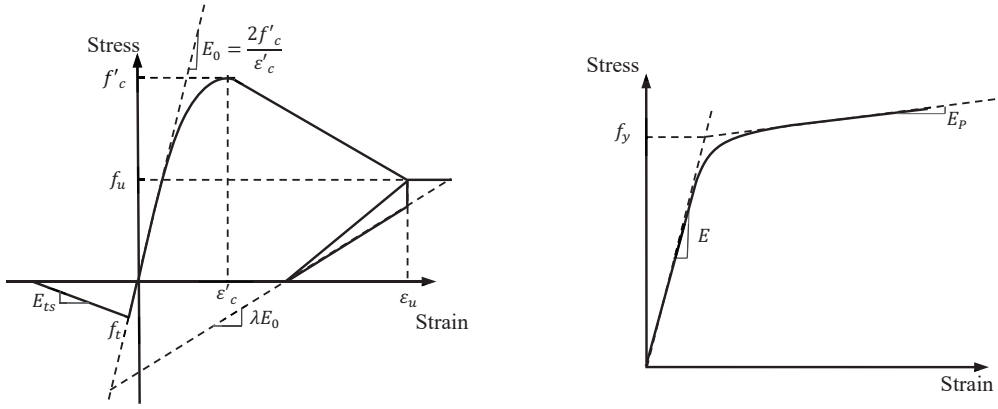

a) Concrete02 material b) Steel02 material

Figure 4.8 Constitutive models of concrete and steel reinforcement

4.6 Modeling of Test Specimens Using Proposed Method

The proposed model was implemented in OpenSees to simulate the behavior of five infilled frame specimens. Three of the specimens were tested under monotonic lateral loading at Dalhousie University (Hosseini, 2020) and the other two specimens were reported in Cavaleri and Di Trapani (2014) and in Crisafulli (1997), respectively, both under constant vertical and cyclic lateral loading. Also noted is that the first three specimens were all-masonry infilled frames of different aspect ratios while the other two specimens were concrete masonry infilled RC frames. These specimens were selected to

verify the capability of the proposed model in dealing with different geometry and material properties of both the infill and the bounding frame as well as in simulating both static pushover and cyclic behavior of infilled frames.

4.6.1 Static pushover analysis

The difference between concrete masonry infilled masonry frames and masonry infilled RC frames is that the bounding frame of the former is also made of masonry units. The motivation of development of this type of infilled system was to facilitate the construction of both infill and frame simultaneously with one material and thus eliminating the need to coordinate with concrete trades as in the case of RC frames. In this case, the columns of the masonry frame were constructed with custom-made concrete C-shaped blocks forming an enclosed square section which were reinforced and fully grouted. The beam of the masonry frame was constructed as a fully grouted bond beam using the C-shaped blocks with reinforcing bars tied into the masonry columns. Except that the masonry frame members consist of masonry components as opposed to one monolithic concrete material as in RC frame members, all reinforcement details can be made the same. Three specimens, in this case, had infill aspect ratios of 0.5, 0.73, and 1.3, respectively. A detailed description of these specimens can be found elsewhere (Roosta & Liu, 2021). These specimens were modeled in OpenSees based on the proposed model and analyzed under a monotonic displacement-controlled lateral load applied at the top beam level. It is also noted that Concrete 02 material and Steel02 material as described in the previous section were also used for modeling the reinforcement masonry bounding frame with masonry compressive strength and corresponding strains replacing those for concrete. As the masonry infill governs the behavior of infilled frame, this simplification on the bounding

frame is justified. As the masonry infill in these specimens were ungrouted, the compressive strut thickness in the model was assumed to be the thickness of mortared face shells.

Mechanical properties of all materials used in the proposed model for the tested specimens are summarized in Table 4.1. Unless otherwise specified, these properties were obtained from auxiliary tests on each of these materials.

Table 4.1 Summary of material properties for test specimens

	Material properties	Symbol and unit	Value	Source/Reference
Masonry frame	Maximum compression strength	f'_m(MPa)	30.6	Experiments on masonry frame prisms
	Strain at maximum strength	ε_0	0.0030	
	Elastic modulus	E_m (MPa)	24,300	
	Ultimate strength	f_{mu}(MPa)	13.7	
	Strain at ultimate strength	ε_{mu}	0.012	
	Tensile strength	f_t(MPa)	3.0	ACI 318-14 ($\frac{f_t}{f'_m}$ = 0.10~0.15)
Steel reinforcement	Elastic modulus	E (MPa)	220,000	Experiments on steel rebars
	Yield strength	f_y (MPa)	446	
	Ultimate strength	f_u (MPa)	665	
Masonry infill	Maximum compression strength	f'_m(MPa)	16.1	Experiments on masonry infill prisms
	Strain at maximum strength	ε_0	0.0022	
	Elastic modulus	E_m (MPa)	10,733	
	Ultimate strength	f_{mu}(MPa)	11.2	
	Strain at ultimate strength	ε_{mu}	0.006	

The validation of the proposed model was conducted through the comparison of experimental and numerical load vs. displacement responses supplemented by the failure and cracking behavior of specimens. Lateral load vs. displacement curves of the three specimens obtained from the model along with their test results are shown in Figure 4.9(a), (b), and (c), respectively. The numerical responses predicted by the three-strut model of El-Dakhakhni et al. (2003) and the parallel strut-spring model of Crisafulli and Carr (2007)

were also included for comparison. Material properties were obtained experimentally for both infills and the frame and they were consistently used in all three models as appropriate. As can be seen, the proposed model is capable of predicting both the stiffness, ultimate load, and also post-ultimate behavior for all specimens. In comparison with El-Dakhakhni et al. and Crisafulli and Carr's models, the proposed model performed better in predicting stiffness, strength, and post-ultimate response in all cases. This much-improved accuracy of the proposed model is believed to be a result of implementing the shear spring such that the sliding shear behavior of bed joints is reflected on the stiffness and strength degradation.

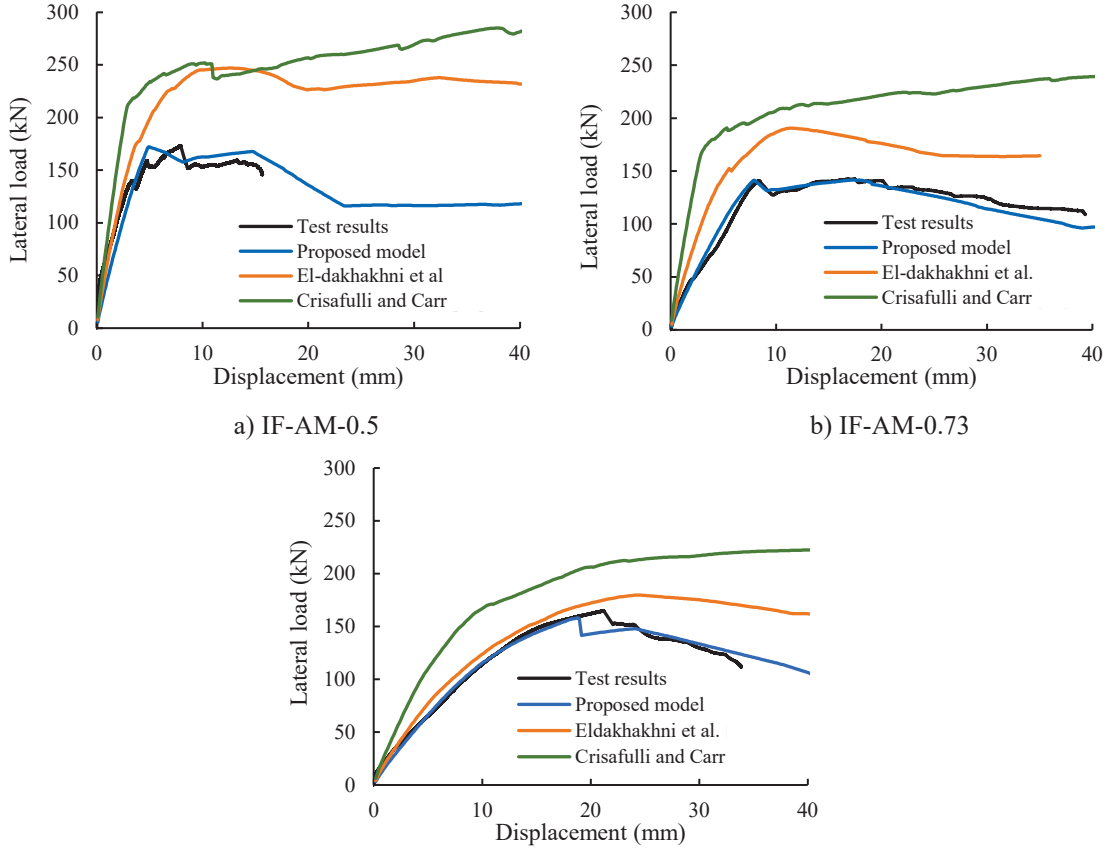

a) IF-AM-0.5

b) IF-AM-0.73

c) IF-AM-1.3

Figure 4.9 Comparison of lateral load vs. displacement curves of specimens

The failure modes of all three specimens are shown in Figure 4.10 where varying degrees of diagonal cracking and shear sliding were observed in all three specimens. It shows that shear sliding cracks predominated the cracking pattern for the specimens of aspect ratios of 0.5 and 0.73. As the specimen became more slender (aspect ratio=1.3), most cracks were in the form of diagonal cracking as opposed to shear sliding, the behavior

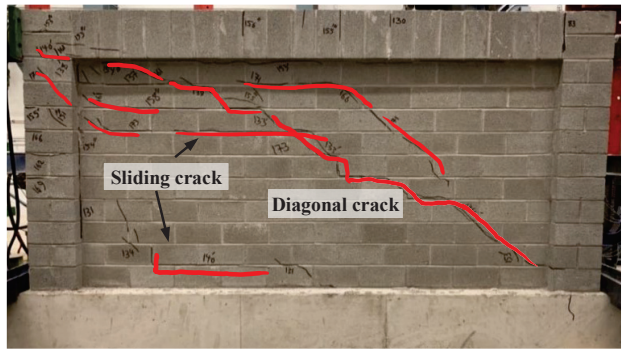

a) IF-AM-0.5

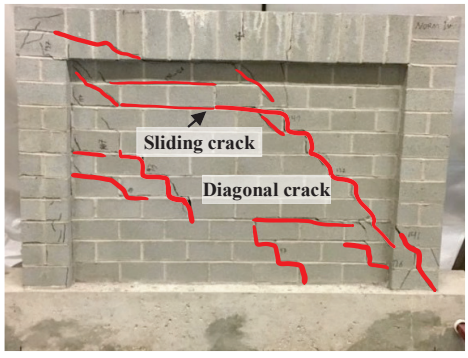

b) IF-AM-0.73

c) IF-AM-1.3

Figure 4.10 Final failure pattern of specimens

shifted to a more flexural behavior and less shear behavior. This shift in cracking pattern was also reflected in the degree of discrepancy between the proposed model and the other two models. The discrepancy appears to be more pronounced for the two specimens where shear sliding behavior predominated and lessened for the slender specimen. This further confirms that the implementation of shear spring and the manner in which it was implemented in the proposed model are the main contributions to an improved model. If the behavior and failure are less controlled by shear, El-Dakhakhni et al.'s three-strut model is shown to perform better. On the other hand, Crisafulli and Carr's model is shown to overestimate both stiffness and strength of the specimens which is believed to be a result of assuming higher initial stiffness for the shear spring and also the parallel configuration of shear spring and struts where shear sliding failure could not be captured accurately.

4.6.2 Sensitivity analysis of shear behavior parameters

The efficacy and validity of the proposed model have been demonstrated through the previous comparison between the experimental and numerical responses. As mentioned earlier, several input parameters, in particular, the unit displacement values of γ_m, γ_u, and γ_r were experimentally observed to have values which are in a predictable range from the triplet tests. The exact value used in the shear spring model were calibrated against the experimental results of this study. A list of these values used for generating response curves of the test specimens is summarized in Table 4.2. A sensitivity analysis on the variation of these parameters was then conducted and results are discussed in this section. This discussion is intended to provide insights and guidance for the model implementation by others. These parameters are deemed critical in defining the shear spring model but the

available literature provides little information on their values. The input parameters and their variations selected for this analysis are summarized in Table 4.3 where the control value represents the value of the parameter held constant while the other parameters varied.

Table 4.2 Summary of shear spring model parameters for test specimens

Properties	Symbol and unit	Specimen aspect ratio	Value	Source/Reference
Maximum shear stress	τ_m (MPa)	0.5 0.73 1.3	2.5 2.6 3.5	Shear triplet test results
Shear unit displacement at maximum stress	γ_m (mm/mm)	0.5 0.73 1.3	0.002 0.0025 0.0027	Shear triplet test with calibration
Ultimate shear stress	τ_u (MPa)	0.5 0.73 1.3	2.25 2.34 3.15	$\tau_u = 0.9\ \tau_m$ (Per Section 4.1.2)
Shear unit displacement at ultimate strength	γ_u (mm/mm)	0.5 0.73 1.3	0.005 0.009 0.007	Shear triplet test with calibration
Residual shear stress	τ_r (MPa)	0.5 0.73 1.3	1.25 1.30 1.75	$\tau_r = 0.5\ \tau_m$ (Per Section 4.1.2)
Residual shear unit displacement	γ_r (mm/mm)	0.5 0.73 1.3	0.01 0.02 0.02	Calibration (Per Section 4.1.2)

Table 4.3 Parameters in the sensitivity analysis of the shear spring model

Parameter	Variation	Control value
Maximum shear strength, τ_m (MPa)	1.5 ~ 4.0 with an increment of 0.5	γ_m = 0.0025 mm/mm γ_u = 0.009 mm/mm γ_r = 0.025 mm/mm
Shear unit displacement at maximum strength, γ_m (mm/mm)	0.002 ~ 0.0035 with an increment of 0.0005	τ_m = 2.5 MPa γ_u = 0.009 mm/mm γ_r = 0.025 mm/mm
Shear unit displacement at ultimate strength, γ_u (mm/mm)	0.005 ~ 0.011 with an increment of 0.002	τ_m = 2.5 MPa γ_m = 0.0025 mm/mm γ_r = 0.025 mm/mm
Residual shear unit displacement, γ_r (mm/mm)	0.01 ~ 0.03 with an increment of 0.005	τ_m = 2.5 MPa γ_m = 0.0025 mm/mm γ_u = 0.009 mm/mm

4.6.2.1 Maximum shear strength, τ_m, and corresponding unit displacement, γ_m

The parameters describing the peak point of phase one on the behavior model are studied in this section. First, the maximum shear strength was varied from 1.5 to 4.0 MPa with a 0.5 MPa increment while shear unit displacements were kept constant at maximum, ultimate, and residual points. Numerical results were obtained in the form of lateral load versus displacement curves for different values of τ_m as shown in Figure 4.11(a) and the ultimate lateral load and cracking stiffness of the infilled frame versus τ_m as shown in Figure 4.11(b) and (c), respectively, using specimen IF-AM-0.73 as an example. The cracking stiffness is defined as the secant stiffness connecting the origin and the first cracking point on the load response curve, and the first cracking point is taken at the point where the load showed a sudden drop followed by an immediate recovery but at a reduced stiffness. It can be seen that the value of τ_m has a marked effect on the response curve in both stiffness and ultimate strength. As shown in Figure 4.11(b), up to a certain level of shear strength, in this case, 3.5 MPa, the ultimate load of the infilled frame increases almost linearly with an increase of the shear strength τ_m. Beyond 3.5 MPa, the failure of the infilled frame begins to be governed by compression failure of struts, therefore the increase in the mortar shear strength has no impact on increasing the ultimate load and it levels off.

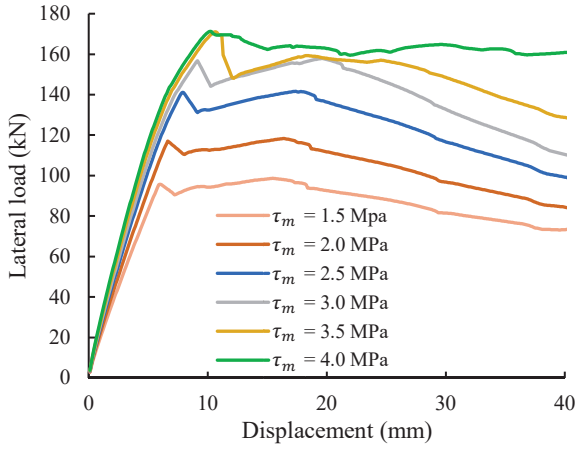

a) Lateral load vs. displacement curves

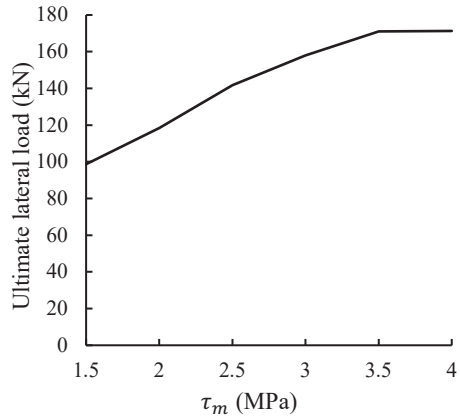

b) Ultimate lateral load of infilled frame

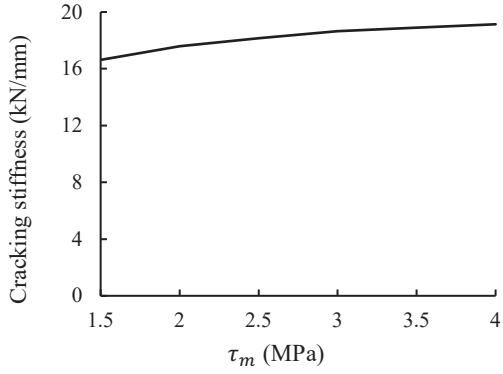

c) Cracking stiffness of infilled frame

Figure 4.11 Sensitivity analysis results of τ_m

Next, the effect of γ_m was studied. Its value was varied from 0.002 to 0.0035 mm/mm with a 0.0005 mm/mm increment while shear strength values (τ_m, τ_u, τ_r) were kept constant. The numerical lateral load versus displacement curves, and the ultimate lateral load and cracking stiffness of the infilled frame as affected by γ_m are shown in Figure 4.12. An increase in γ_m resulted in a decrease in the cracking stiffness of the infilled frame but its effect on the ultimate load is insignificant. Further shown in Figure 4.12(b), the ultimate load remained almost constant as γ_m increased.

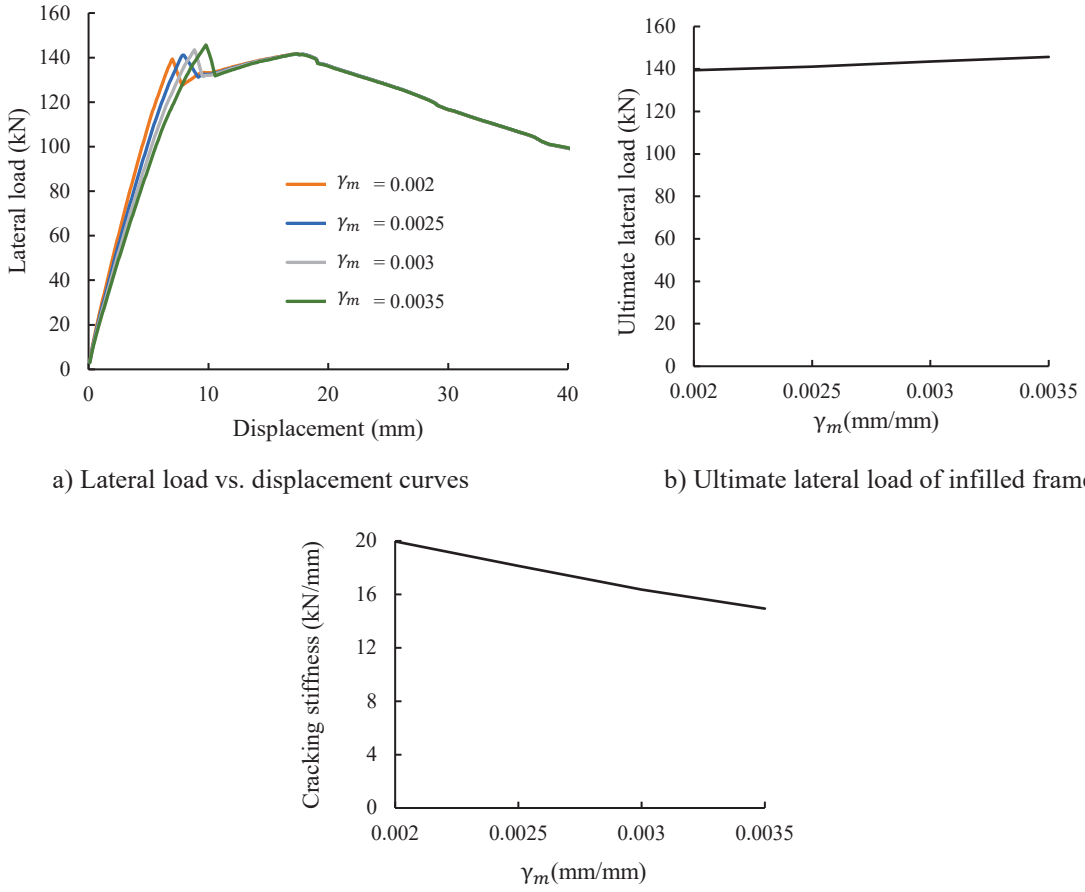

a) Lateral load vs. displacement curves

b) Ultimate lateral load of infilled frame

c) Cracking stiffness of infilled frame

Figure 4.12 Sensitivity analysis results of γ_m

4.6.2.2 Shear unit displacement, γ_u and γ_r

The results of sensitivity study of γ_u and γ_r are shown in Figure 4.13 where lateral load vs. displacement curves are plotted in each case. The figure showed that the effect of either parameter is most pronounced in influencing the post-ultimate behavior (falling branch) but is insignificant on the rising branch of the response curve in terms of the stiffness and ultimate load of the infilled system.

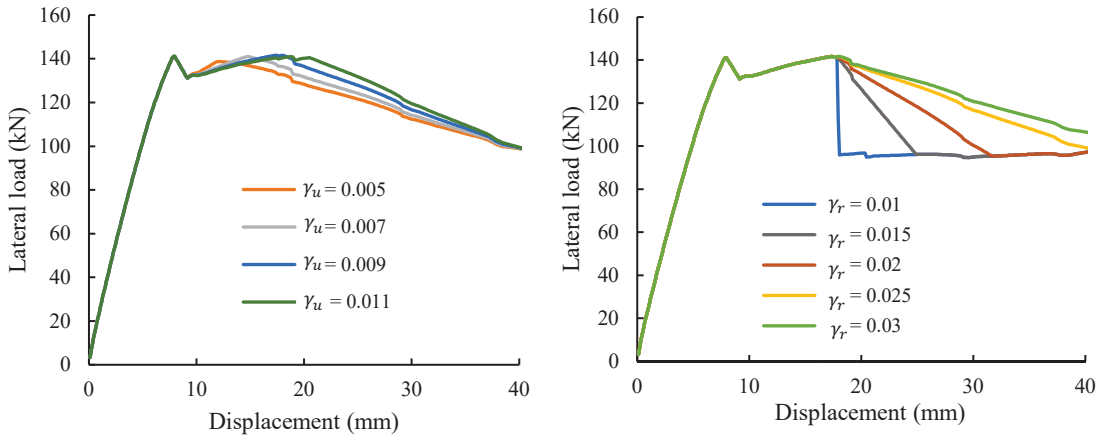

a) γ_u b) γ_r

Figure 4.13 Sensitivity analysis results of shear unit displacements, γ_u and γ_r

In summary, the sensitivity study of the shear material model shows that overall, the maximum shear strength is the most influential parameter in modeling the stiffness and strength of the infilled frame. The corresponding unit displacement affects the stiffness but does little to the strength of the infilled frame. The effect of unit displacements at the ultimate strength and the residual strength is most pronounced in the post-ultimate behavior but negligible in the rising branch of the load response.

4.6.3 Quasi-static cyclic analysis

For quasi-static cyclic loading conditions, two sets of struts with same material properties were implemented to the proposed model for reversal loading, as shown in Figure 4.4. The shear spring has symmetric constitutive behavior (Figure 4.7) and its relative displacement can be either positive or negative. The RC masonry infilled frame (Unit 2) tested by Crisafulli (1997) was constructed with ¾ scale solid concrete bricks with an infill aspect ratio of 0.8. This specimen was tested under 20 kN vertical load applied on columns while

a quasi-static cyclic lateral load was applied up to a maximum story drift of 2%. The specimen (S1C-2) tested by Cavaleri and Di Trapani (2014) was constructed with lightweight concrete masonry blocks with a frame aspect ratio of approximately 1.0. This specimen was tested under 200 kN constant vertical load applied on each column and a quasi-static cyclic lateral load up to a drift of 2.5%. The material properties for both specimens as reported in the literature were used in the analysis. The cyclic parameters representing cyclic strength and stiffness degradation, such as unloading and reloading stiffness and strength degradation, were needed to be defined in the cyclic analysis. For these parameters as in Concrete01, Concrete02, Steel02 and Pinching4 materials, the default values suggested in the OpenSees manual (Mazzoni et al., 2006) were directly used. No calibration of these parameters against the test results was performed. The model and experimental hysteretic curves are compared in Figure 4.14 for the Crisafulli's specimen. It is worth noting that the maximum shear strength of mortar joints in Crisafulli's study was also determined using triplet tests and was determined to be 0.41 MPa. Sliding shear failure along horizontal and stepped cracks, running through mortar joints was observed to initiate the failure of the specimen during the test. The early stage loading comparison presented in Figure 4.14(a) shows that the proposed model predicted the sliding failure at the third cycle and 72.4 kN load whereas the experimental values were observed to be 65 kN at the third cycle. This suggests that the proposed shear sliding material model is adequate in representing shear behavior of different material and geometric properties. The entire hyterestic response comparison presented in Figure 4.14(b) shows that the model is capable of simulating strength and stiffness and their degradation and pinching under cyclic loading reasonably well. As the system nonlinearity grew with increasing displacement, the discrepancy between the numerical and

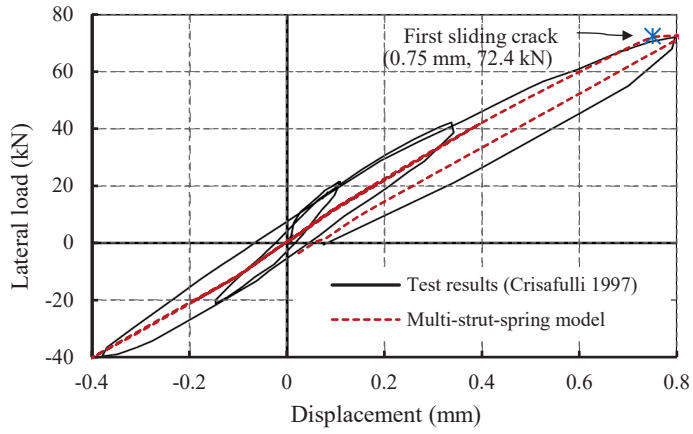

a) First sliding crack

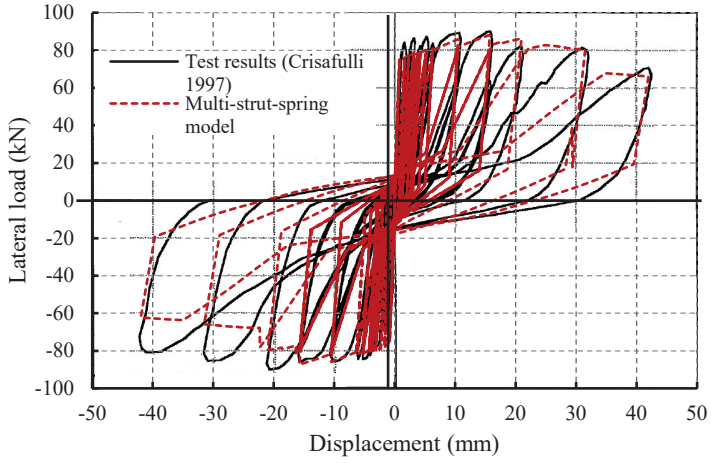

b) Overal response up to 2.0% story drift

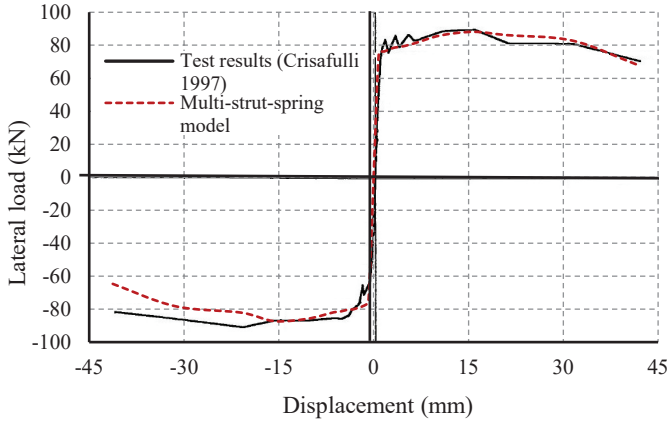

c) Backbone curve

Figure 4.14 Hysteretic response and backbone curve of specimen Unit 2 tested by Crisafulli (1997)

experimental curves seems to be more pronounced, indicating the stiffness degradation post-ultimate is still a challenge to capture. This can be further demonstrated in the backbone curve comparison shown in Figure 4.14(c) where the model performed better in predicting the initial behavior and ultimate strength than the post-ultimate behavior.

Figure 4.15 shows the model and experimental hysteretic responses are compared for the Cavaleri and Di Trapani's specimen. Again, the model performed reasonably well in capturing the overall strength and stiffness and their degradation under cyclic loading. The stiffness degradation at the large non-linearity region and post-ultimate behavior is less representative of the experimental results. As mentioned previously, the default hysteretic and cyclic parameters as suggested in the OpenSees manual were used without calibration to the specific experimental curves. A better fit in the hysteresis response might be achieved by calibrating those parameters against the experimental results. As the objective of the paper was to develop a functional model using the fundamental component material constitutive laws, it is believed that the results show that the proposed model as described is reasonably accurate for analysis of the infilled frames of varying properties under lateral load.

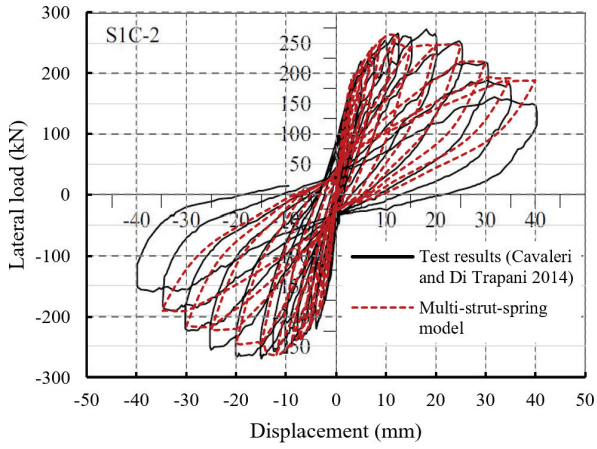

a) Hysteretic response

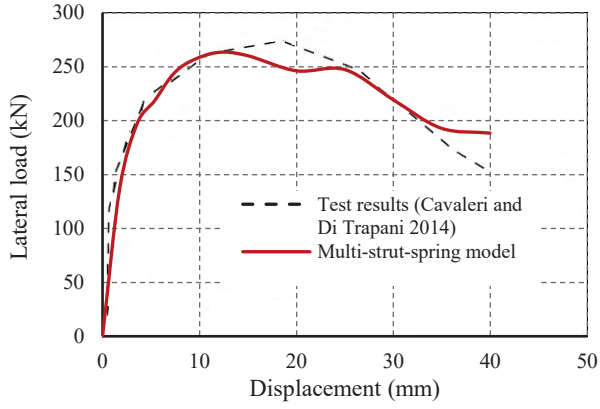

b) Backbone curve

Figure 4.15 Hysteretic response and backbone curve of specimen S1C-2 tested by Cavaleri and Di Trapani (2014)

4.7 Conclusion

This paper proposed a multi-strut-spring macro-model for masonry infilled frames under lateral in-plane monotonic and cyclic loading. The model accounted for compressive failure and shear failure of the infill as well as the infill effect on the bounding frames through the use of two sets of three struts each and a shear spring in a serial configuration.

The three struts were assigned with compressive stress-strain behavior taking into account the directional effect of masonry assemblage. Furthermore, the struts, connecting to the frame members at designated points, were to reflect more accurately the interaction between the infill and the bounding frame. The shear spring model was defined at a material level through experimental triplet tests. The sensitivity analysis of several critical input parameters of the model was further conducted and presented. The proposed model was verified using experimental results of masonry infilled RC frame specimens from literature as well as masonry infilled masonry frame specimens from this study.

The comparison between numerical results and experimental results showed that the proposed model can accurately simulate the lateral behavior of infilled frames of both bounding frame materials and in both static and cyclic analysis. The shear spring model in a serial configuration with struts can predict both sliding shear failure of mortar joints and compression failure of struts. Furthermore, the comparison between this model and the other two models proposed by others showed that given the same input parameters, the proposed model provided better simulation in terms of stiffness, strength, and post-ultimate behavior than the other two models. It should be pointed out that the proposed model focused on an accurate representation of the infill behavior and the infill effect on the bounding frame, but it does not represent the column base shear failure directly. It is recommended that more validation of the proposed model and further refinement of the shear material model are needed for infilled frames with other failure modes.

4.8 Acknowledgments

The authors wish to gratefully acknowledge the contribution of the financial assistance provided by the Natural Sciences and Engineering Research Council (NSERC) of Canada and the Canadian Concrete Masonry Producers Association for conducting this research.

CHAPTER 5 SEISMIC PERFORMANCE ASSESSMENT OF ALL-MASONRY INFILLED FRAMES

5.1 Abstract

This paper presents a systematic study on the seismic performance of a new type of masonry infilled frame systems, referred to as all-masonry infilled frames. All-masonry infilled frames consist of masonry infills built within reinforced masonry frames. The masonry boundary frame is constructed using custom-made boundary blocks allowing large opening area to facilitate concentrated steel reinforcement and the masonry infill is left ungrouted and unreinforced. A considerable amount of experimental research in literature showed that masonry infills can enhance the stiffness, strength, ductility, and energy dissipation of the frame structure. However, there is a lack of systematic studies to quantify the seismic performance of masonry infilled frames regardless of the boundary materials. The masonry infills are currently designed as non-structural elements and masonry infilled frame system is not a code-recognized seismic force resisting system. This study was conducted to investigate the seismic performance, in particular, fragility curves and seismic modification factors, of all-masonry infilled frames. A macro-model developed in this study was used in OpenSees to simulate the seismic response of eight archetype infilled systems with different design parameters. The models were studied under both nonlinear static pushover analysis and incremental dynamic analysis framework using 22 pairs of strong ground motion records. The performance of all-masonry infilled frame archetypes in terms of their fragility curves for immediate

occupancy (IO), life safety (LS), and collapse prevention (CP) performance limit states, and their seismic modification factors were presented and discussed in this paper. The results show that seismic performance and seismic modification factors of all-masonry infilled frames are in a similar range to the reinforced masonry shear walls with boundary elements.

5.2 Introduction

Masonry infilled frames are composed of a bounding frame and a masonry infill panel built within. The bounding frame is conventionally made of steel or reinforced concrete (RC). This study proposes a new type of masonry infilled frames, referred to as all-masonry infilled frames (Roosta & Liu, 2021). In essence, the bounding frame of this type of masonry infilled frame is also made of masonry materials. Its construction is similar to traditional masonry infilled RC frames except that the bounding frame is composed of masonry reinforced columns and tied in reinforced masonry beams. The advantage of this type of infilled frame is that the construction for the frame and infill can occur at the same time and thus eliminates the need to coordinate with concrete or steel trades as in the case of steel or RC frames. In this case, the masonry columns are constructed with custom-made C-shaped concrete blocks similar to the boundary elements in masonry shear walls, which allows for a large open area for concentrated reinforcing in the masonry columns. The masonry infill is constructed with standard concrete masonry blocks and is left ungrouted and unreinforced. The use of boundary elements has seen success in improving ductility and energy dissipation of masonry shear walls under cyclic loading (Abo El Ezz et al., 2015; Banting & El-Dakhakhni, 2014; Ezzeldin et al., 2016; Obaidat et al., 2018).

By incorporating the concept of boundary elements in the masonry frame, all-masonry infilled frame derives its lateral load capacity from both the frame flexural behaviour and the shear behaviour of the infill. Roosta and Liu (2021) experimentally studied the behaviour and capacity of the all-masonry infilled frames subjected to in-plane lateral loading. The results revealed that while showing similar lateral behaviour and capacity to masonry infilled RC frame counterparts, all-masonry infilled frames exhibited better ductility. Subsequently, Roosta and Liu (2022) developed a macro-model to aid the lateral behaviour analysis of all-masonry infilled frames. The model was shown to be capable of accurately simulating the behaviour and capacity of all-masonry infilled frames and masonry infilled RC frames under both static and cyclic loading. As a continuation of that study, this paper focuses on the seismic performance assessment of all-masonry infilled frames using the developed numerical model.

5.3 Seismic Analysis of Masonry Infilled Frames

The design practice has regarded the infills as non-structural elements. However, the available literature contains considerable research showing the significant effect of masonry infills on the behaviour of the frame structure subjected to lateral loading. In seismic regions, the accurate evaluation of system seismic characteristics such as stiffness, strength, ductility, and energy dissipation has a critical implication in the load distribution and design. Thus, simply ignoring the infill effect on the frame structure will lead to erroneous and unsafe design. Recent strong earthquakes (L'Aquila, Italy, 2009 (Braga et al., 2011); Maule, Chile, 2010 (Miranda et al., 2012); Muisne, Ecuador, 2016 (EEFIT, 2018)) showed that if not designed properly, the masonry infills can cause large damage

to the frame structures (Chiozzi & Miranda, 2017). While the existing research focused on the masonry infilled frames under static and cyclic loading, comprehensive studies on their seismic performance assessment are limited. A few available studies on the seismic analysis of masonry infilled frames adopted the approach of implementing the incremental dynamic analysis (IDA) technique through a numerical model in the seismic performance assessment. Due to its simplicity, the equivalent strut model of some form was often used as the model of choice in the seismic performance analysis of infilled frames where the masonry infill was replaced by one, or multiple struts in compression (Celarec & Dolšek, 2013; Di Trapani et al., 2020; Jeon et al., 2015). While the IDA technique necessitates the use of a simple model, the trade-off of a strut model has been that certain behaviour and failure characteristics of masonry infilled frames of specific geometric and material properties may not be captured. For instance, Celarec and Dolsek (2013) utilized a single strut model calibrated against iterative pushover analyses for masonry infilled RC frames and approximated column shear and flexural failures. They did not, however, consider shear sliding failure of infills. Jeon et al. (2015) assessed the seismic response and fragility of lightly reinforced concrete frames with masonry infills using a three-strut model for masonry infills. It showed that the effect of masonry infills on the seismic vulnerability of lightly reinforced RC frames depends on ground motion intensities and infill properties. Di Trapani et al. (2020) studied the seismic performance of clay brick infills based on the IDA technique where the infill was modeled using an equivalent strut model with an eccentric positioning to account for the infill-frame interaction. These studies showed that overall, the presence of masonry infills mitigates the seismic fragility of the surrounding frame and decreases the probability of exceeding a specific performance level. However, one limitation observed in these studies is that none of the numerical models they adopted

predict the shear failure in the masonry infills. For those infills that shear sliding is the main governing failure mode, the strut model is not adequate.

5.4 Summary of the Proposed Macro-Model

The proposed macro-model is a multi-strut-spring model. The details of the model development and its implementation in OpenSees can be found in Roosta and Liu (2022). For the completeness of this paper and ease of reference, the following section provides a brief summary of the model and its validation against experimental results. This multi-strut-spring model consists of diagonal and off-diagonal strut elements to represent the interaction between infill and the bounding frame, and a shear spring in the middle of the infill panel to simulate the sliding shear behaviour of mortar joints, as shown in Figure 5.1. For each direction of loading, six struts were connected at the center point of the infill panel, and they were compression-only truss elements pinned to beam-column joints and at the middle of contact lengths along either columns or beam. The total strut width was assigned based on the strut width equation developed by Stafford Smith and Carter (1969) and 50% of which was assigned to the center diagonal elements, and 25% to the off-center diagonal ones. The purpose of shear spring was to model shear behavior and shear failure along mortar joints. A nonlinear shear constitutive model was developed and calibrated with experimental results, and it included the initial elastic phase up to the maximum mortar bond strength, strength hardening phase, and frictional resistance of sliding surfaces of bed joints.

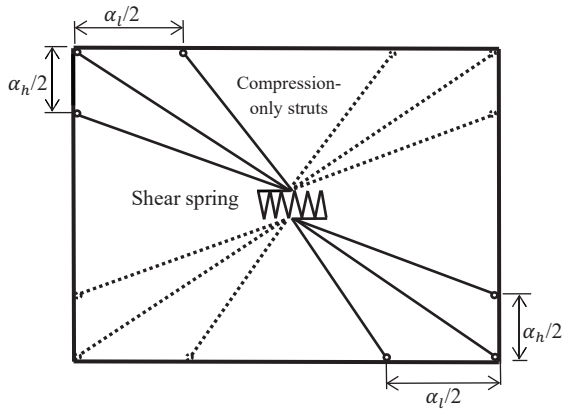

Figure 5.1 The multi-strut-spring model proposed by Roosta and Liu (2022)

This macro model was examined under pushover and cyclic analyses for both masonry infilled RC and all-masonry infilled frames against experimental results of specimens reported in the literature. The results showed that the model is capable of capturing failure modes of infilled frames including compression and sliding shear failure of infill, and also frame failure. One example shown in the previous paper (Roosta & Liu, 2022) is reproduced in Figure 5.2 for reference.

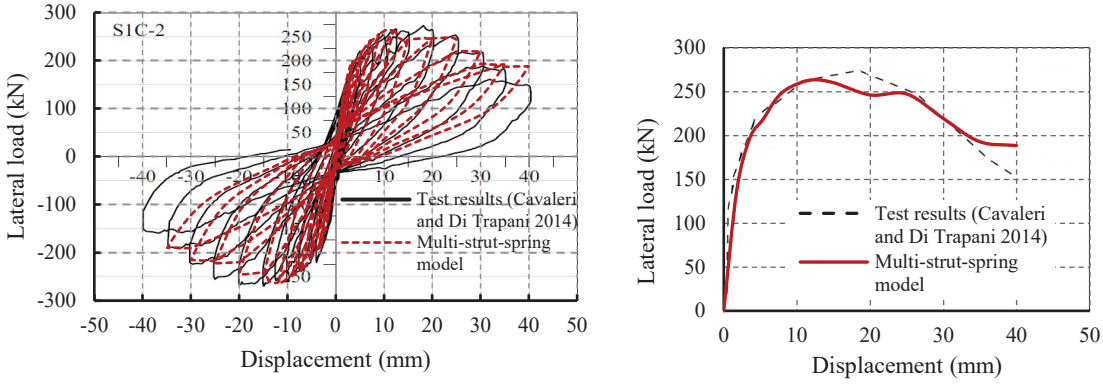

a) Hysteretic response b) Backbone curve

Figure 5.2 Hysteretic response (Roosta & Liu, 2022) and backbone curve of specimen S1C-2 tested by Cavaleri and Di Trapani (2014)

5.5 All-Masonry Infilled Frame Archetypes

In developing the all-masonry infilled frame archetypes for the seismic analysis, the parameters considered included the infill aspect ratio, the infill grouting, frame column dimension and reinforcing amount, and the presence of axial load in frame columns. The selection of dimension, reinforcement, and infill material property of the standard archetype used reference to archetype S1 in NIST (2010), a report on seismic performance assessment of reinforced masonry (RM) walls. Archetype S1 is designed and detailed as a "special reinforced masonry shear wall" in accordance with TMS 402/602. Ezzeldin et al (2016) used a similar archetype (S1-B) with the same properties as S1 except with the boundary elements implemented on the RM walls at ends. To facilitate comparison between all-masonry infilled frames and RM walls mentioned above, the standard archetype (S1-AM) was created with similar properties as S1 and S1-B. The details of all archetypes considered in this study are listed in Table 5.1 and further illustrated in Figure 5.3.

Unlike the RM walls where the vertical reinforcement was employed along the entire length of the wall, the infilled frame archetypes were designed so that the vertical reinforcement was concentrated in the frame columns and the masonry infills were left unreinforced. This was to comply with the typical construction practice of masonry infills. In all these archetypes, the infill thickness was assumed to be 200 mm as for standard concrete masonry units and the infill is either fully grouted (Figure 5.3a) or ungrouted (Figure 5.3b). The first seven archetypes were one-storey infilled frames and the eighth one (AM-2S) was a two-storey infilled frame (Figure 5.3c). The axial load was applied to frame columns with the magnitude at either 2% or 1% of the product of A_g and f'_m, where

A_g is the gross cross-sectional area of archetypes and f'_m is the compressive strength of masonry.

To evaluate the seismic performance of these archetypes, both non-linear static pushover analysis and incremental dynamic analysis (IDA) were performed. The following section describes details of the IDA analysis on these archetypes.

Table 5.1 Material properties, dimensions, and reinforcement details of all-masonry infilled frames

Archetype	f'_m (MPa)	Grouted (yes/no)	Infill height (m)	Infill length (m)	Size (mm) and reinf.		Axial load (kN) ($\%A_g f'_m$)
					Column	Beam	
S1-AM	10.34	yes	3.25	6.51	400x400 4-15M	400x400 4-15M	330 (2%)
AM-UG	10.34	no	3.25	6.51	400x400 4-15M	400x400 4-15M	201 (2%)
AM-LA	10.34	yes	3.25	6.51	400x400 4-15M	400x400 4-15M	165 (1%)
AM-Square	10.34	yes	3.25	3.25	400x400 4-15M	400x400 4-15M	200 (2%)
AM-Slender	10.34	yes	4.87	3.25	400x400 4-15M	400x400 4-15M	200 (2%)
AM-600	10.34	yes	3.25	6.51	600x600 4-20M	600x600 4-20M	418 (2%)
AM-600-UG	10.34	no	3.25	6.51	600x600 4-20M	600x600 4-20M	284 (2%)
AM-2S	10.34	yes	3.25	6.51	400x400 4-15M	400x400 4-15M	330 (2%)

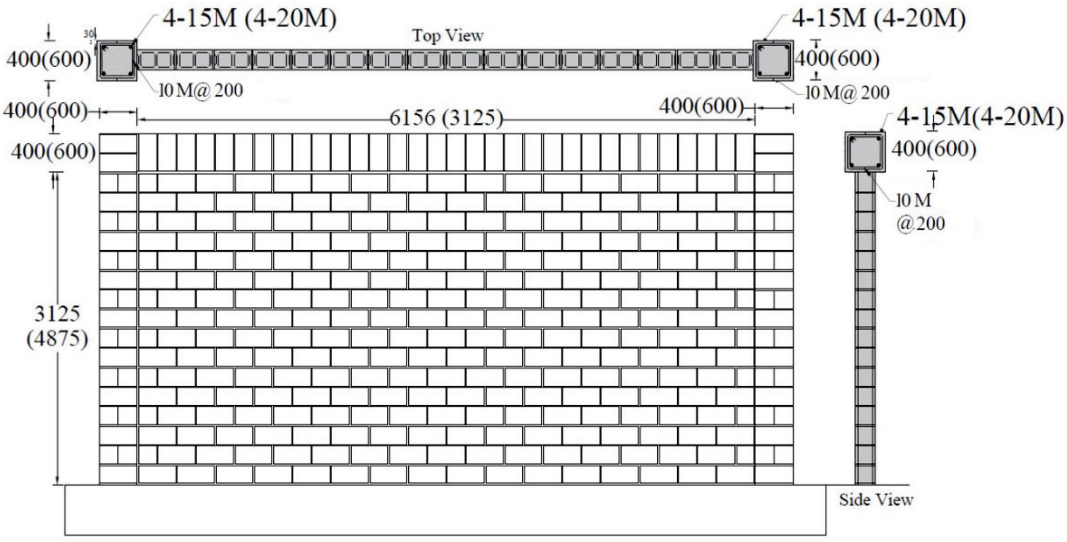

a) S1-AM, AM-LA, AM-Square, AM-Slender, AM-600

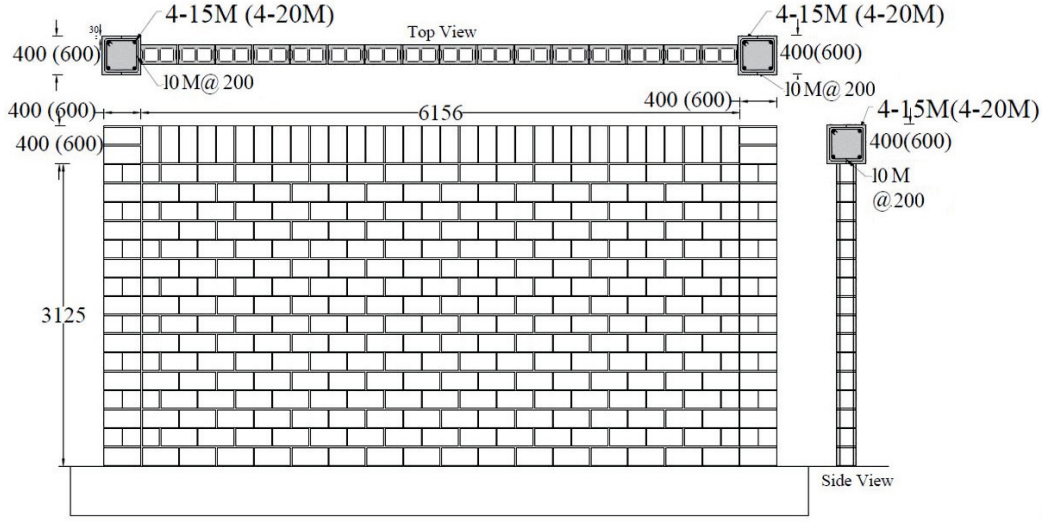

b) AM-UG, AM-600-UG

Figure 5.3 Geometry and reinforcement details of archetypes (unit: mm) - cont'd

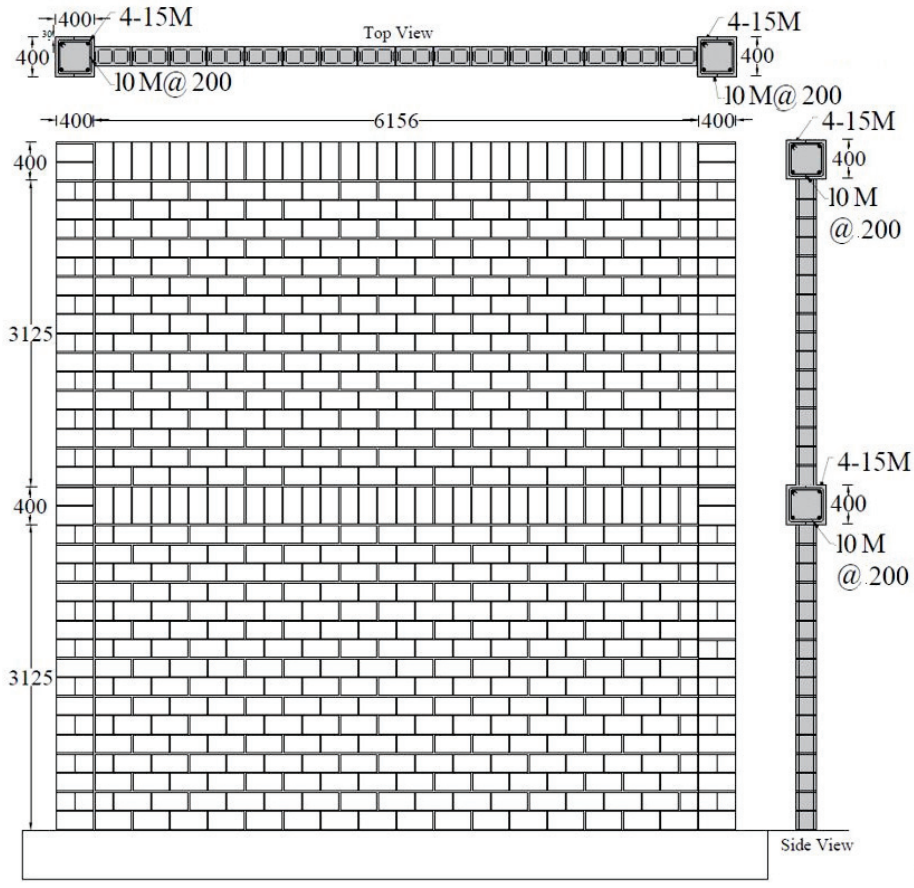

c) AM-2S

Figure 5.3 Geometry and reinforcement details of archetypes (unit: mm)

5.6 Incremental Dynamic Analysis (IDA)

Incremental Dynamic Analysis (IDA) is a suite of nonlinear time history analyses performed on a structural model using a group of seismic ground acceleration records, each scaled to several intensity levels to predict seismic demand and capacity of the structure. The framework of IDA as presented in the study by Vamvatsikos and Cornell (2002b) was adopted to conduct the IDA analysis of the archetypes.

5.6.1 Ground motion records

The seismic ground acceleration records used in this study consist of a set of 22 far-field ground motion record pairs from the Pacific Earthquake Engineering Research Center (PEER) Next-Generation Attenuation (NGA) West2 database (PEER, 2022). They are summarized in Table 5.2.

Table 5.2 Summary of the 22 far-field record sets

ID No.	Earthquake			Recording station	
	M	Year	Name	Name	Owner
1	6.7	1994	Northridge	Beverly Hills-Mulhol	USC
2	6.7	1994	Northridge	Canyon Country-WLC	USC
3	7.1	1999	Duzce, Turkey	Bolu	ERD
4	7.1	1999	Hector Mine	Hector	SCSN
5	6.5	1979	Imperial Valley	Delta	UNAMUCSD
6	6.5	1979	Imperial Valley	El Centro Array #11	USGS
7	6.9	1995	Kobe, Japan	Nishi-Akashi	CUE
8	6.9	1995	Kobe, Japan	Shin-Osaka	CUE
9	7.5	1999	Kocaeli, Turkey	Duzce	ERD
10	7.5	1999	Kocaeli, Turkey	Arcelik	KOERI
11	7.3	1992	Landers	Yermo Fire Station	CDMG
12	7.3	1992	Landers	Coolwater	SCE
13	6.9	1989	Loma Prieta	Capitola	CDMG
14	6.9	1989	Loma Prieta	Gilroy Array #3	CDMG
15	7.4	1990	Manjil, Iran	Abbar	BHRC
16	6.5	1987	Superstition Hills	El Centro Imp. Co.	CDMG
17	6.5	1987	Superstition Hills	Poe Road (temp)	USGS
18	7.0	1992	Cape Mendocino	Rio Dell Overpass	CDMG
19	7.6	1999	Chi-Chi, Taiwan	CHY101	CWB
20	7.6	1999	Chi-Chi, Taiwan	TCU045	CWB
21	6.6	1971	San Fernando	LA – Hollywood Stor	CDMG
22	6.5	1976	Friuli, Italy	Tolmezzo	--

These records were obtained at sites located greater than or equal to 10 km from fault rupture in all large-magnitude events. This set was also used by the FEMA P695 (2009) in the seismic performance assessment. Each of the 22 earthquakes shown in Table 5.2 has

two horizontal component records, totaling 44 individual ground motion records. Response spectra of all 44 ground motions and their mean spectrum are illustrated in Figure 5.4.

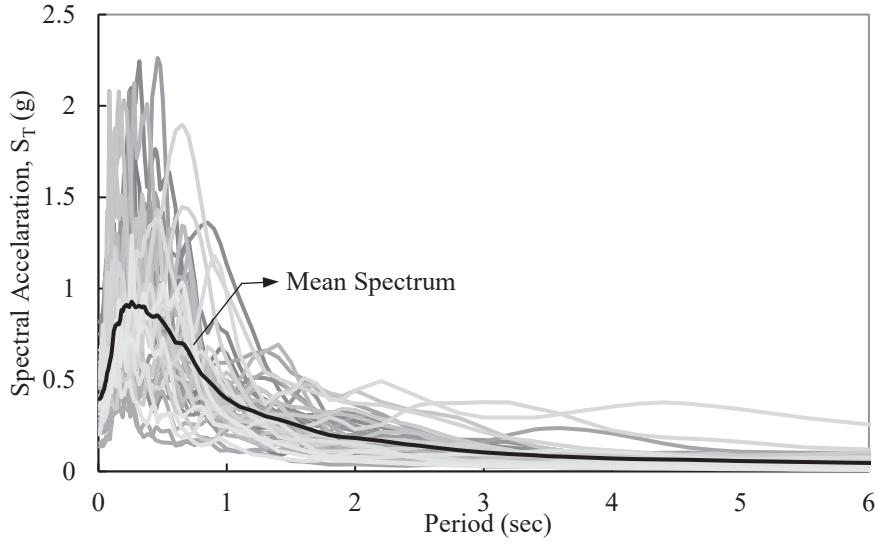

Figure 5.4 Response spectra of the 44 records and their mean response spectra

To eliminate the effect of variabilities between records due to differences in earthquake magnitudes and geographical characteristics, each ground motion record used in the IDA analysis was normalized by its respective geometric peak ground velocity (NIST GCR 10-917-8, 2010). Geometric peak ground velocity is the geometric mean of two horizontal components of the records and is computed as PGV_{PEER} in the PEER NGA database. The two horizontal time history components of ith ground motion are then normalized using the following equations.

$$NTH_{1,i} = NM_i * TH_{1,i} \quad (5.1)$$

$$NTH_{2,i} = NM_i * TH_{2,i} \quad (5.2)$$

$$NM_i = Median(\mathrm{PGV}_{PEER,i})/\mathrm{PGV}_{PEER,i} \quad (5.3)$$

where $TH_{1,i}$ and $TH_{2,i}$ are the original time history records of ith ground motion from PEER NGA database for horizontal components 1 and 2; $NTH_{1,i}$ and $NTH_{2,i}$ are the normalized time history records of the ith ground motion for horizontal components (1 and 2); and NM_i is the normalized factor used for both horizontal components of the ith record where $\mathrm{PGV}_{PEER,i}$ is the $\mathrm{PGV}_{\mathrm{PEER}}$ of the ith record, taken from the PEER NGA database, and $Median(\mathrm{PGV}_{PEER,i})$ is the median of $\mathrm{PGV}_{\mathrm{PEER}}$ values of the 22 pairs which is equal to 37.2 cm/s. Table 5.3 shows $\mathrm{PGV}_{\mathrm{PEER}}$, NM_i, and maximum values of peak ground acceleration, $\mathrm{PGA}_{\mathrm{max}}$, and peak ground velocity, $\mathrm{PGV}_{\mathrm{max}}$, as recorded and after normalization for each record pair. The normalization of the records by using their $\mathrm{PGV}_{\mathrm{PEER}}$ has decreased the extent of spread of $\mathrm{PGV}_{\mathrm{max}}$ and $\mathrm{PGA}_{\mathrm{max}}$ values of the record set, without noticeably impacting their average values.

5.6.2 Performing IDA

Using the normalized ground motion records, the IDA was conducted on all-masonry infilled frame archetypes in OpenSees. As described earlier, the multi-strut-spring model depicted in Figure 5.1 was used in the modeling of the archetypes. To generate the IDA curves of a structure, a damage measure (DM) for the structure and an intensity measure (IM) for the ground motion records need to be defined. In this study, the maximum inter-

Table 5.3 As-recorded and normalized parameters of the record set

ID No.	As recorded		PGV_{PEER} (cm/s)	Normalization factors, NM_i	Normalized records	
	Max of PGA_{max} (g)	Max of PGV_{max} (cm/s)			Max of PGA_{max} (g)	Max of PGV_{max} (cm/s)
1	0.52	63	57.2	0.65	0.34	41
2	0.48	45	44.8	0.83	0.40	38
3	0.82	62	59.2	0.63	0.52	39
4	0.34	42	34.1	1.09	0.37	46
5	0.35	33	28.4	1.31	0.46	43
6	0.38	42	36.7	1.01	0.39	43
7	0.51	37	26.0	1.03	0.53	39
8	0.24	38	33.9	1.10	0.26	42
9	0.36	59	54.1	0.69	0.25	41
10	0.22	40	27.4	1.36	0.30	54
11	0.24	52	37.7	0.99	0.24	51
12	0.42	42	32.4	1.15	0.48	49
13	0.53	35	34.2	1.09	0.58	38
14	0.56	45	42.3	0.88	0.49	39
15	0.51	54	47.3	0.79	0.40	43
16	0.36	46	42.8	0.87	0.31	40
17	0.45	36	31.7	1.17	0.53	42
18	0.55	44	45.4	0.82	0.45	36
19	0.44	115	90.7	0.41	0.18	47
20	0.51	39	38.8	0.96	0.49	38
21	0.21	19	17.8	2.10	0.44	40
22	0.35	31	25.9	1.44	0.50	44

storey drift ratio, θ_{max}, was selected as the DM, and the 5%-damped first mode spectral acceleration, S_a (T_1,5%), was selected as the IM. This pairing of DM and IM was used in some existing seismic IDA studies (FEMA, 2000; Vamvatsikos & Cornell, 2002b) where the DM as defined was shown to adequately represent the global dynamic instability of the structure, and the IM as defined minimized dispersion of analysis results. For conducting the IDA, each of the 44 ground motion records was scaled systematically and applied to the archetype such that the entire range of structural response from elastic behaviour, to yielding and finally, global dynamic instability were covered (Vamvatsikos & Cornell, 2002b). The scaling was performed such that the corresponding spectral acceleration of the first mode period (T_1) of the archetype was divided into 20 levels. For

each scaling level of each ground motion record, a time history dynamic analysis was conducted to obtain the maximum inter-storey drift, θ_{max}, vs. spectral acceleration S_a (T_1,5%) response of the archetype. Hence, the final IDA curve of the IM-DM plane has twenty discrete response points for each ground motion record.

One example of the IDA curves is shown in Figure 5.5 for the archetype S1-AM with the ground motion of the Northridge earthquake recorded at Beverly Hills station (first row of Table 5.2). The two curves represent two horizontal components of the ground motion. As can be seen, both curves exhibited an elastic phase up to the yielding point (S_a^{yeild}(T_1,5%)≈0.8g, θ_{max}^{yeild} ≈0.37%). After the yielding point, the curves showed a zig-zag pattern including softening and hardening regions. The hardening regions indicate that increasing the intensity of a record, in some cases, causes a lower drift response in a structure as damages under earlier cycles can act as a fuse to relieve the subsequent, stronger cycles (Vamvatsikos & Cornell, 2002a). For the Horizontal-2 record of the earthquake, dynamic instability of the archetype was observed at approximately S_a (T_1,5%) =2.0g while under the Horizontal-1 record, the archetype sustained a maximum drift of 2.47% at a higher intensity level of 3.0g. At the maximum value of S_a (T_1,5%) = 3.2g, the IDA curve of Horizontal-1 record shows a flatline as the dynamic analysis failed to converge, signaling the global dynamic instability of the structure.

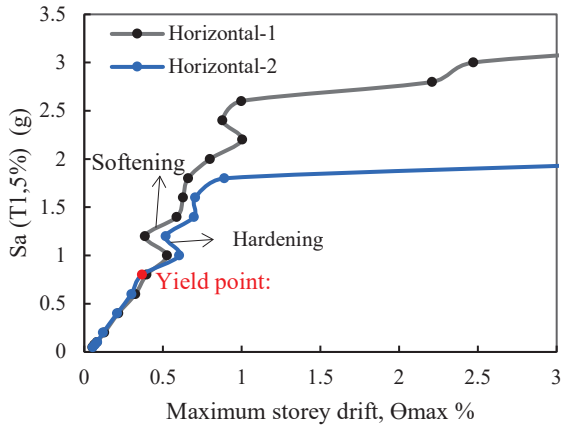

Figure 5.5 IDA curves of S1-AM archetype under horizontal records of Northridge earthquake (Beverly Hills station)

The same analysis was performed on archetype S1-AM for all ground motions. All generated IDA curves for the 44 records are shown in Figure 5.6(a). It can be seen that a similar trend of IDA response as described above was observed for other ground motions. The statistical properties of DM values are further illustrated in Figure 5.6(b) where the median, 16%, and 84% fractiles of DM corresponding to each value of IM are plotted for archetype S1-AM. The median IDA curve is often used as a probabilistic measure to show the central tendency of the dynamic response of a structure and 16% and 84% fractiles can be viewed as measures of dispersion of DM values. For example, it can be seen that at S_a (T_1,5%) =2.4g, 16% of records cause maximum inter-storey drifts equal and less than 1.1%, 50% of records produce maximum inter-storey drifts equal and less than 2.3%, and at least 84% of records caused dynamic instability for the S1-AM archetype.

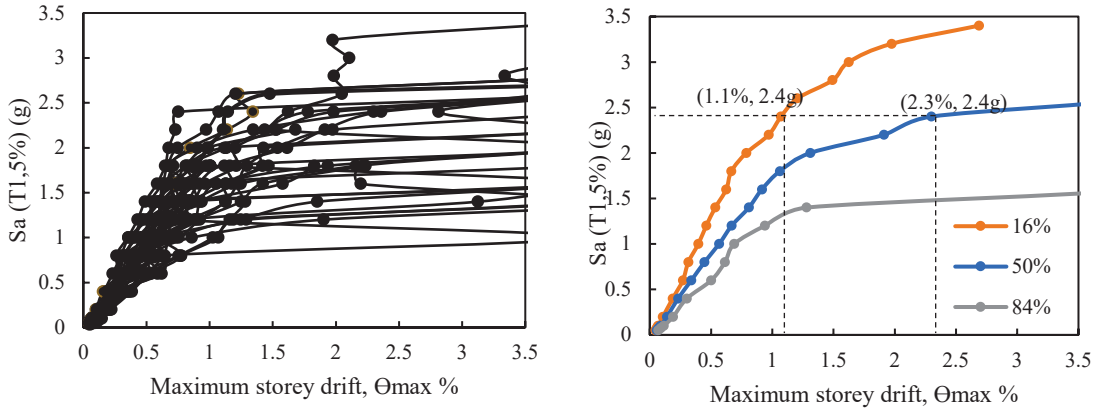

a) Forty-four IDA curves b) The 16%, 50%, and 84% fractile curves

Figure 5.6 IDA study of S1-AM archetype

Next, the same IDA analysis procedure was performed for all archetypes. The resulting median IDA curves of all archetypes are shown in Figure 5.7 as grouped to demonstrate the effect of the design parameters. The effect of varying axial load can be observed in Figure 5.7(a) where archetypes S1-AM and AM-LA are compared. It shows that when all other parameters kept the same, a reduction in the axial load (50% in archetype AM-LA in this case) had insignificant effect on the elastic phase of the response but resulted in a lower ultimate dynamic strength. At about S_a (T_1,5%) =2.0g, AM-LA reached its maximum inter-storey drift of 1.5% while S1-AM attained a maximum inter-storey drift of 2.3% at S_a (T_1,5%) =2.4g. Figure 5.7(b) shows the median IDA curves of archetypes with aspect ratios of 0.5 (S1-AM), 1.0 (AM-Square), and 1.5 (AM-Slender). At the initial elastic stage, the curves show that the slender infill had much lower initial stiffness when compared with the squat and square infills while the behaviour of the latter two was comparable. It suggests that as the infill becomes slender, flexural deformation becomes an increasingly governing mechanism in the system deformation which results

in a greater deformation at a given seismic IM. The square and squat infills, on the other hand, may still rely mainly on the diagonal strut mechanism and thus remained relatively similar in behaviour. When the ultimate dynamic strength is concerned, the slender infill reached dynamic instability at around S_a (T_1,5%) =1.0g and the square one at around 2.0g. The squat one attained the highest IM at 2.4g. The effects of grouting and frame cross-section are shown collectively in Figure 5.7(c). The effect of grouting can be observed by comparing S1-AM and AM-UG, and AM-600 and AM-600-UG. It shows that grouted infills attained markedly greater initial stiffness and ultimate dynamic strength in both cases. When it comes to the frame cross-section, the comparison of S1-AM and AM-600 shows that using a larger frame section with more reinforcement had a negligible impact on the initial elastic response but resulted in greater ultimate dynamic strength, i.e., greater maximum storey drift at higher magnitude of seismic IM. Figure 5.7(d) shows the difference between the dynamic behaviour of a two-storey infilled frame (AM-2S) and a single-storey one (S1-AM). When all other parameters are kept the same, the two-storey infilled frame system had much lower initial stiffness (60% lower) and began to lose dynamic stability at S_a (T_1,5%) less than 0.8g, a 67% decrease from 2.4g observed for S1-AM.

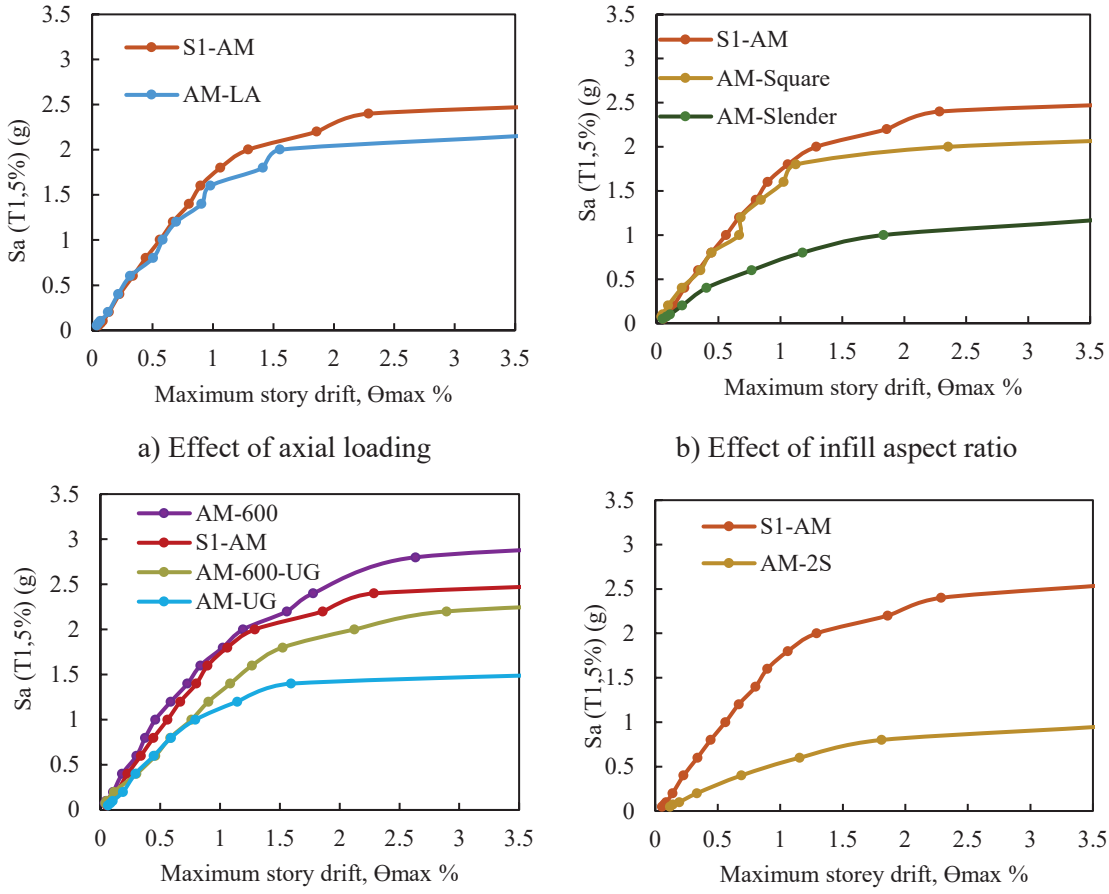

Figure 5.7 Median IDA curves of all-masonry infilled frame archetypes

5.7 Structural Performance Limit States and Pushover Analysis

In this study, three performance limit states including Collapse Prevention (CP), Immediate Occupancy (IO) and Life Safety (LS) limit states were considered. As the most critical limit state, Collapse Prevention (CP) limit state defines the collapse point of the structure. It can be identified as the point where the IDA curve flattens and approaches a zero slope, indicating the global dynamic instability of the structure (Vamvatsikos & Cornell, 2002a). As for IO and LS limit states, there are no widely accepted definitions

specifically for masonry infilled frames. The following definitions are specified in ATC-40 (1996) for reinforced concrete structures. At IO limit state, very limited cracking and structural damage has occurred, and at LS limit state, hinges have formed at the base of the building with spalling at beam-column joints along with shear and flexural cracking, however, lateral capacity of the structure is still maintained. ATC 40 also suggests that quantifying the limit states for specific structures be based on engineering judgment and observed damages in laboratory tests. In this study, the definitions of IO and LS limit states suggested by Jeon et al. (2015) were adopted where the IO and LS limit states are defined, respectively, as the yielding point and maximum lateral load point derived from pushover response curves.

Nonlinear static pushover analysis was then conducted for each archetype subjected to a point lateral load applied at the roof level. A typical pushover curve using S1-AM archetype as an example is shown in Figure 5.8. While the maximum lateral load, V_{max}, is easily identified on the curve, the yielding point is determined using the idealized curve method suggested by ASCE41-17 (2017b) The idealized curve is constructed such that the areas under the actual and idealized curve up to the V_{max} point are equal. The point where the first line segment of the idealized curve intercepts the actual curve is considered at a load equal to 60% of the yielding force. The yielding point can then be determined. The drift values at the yielding point (δ_y) and at the maximum lateral load point (δ_{max}) represent the IO and LS limit states, respectively. The same pushover analysis was performed for all archetypes and the inter-storey drifts corresponding to IO and LS limit states for all are summarized in Table 5.4 along with the CP limit state. The CP limit state was identified as the storey drift corresponding to the dynamic instability of IDA curves (δ_D).

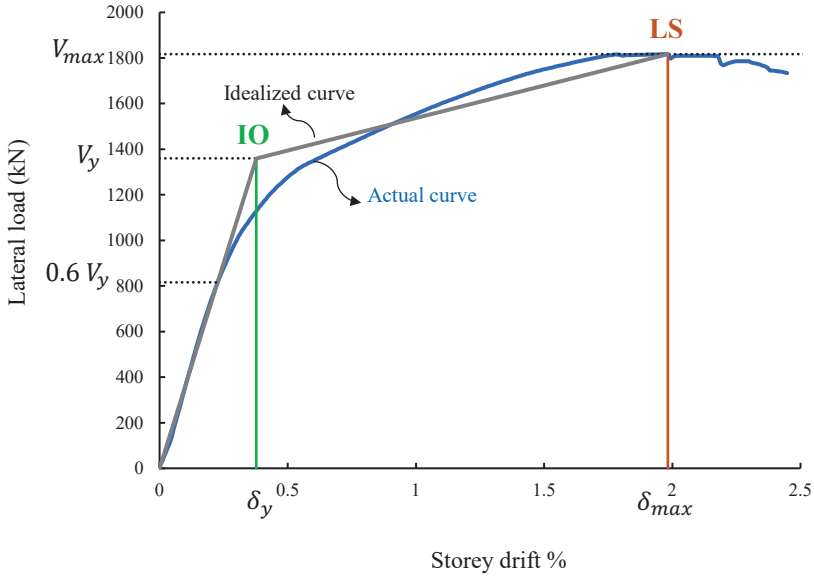

Figure 5.8 Definition of IO and LS limit states for all archetypes

Table 5.4 Storey drifts (%) corresponding to different limit states

Archetype	Pushover results		IDA results
	IO (δ_y %)	LS (δ_{max} %)	CP (δ_D %)
S1-AM	0.38	1.98	2.86
AM-UG	0.33	1.70	2.62
AM-LA	0.42	1.24	2.67
AM-Square	0.31	1.28	2.07
AM-Slender	0.35	2.14	3.74
AM-600	0.42	1.30	2.30
AM-600-UG	0.42	1.36	2.89
AM-2S	0.41	3.08	2.56

The pushover curves of all archetypes are shown in Figure 5.9 in groups based on the design parameters. Overall, the effect of design parameters on the pushover behaviour trend is similar to that discussed under IDA curves. As shown in Figure 5.9(a), the impact of varying axial load on the archetype is more pronounced on the ultimate lateral strength

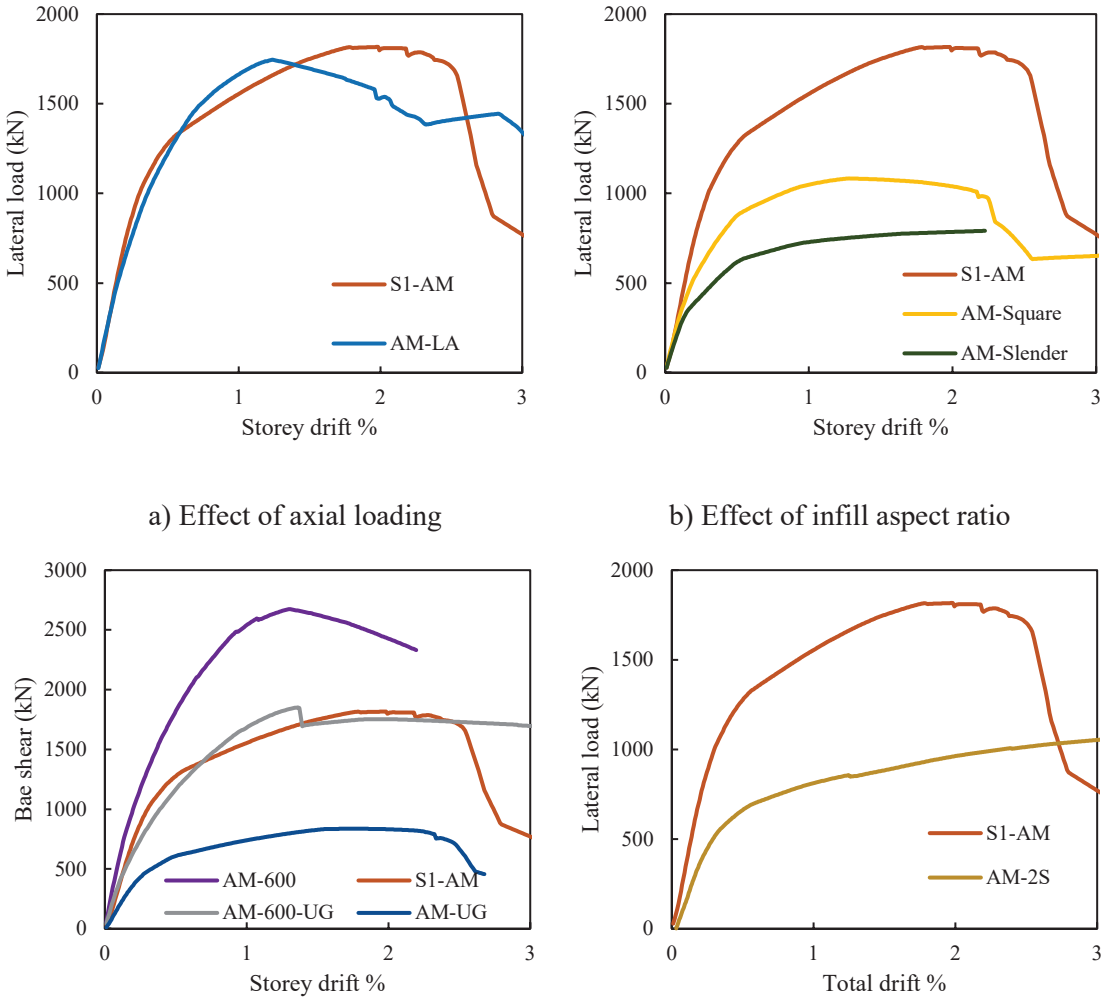

a) Effect of axial loading

b) Effect of infill aspect ratio

c) Effect of grouting and frame cross-section

d) Effect of number of stories

Figure 5.9 Pushover curves of all-masonry infilled frame archetypes

and the corresponding displacement where a lower axial load (AM-LA) resulted in a decrease in the lateral strength and reached at a lower level of story drift. Figure 5.9 (b) shows that as the infill becomes increasingly squat, both the stiffness and lateral strength increases, indicating for infilled frames, the strut action is a more effective load transferring mechanism as opposed to flexural behaviour. Figure 5.9(c) demonstrates the effect of infill grouting and frame cross-section. It can be seen that for a given frame cross-

section, grouting infill resulted in markedly greater initial stiffness (67%) and ultimate strength (80%) when compared with the ungrouted infill. For a given grouting situation, increasing the frame cross-section dimension from 400x400 mm to 600x600 mm resulted in an increase in the initial stiffness of 66% and 41%, and ultimate strength of 120% and 47% for ungrouted and grouted infill respectively. Figure 5.9 (d) shows that the lateral strength of AM-2S is about half the strength of S1-AM.

5.8 Fragility Curves

Fragility curves are used to show the probability of a structure exceeding a certain limit state or performance level under a given intensity measure (IM) of ground motion records. Based on the results of IDA curves for the 44 ground motion records, the percentage of records exceeding a limit state for the specific IM level is shown as a fragility curve. Figure 5.10 shows the fragility curves of archetype S1-AM in terms of probability of exceedance versus S_a (T_1,5%) for IO, LS, and CP performance limit states. It can be seen that at ground motion intensity S_a (T_1,5%) equal to 1.4g, 100% of earthquakes caused S1-AM to exceed the IO limit state. When comparing LS and CP limit states, it shows that for a given ground motion intensity measure, the probability of exceeding the LS limit state is about 10% higher than that of the CP limit state for this archetype. The median collapse spectral acceleration, $\widehat{S}_{CT}$, is defined as the first mode spectral acceleration in which 50% of the records caused collapse of the archetype (FEMA P695, 2009). For S1-AM, $\widehat{S}_{CT}$ is equal to 2.4g in which 50% of the records caused the archetype to exceed the CP limit state. It is noted that the standard RM shear wall archetype (S1) studied in NIST (NIST GCR 10-917-8, 2010) had a $\widehat{S}_{CT}$ of 0.78g, and the RM archetype with boundary element (S1-B)

studied by Ezzeldin et al (2016) had a $\widehat{S}_{CT}$ of 3.17g. The standard all-masonry infilled frame S1-AM constructed with similar geometric and material properties as the other two archetypes had a $\widehat{S}_{CT}$ in between.

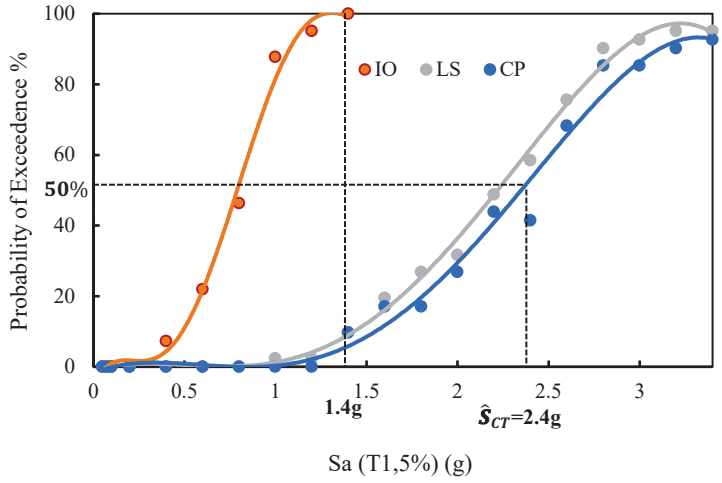

Figure 5.10 Fragility curves of archetype S1-AM for different performance levels

Fragility curves for the CP limit state for all archetypes are depicted in Figure 5.11. For all archetypes considered, the probability of exceeding the CP limit state under ground motions with IM up to 0.6g is nearly 0%. The median collapse spectral acceleration, $\widehat{S}_{CT}$, along with the first mode fundamental period, T_1, for all archetypes are summarized in Table 5.5. The highest value of $\widehat{S}_{CT}$, 2.5g, was observed in AM-600 archetype with a fundamental period of 0.16 sec., and the lowest $\hat{S}_{CT}$ of 1.0g was recorded for AM-2S with a fundamental period of 0.34 sec. The effects of design parameters as discussed in pushover analysis and incremental dynamic analysis sections are similarly reflected in the

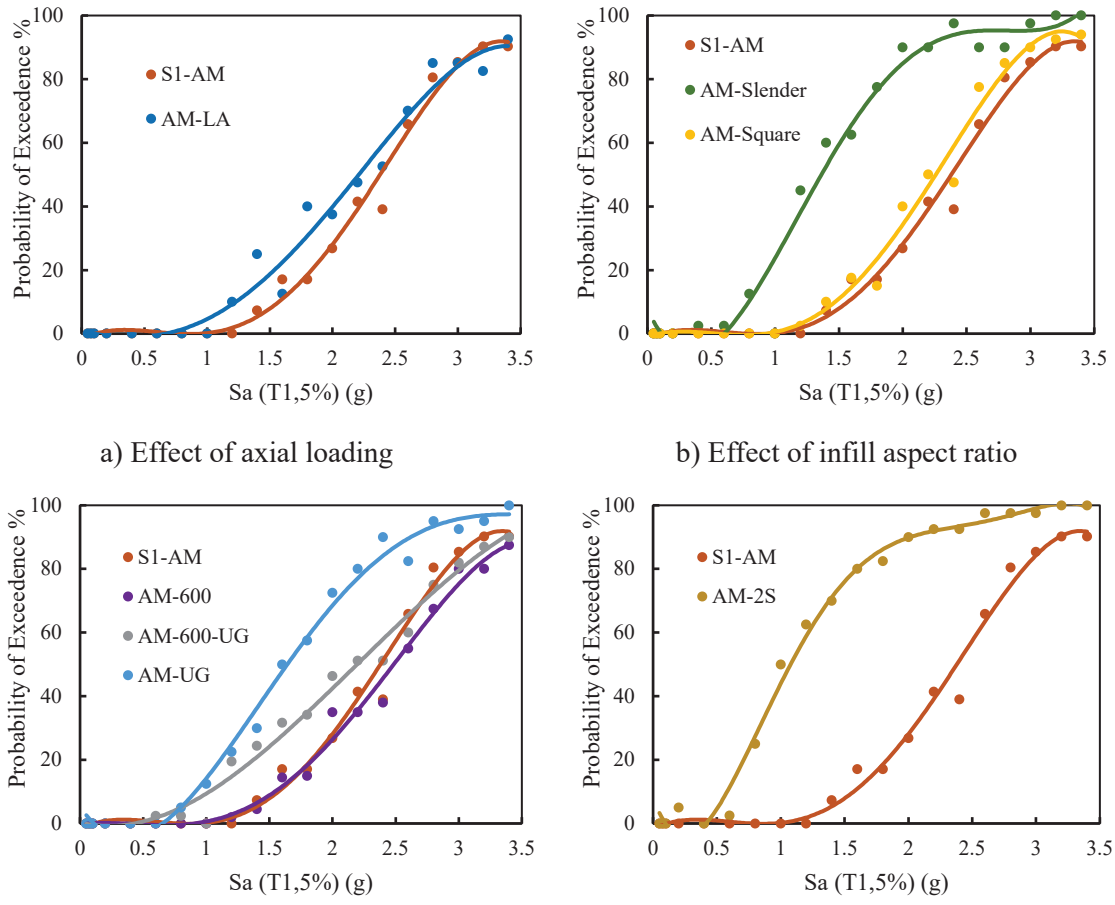

a) Effect of axial loading

b) Effect of infill aspect ratio

c) Effect of grouting and frame cross-section

d) Effect of number of stories

Figure 5.11 Fragility curves of all archetypes for CP limit states

Table 5.5 First mode period and median collapse spectral acceleration of all archetypes

Archetype	T (sec)	$\hat{S}_{CT}$ (g)
S1-AM	0.16	2.4
AM-UG	0.22	1.6
AM-LA	0.16	2.2
AM-Square	0.12	2.3
AM-Slender	0.19	1.4
AM-600	0.16	2.5
AM-600-UG	0.17	2.2
AM-2S	0.34	1.0

fragility curves. As shown in Figure 5.11(a), a reduction in axial load (AM-LA) resulted in a higher probability of exceeding the CP limit state especially in the region of 0.6g < S_a (T_1,5%)< 2.5g. Figure 5.11(b) shows that AM-Slender shows a significantly higher probability of collapse over a wide range of S_a in comparison to S1-AM and AM-Square whereas the latter two archetypes exhibit comparable performance with S1-AM having the lower probability of collapse of the two. Figure 5.11(c) shows that in general, grouting infills and/or increasing the frame cross-section result in improved seismic performance by lowering the probability of collapse. However, it indicates that the degree of improvement as a result of increasing frame cross-section is more pronounced when the infill is ungrouted. On the other hand, the degree of improvement as a result of grouting infill is more pronounced for the smaller frame cross-section. In Figure 5.11(d), it can be seen that the fragility of two-storey (AM-2S) archetype is considerably greater than one-storey archetype.

5.9 Response Modification Factor

Seismic response modification factors are key parameters for the seismic design of recognized seismic force resisting systems (SFRS). They are indicators of ductility and energy dissipation capability of an SFRS. There are different methods for calculating response modification factors in the literature. According to FEMA 451B (2007), the response modification coefficient of a system is defined as $R = R_d\Omega_o$, where Ω_o is the overstrength factor, and R_d is the ductility reduction factor. Overstrength factor, $\Omega_o = \frac{V_{max}}{V_y}$ is the ratio of maximum strength (V_{max}) to design strength (V_y) (Eq. 5.4) and can be obtained from the pushover response curve. Ductility reduction factor, R_d, is the ratio of

elastic strength demand (V_e) corresponding to δ_{max} to the maximum strength (V_{max}) (Eq. 5.5). The definitions of R, R_d, and Ω_o are illustrated on the pushover curve of archetype S1-AM as an example in Figure 5.12. The idealized curves were determined as previously described in Section 5.7.

$$\Omega_o = \frac{V_{max}}{V_y} \tag{5.4}$$

$$R_d = \frac{V_e}{V_{max}} \tag{5.5}$$

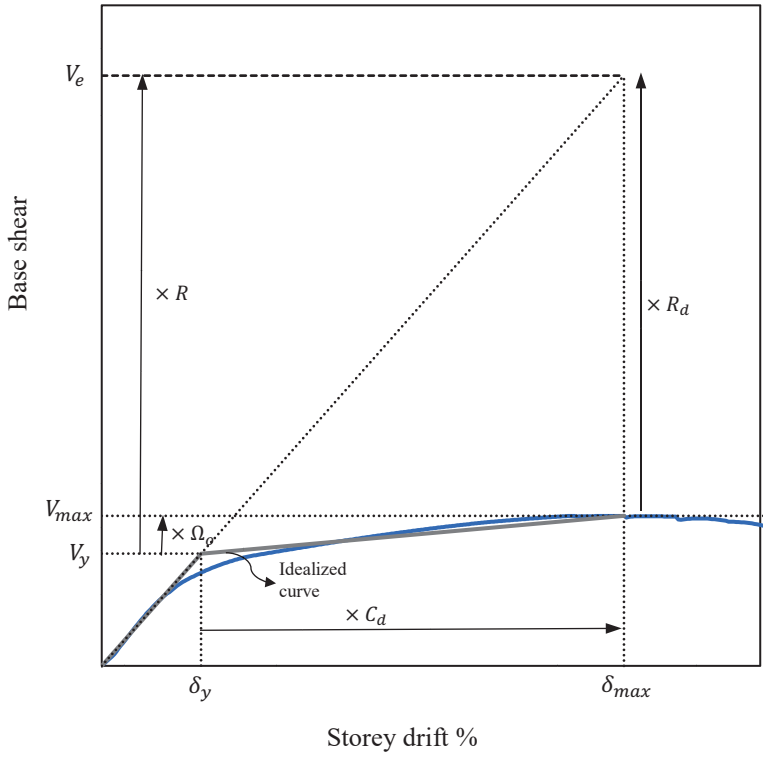

Figure 5.12 Definition of seismic modification factors

Design strength is defined as the shear capacity of the structure at the first significant yielding and thus the yielding point found from the idealization curve can be used as the design strength of the structure (V_y). Elastic strength demand (V_e) is the elastic base shear corresponding to δ_{max} which can be obtained from elastic IDA on the structure (Mwafy & Elnashai, 2002). From Eqs (5.4) and (5.5), the response modification coefficient can be expressed as the ratio of elastic strength demand (V_e) to the yielding strength (V_y) as shown in Eq (5.6).

$$R = \frac{V_e}{V_y} \tag{5.6}$$

Displacement amplification factor, C_d, is used to compute the maximum inelastic displacement from the elastic displacement induced by the design seismic forces, as shown in Figure 5.12 and is computed as the ratio between δ_{max} and δ_y.

$$C_d = \frac{\delta_{max}}{\delta_y} \tag{5.7}$$

In Table 5.6, all strength values and computed seismic performance factors are summarized for all archetypes. Overstrength factors, Ω_o, calculated for all-masonry infilled frames ranged from 1.2 to 1.58 with a median of 1.375. The ductility reduction factors, R_d, for these archetypes was in the range of 2.95 for the AM-LA archetype to 6.43 for the two-storey archetype, AM-2S. Similarly, the lowest displacement amplification factor, C_d, was observed for AM-LA and the highest value of 8.0 was calculated for the two-storey archetype, AM-2S. The response modification factor, R, showed a lowest value of 3.98 for AM-LA and a highest number of 8.55 for the slender archetype, AM-Slender.

Overall, the median R factor observed was about 5.5 for all-masonry infilled frames. The higher the R value, the greater ability for the system to absorb the energy through ductility and energy dissipation and thus greater modification in seismic load.

Table 5.6 Strengths and seismic modification factors of all archetypes

Archetype	V_y (kN)	V_{max} (kN)	V_e (kN)	Ω_o	R_d.	R	C_d
S1-AM	1359.7	1816.8	7442.9	1.34	4.10	5.47	5.2
AM-UG	607.6	836.8	3641.8	1.38	4.35	5.99	5.2
AM-LA	1292.4	1745.4	5145.7	1.35	2.95	3.98	2.9
AM-Square	830.3	1083.5	4115.7	1.3	3.80	4.96	4.2
AM-Slender	669.7	791.5	5729.8	1.2	7.24	8.55	6.1
AM-600	1955.1	2674.4	9084.4	1.37	3.40	4.65	3.1
AM-600-UG	1241.2	1850.7	6887.1	1.49	3.72	5.55	3.27
AM-2S	1258.8	1560.2	10039.3	1.58	6.43	7.97	8.0

It is pointed out that masonry infilled frames are currently not categorized as a seismic force resisting system (SFRS) in the North American design practice. However, the current American masonry design standard TMS 402/602-16 recognizes the special reinforced masonry (RM) shear walls as SFRS with an *R* factor of 5. Similarly, the Canadian masonry design standard CSA S304-14 also specifies moderately ductile and ductile masonry shear walls as SFRSs with ductility-related force modification factors (R_d) of 2 and 3, respectively, and overstrength-related force modification factors (R_o) of 1.5 for both types. Note that the symbol R_o in the Canadian standard is equivalent to Ω_o as described previously. Thus, for moderately ductile and ductile masonry shear walls, the *R* factors assigned in the Canadian standard are 3 and 4.5 respectively.

Based on the calculation and discussion presented above, the seismic modification factors for all-masonry infilled frames studied in this paper all exceeded the threshold value of 3 set for moderately ductile masonry shear walls and many were in the range of ductile shear wall category. This indicates that the all-masonry infilled frames have great potential to be recognized as a SFRS.

5.10 Conclusion

This paper presents a study on the seismic performance assessment of all-masonry infilled frames using a macro-model developed by the authors. Incorporating multi-strut and a shear spring, this model was intended to capture the compressive and sliding shear behaviour of masonry infills as well as the frame-infill interaction. Encoded in OpenSees, the model was used to perform Incremental Dynamic Analysis (IDA) on eight all-masonry infilled frame archetypes under 22 pairs of far-field ground motion records. The nonlinear static pushover analysis was also conducted on each archetype. The results of IDA and pushover analysis were used to develop the fragility curves for all-masonry infilled frames for Immediate Occupancy, Life Safety, and Collapse Prevention performance limit states. For all archetypes considered, the probability of exceeding the CP limit state under ground motions with IM up to 0.6g is nearly 0%. The median collapse spectral acceleration, $\widehat{S}_{CT}$, ranged from 1.0g to 2.5g. For one-storey all-masonry infilled frames, infill grouting and infill aspect ratio, among all parameters considered, had the most pronounced effect on the fragility curves. When all other parameters were kept the same, a fully grouted infill showed a significantly reduced probability of collapse in comparison to an ungrouted infill. Similar observation was also made for a squat infill vs. a slender infill. When the

storey of infilled frame is concerned, the results showed that the two-storey all-masonry infilled frame had the lowest value of $\widehat{S}_{CT}$, indicating the most vulnerability for collapse.

The seismic performance factors of the all-masonry infilled frame archetypes were also determined based on the IDA and pushover analysis results. The response modification factor, R, was found to range from 3.98 to 8.55 for the archetypes considered, with a median R factor of about 5.5. These R values, in most cases, exceeds the R values assigned to ductile masonry shear walls by the Canadian masonry design standard. Overall, this study has shown that all-masonry infilled frames have the potential to be recognized as SFRS. It is recognized that the numerical model needs to be further validated with infilled frames of varying material and geometric properties. Experimental tests on masonry infilled frames under seismic loading conditions are thus recommended as part of future work to provide physical evidence to further the study.

5.11 Acknowledgments

The authors wish to gratefully acknowledge the contribution of the financial assistance provided by the Natural Sciences and Engineering Research Council (NSERC) of Canada and the Canadian Concrete Masonry Producers Association for conducting this research.

CHAPTER 6 SUMMARY AND CONCLUSIONS

This study was conducted as part of an on-going research on the in-plane behaviour and capacity of masonry infilled frames. Numerical study using finite element modeling supplemented by experimental testing was the main methodology used in the investigation, and the focus of the study was on all-masonry infilled frames. The concept of all-masonry infilled frames was first proposed at Dalhousie University and their uniqueness from conventional masonry infilled RC frames is that the boundary frame is also made of masonry materials. The numerical work consisted of two distinctive components. First, a finite element macro-model was developed in OpenSees to simulate the in-plane lateral response of masonry infilled frames under both monotonic and cyclic loading. The proposed model is a multi-strut-spring model which accounted for diagonal and off-diagonal compressive behaviour of the infill panel, shear sliding of mortar bed joints, and infill-frame interaction. Concurrent with the numerical work, an experimental program was conducted to 1) examine the performance of all-masonry infilled frames under in-plane lateral loading; and 2) provide test results for numerical model validation. The proposed model was verified against the experimental results from this study as well as those under cyclic loading from literature. Next, the model was used in a seismic performance assessment where eight archetypes of varying design parameters were considered. Fragility curves and seismic modification factors were determined and discussed.

Conclusions drawn from the results of this research are summarized in the following.

6.1 Experimental Behaviour

- The general behaviour of all-masonry infilled frames is similar to their infilled RC frame counterparts under both monotonic and cyclic loading. The final failure modes of all-masonry infilled frames was mainly governed by the extension of diagonal cracks into the boundary columns as opposed to corner crushing for masonry infilled RC frames.
- Under cyclic loading, the all-masonry infilled frames were found to attain greater ductility, energy dissipation and ultimate load than the RC framed specimens with the same design parameters.
- Overall, both infilled frame systems showed significantly greater ductility at ultimate than what is specified for masonry infilled frames in the design practice.

6.2 Development of a Macro-Model

- The shear spring model in a serial configuration with struts can predict both bed-joint sliding failure of mortar joints and compression failure of struts.
- The shear spring model was most influenced by the maximum shear strength and its corresponding shear displacement.
- The comparison between this model and the two models proposed by El-Dakhakhni et al. (2003) and Crisafulli and Carr (2007) showed that given the same

input parameters, the proposed model provided better simulation in terms of stiffness, strength, and post-ultimate behavior than the other two models.

6.3 Seismic Performance Assessment

- For all-masonry infilled frame archetypes considered in this study, the probability of exceeding the CP limit state under ground motions with IM up to 0.6g is nearly 0% and the median collapse spectral acceleration, $\widehat{S}_{CT}$, ranged from 1.0g to 2.5g.
- It was observed that the probability of exceeding the LS limit state under ground motions with IM up to 0.6g is about 0% and for IM ranging from 1.0g to 2.2g, all-masonry infilled frame archetypes exceeded the LS limit state under 50% of the ground motion records.
- Fully grouted infills showed a significantly reduced probability of collapse in comparison to ungrouted infills while the slender and two-storey all-masonry infilled frame archetypes had the lowest value of $\widehat{S}_{CT}$, indicating the most vulnerability for collapse.
- The response modification factor, R, was found to range from 3.98 to 8.55 for the all-masonry infilled frame archetypes considered, with a median R factor of 5.5. These R values, in most cases, exceeds the R values assigned to ductile masonry shear walls by the Canadian masonry design standard.

6.4 Recommendations for Future Research

For future research, the following items are recommended:

- Further experimental studies on all-masonry infilled frames with large-scaled specimens, specimens with different infill-frame anchorage connections, and all-masonry infilled frames with multiple stories are recommended to provide more information on the behaviour of the newly proposed system.
- The proposed multi-strut-spring model focused on the sliding shear behaviour of mortar bed joints, infill compression behaviour, and the interaction between the masonry infill panel and its surrounding frame. However, the columns' shear failure mode was not reflected in the model. It is recommended to further validate the proposed model and consider the use of another type of element to model frame columns which can simulate not only the flexural and axial behaviour of columns but also is capable of modeling the shear failure of columns.
- In this study, the results of the triplet tests, conducted as per the specification EN1052-3, were used to propose a constitutive model for mortar bed joints. Nevertheless, more shear tests are recommended to further study the sliding shear behaviour of mortar joints considering other suggested shear test methods available in the literature.
- Experimental tests on masonry infilled frames under seismic loading conditions are recommended to provide physical evidence about dynamic behaviour of infilled frames.

REFERENCES

Abo El Ezz, A., Seif Eldin, H. M., & Galal, K. (2015). Influence of confinement reinforcement on the compression stress–strain of grouted reinforced concrete block masonry boundary elements. *Structures*, *2*, 32–43. https://doi.org/https://doi.org/10.1016/j.istruc.2015.01.001

Al-Chaar, G. (2002). *Evaluating Strength and Stiffness of Unreinforced Masonry Infill Structures*. 86.

Al-Chaar, G., Issa, M., & Sweeney, S. (2002). Behavior of Masonry-Infilled Nonductile Reinforced Concrete Frames. *Journal of Structural Engineering*, *128*(8), 1055–1063. https://doi.org/10.1061/(ASCE)0733-9445(2002)128:8(1055)

Al-Nimry, H., Resheidat, M., & Al-Jamal, M. (2014). Ambient vibration testing of low and medium rise infilled RC frame buildings in Jordan. *Soil Dynamics and Earthquake Engineering*, *59*, 21–29. https://doi.org/https://doi.org/10.1016/j.soildyn.2014.01.002

Andreotti, G., Graziotti, F., & Magenes, G. (2018). Detailed micro-modelling of the direct shear tests of brick masonry specimens: The role of dilatancy. *Engineering Structures*, *168*, 929–949. https://doi.org/https://doi.org/10.1016/j.engstruct.2018.05.019

Anić, F., Penava, D., Abrahamczyk, L., & Sarhosis, V. (2020). A review of experimental and analytical studies on the out-of-plane behaviour of masonry infilled frames. *Bulletin of Earthquake Engineering*, *18*(5), 2191–2246. https://doi.org/10.1007/s10518-019-00771-5

Anil, Ö., & Altin, S. (2007). An experimental study on reinforced concrete partially infilled frames. *Engineering Structures*, *29*(3), 449–460. https://doi.org/https://doi.org/10.1016/j.engstruct.2006.05.011

Armaanidis, V. I. (1998). *A model for the shear strength of rough rock discontinuities under low normal stress*. M. Sc. dissertation, School of Civil Engineering and Geosciences, University of Newcastle, Upon Tyne, UK.

ASCE/SEI 41-17. (2017). *Seismic Evaluation and Retrofit of Existing Buildings*. https://doi.org/10.1061/9780784414859

Asteris, P. G., Chrysostomou, C. Z., Giannopoulos, I. P., & Smyrou, E. (2011). Masonry infilled reinforced concrete frames with openings. *III ECCOMAS Thematic Conference on Computational Methods in Structural Dynamics and Earthquake Engineering*, 25–28.

ASTM C39 / C39M-01. (1999). *Standard Test Method for Compressive Strength of Cylindrical Concrete Specimens*. https://doi.org/10.1520/C0039_C0039M-01

ASTM E8 / E8M-16. (2016). *Standard Test Methods for Tension Testing of Metallic Materials*. ASTM International. https://doi.org/10.1520/E0008_E0008M-16A

ATC-24. (1992). *Buildings, Guidelines for cyclic seismic testing of components of steel structures for* (ATC-24).

ATC-40. (1996). *Seismic Evaluation and Retrofit of Concrete Buildings*.

Attard, M. M., Alfonso, N., & Francis, T.-L. (2007). Modeling Fracture in Masonry. *Journal of Structural Engineering*, *133*(10), 1385–1392. https://doi.org/10.1061/(ASCE)0733-9445(2007)133:10(1385)

Augenti, N., & Parisi, F. (2011). Constitutive modelling of tuff masonry in direct shear. *Construction and Building Materials*, *25*(4), 1612–1620. https://doi.org/https://doi.org/10.1016/j.conbuildmat.2010.10.002

Banting, B. R., & El-Dakhakhni, W. W. (2012). Force- and Displacement-Based Seismic Performance Parameters for Reinforced Masonry Structural Walls with Boundary Elements. *Journal of Structural Engineering*, *138*(12), 1477–1491. https://doi.org/10.1061/(ASCE)ST.1943-541X.0000572

Banting, B. R., & El-Dakhakhni, W. W. (2014). Seismic Performance Quantification of Reinforced Masonry Structural Walls with Boundary Elements. *Journal of Structural Engineering*, *140*(5), 4014001. https://doi.org/10.1061/(ASCE)ST.1943-541X.0000895

Bertero, V., & Brokken, S. (1983). Infills in seismic resistant building. *Journal of Structural Engineering*, *109*(6), 1337–1361.

Bhatt, C., & Bento, R. (2012). Comparison of Nonlinear Static Methods for the Seismic Assessment of Plan Irregular Frame Buildings with Non Seismic Details. *Journal of Earthquake Engineering*, *16*(1), 15–39. https://doi.org/10.1080/13632469.2011.586085

Blackard, B., Willam, K., & Mettupalayam, S. (2009). Experimental observations of masonry infilled reinforced concrete frames with openings. *Special Publication*, *265*, 122–199. https://doi.org/10.14359/51663296

Braga, F., Gigliotti, R., & Laterza, M. (2006). Analytical Stress–Strain Relationship for Concrete Confined by Steel Stirrups and/or FRP Jackets. *Journal of Structural*

Engineering, *132*(9), 1402–1416. https://doi.org/10.1061/(ASCE)0733-9445(2006)132:9(1402)

Braga, F., Manfredi, V., Masi, A., Salvatori, A., & Vona, M. (2011). Performance of non-structural elements in RC buildings during the L'Aquila, 2009 earthquake. *Bulletin of Earthquake Engineering*, *9*(1), 307–324. https://doi.org/10.1007/s10518-010-9205-7

Buonopane, S. G., & White, R. N. (1999a). *Seismic Evaluation of a Masonry Infilled Reinforced Concrete Frame by Pseudodynamic Testing.*

Buonopane, S. G., & White, R. N. (1999b). Pseudodynamic Testing of Masonry Infilled Reinforced Concrete Frame. *Journal of Structural Engineering*, *125*(6), 578–589. https://doi.org/10.1061/(ASCE)0733-9445(1999)125:6(578)

Burton, H., & Deierlein, G. (2014). Simulation of seismic collapse in nonductile reinforced concrete frame buildings with masonry infills. *Journal of Structural Engineering*, *140*(8), A4014016. https://doi.org/https://doi.org/10.1061/(ASCE)ST.1943-541X.0000921

Campione, G., Cavaleri, L., Macaluso, G., Amato, G., & Di Trapani, F. (2015). Evaluation of infilled frames: an updated in-plane-stiffness macro-model considering the effects of vertical loads. *Bulletin of Earthquake Engineering*, *13*(8), 2265–2281. https://doi.org/10.1007/s10518-014-9714-x

Cavaleri, L., & Di Trapani, F. (2014). Cyclic response of masonry infilled RC frames: Experimental results and simplified modeling. *Soil Dynamics and Earthquake Engineering*, *65*, 224–242. https://doi.org/10.1016/j.soildyn.2014.06.016

Cavaleri, L., & Di Trapani, F. (2015). Prediction of the additional shear action on frame members due to infills. *Bulletin of Earthquake Engineering*, *13*(5), 1425–1454. https://doi.org/10.1007/s10518-014-9668-z

Cavaleri, L., & Papia, M. (2003). A new dynamic identification technique: application to the evaluation of the equivalent strut for infilled frames. *Engineering Structures*, *25*(7), 889–901. https://doi.org/https://doi.org/10.1016/S0141-0296(03)00023-3

Celarec, D., & Dolšek, M. (2013). Practice-oriented probabilistic seismic performance assessment of infilled frames with consideration of shear failure of columns. *Earthquake Engineering \& Structural Dynamics*, *42*(9), 1339–1360. https://doi.org/https://doi.org/10.1002/eqe.2275

Chaimoon, K., & Attard, M. M. (2009). Experimental and numerical investigation of masonry under three-point bending (in-plane). *Engineering Structures*, *31*, 103–112.

Chandel, V. S., & Yamini Sreevalli, I. (2019). Numerical study on influence of masonry infill in an RC frame. *Asian Journal of Civil Engineering*, *20*(1), 1–8. https://doi.org/10.1007/s42107-018-0083-7

Charleson, A. (2008). Seismic Design for Architects. *Architectural Press*, 64.

Chen, X. (2016). *Numerical study of the in-plane behaviour of concrete masonry infills bounded by steel frames*. Dalhousie University.

Chen, X., & Liu, Y. (2016). A finite element study of the effect of vertical loading on the in-plane behavior of concrete masonry infills bounded by steel frames. *Engineering Structures*, *117*, 118–129. https://doi.org/https://doi.org/10.1016/j.engstruct.2016.03.010

Chiozzi, A., & Miranda, E. (2017). Fragility functions for masonry infill walls with in-plane loading. *Earthquake Engineering \& Structural Dynamics*, *46*(15), 2831–2850. https://doi.org/https://doi.org/10.1002/eqe.2934

Chrysostomou, C. Z., Gergely, P., & Abel, J. F. (2002). A six-strut model for nonlinear dynamic analysis of steel infilled frames. *International Journal of Structural Stability and Dynamics*, *2*(03), 335–353.

Cope, R. J., Rao, P. V, Clark, L. A., & Norris, P. (1980). *Modelling of reinforced concrete behaviour for finite element analyses of bridge slabs. Numerical methods for nonlinear problems I*. New York: Taylor & Francis.

Crisafulli, F. (1997). *Seismic behaviour of reinforced concrete structures with masonry infills*. University of Canterbury.

Crisafulli, F., & Carr, A. J. (2007). Proposed macro-model for the analysis of infilled frame structures. *Bulletin of the New Zealand Society for Earthquake Engineering*, *40*(2), 69–77. https://doi.org/https://doi.org/10.5459/bnzsee.40.2.69-77

CSA A23-3. (2014). *Design of concrete structures*.

CSA S304-14. (2014). *Design of masonry structures*.

Dawe, J. L., & Seah, C. K. (1989). Behaviour of masonry infilled steel frames. *Canadian Journal of Civil Engineering*, *16*(6), 865–876. https://doi.org/10.1139/l89-129

de Borst, R., & Nauta, P. (1985). Non-orthogonal cracks in a smeared finite element model. *Engineering Computations*.

De Risi, M. T., Del Gaudio, C., Ricci, P., & Verderame, G. M. (2018). In-plane behaviour and damage assessment of masonry infills with hollow clay bricks in RC frames.

Engineering Structures, *168*(April), 257–275. https://doi.org/10.1016/j.engstruct.2018.04.065

Decanini, L. D., & Fantin, G. E. (1986). Modelos simplificados de la mampostería incluida en porticos. *Caracteristicas de Stiffnessy Resistencia Lateral En Estado Limite. Jornadas Argentinas de Ingeniería Estructural*, *2*, 817–836.

Di Trapani, F. (2021). A novel data-driven force–displacement macro-model for nonlinear analysis of infilled frames: development, validation and reliability comparison. *Bulletin of Earthquake Engineering*, *19*(14), 6157–6186. https://doi.org/10.1007/s10518-021-01211-z

Di Trapani, F., Bertagnoli, G., Ferrotto, M. F., & Gino, D. (2018). Empirical Equations for the Direct Definition of Stress–Strain Laws for Fiber-Section-Based Macromodeling of Infilled Frames. *Journal of Engineering Mechanics*, *144*(11), 04018101. https://doi.org/10.1061/(asce)em.1943-7889.0001532

Di Trapani, F., Bolis, V., Basone, F., & Preti, M. (2020). Seismic reliability and loss assessment of RC frame structures with traditional and innovative masonry infills. *Engineering Structures*, *208*, 110306. https://doi.org/https://doi.org/10.1016/j.engstruct.2020.110306

Dolšek, M., & Fajfar, P. (2008). The effect of masonry infills on the seismic response of a four-storey reinforced concrete frame — a deterministic assessment. *Engineering Structures*, *30*(7), 1991–2001. https://doi.org/https://doi.org/10.1016/j.engstruct.2008.01.001

Drysdale, R. G., & Hamid, A. A. (2005). *Masonry Structures: Behaviour and Design* (Canadian Edition, Ed.). Canada Masonry Design Centre.

EEFIT. (2018). *The Muisne, Ecuador Earthquake of 16 April 2016. A field Report by EEFIT* (Issue April).

El-Dakhakhni, W. W. (2002). Experimental and analytical seismic evaluation of concrete masonry -infilled steel frames retrofitted using GFRP laminates. In *ProQuest Dissertations and Theses*. Drexel University.

El-Dakhakhni, W. W., Elgaaly, M., & Hamid, A. A. (2003). Three-Strut Model for Concrete Masonry-Infilled Steel Frames. *Journal of Structural Engineering*, *129*(2), 177–185. https://doi.org/10.1061/(ASCE)0733-9445(2003)129:2(177)

Eurocode 6. (2009). *Design of masonry structures - Part 3: Simplified calculation methods for unreinforced masonry structures* (BS EN 1996).

European Committee for Standardization (CEN). (2007). *EN 1052-3: Methods of test for masonry–Part 3: Determination of initial shear strength*. European Committee for Standardization Brussels, Belgium.

Ezzeldin, M., Wiebe, L., & El-Dakhakhni, W. (2016). Seismic Collapse Risk Assessment of Reinforced Masonry Walls with Boundary Elements Using the FEMA P695 Methodology. *Journal of Structural Engineering*, *142*(11), 04016108. https://doi.org/10.1061/(asce)st.1943-541x.0001579

Facconi, L., Plizzari, G., & Vecchio, F. (2014). Disturbed stress field model for unreinforced masonry. *Journal of Structural Engineering*, *140*(4), 4013085.

FEMA. (2000). *Seismic design criteria for steel moment-frame structures* (FEMA 350). SAC Joint Venture, Federal Emergency Management Agency.

FEMA 306. (1998). *Evaluation of earthquake damaged concrete and masonry wall buildings*. Federal Emergency Management Agency.

FEMA 451B. (2007). *NEHRP Recommended Provisions For New Buildings And Other Structures: Training And Instructional Materials*. Federal Emergency Management Agency (FEMA).

FEMA P695. (2009). *Quantification of Building System Performance Factors*. FEMA.

Filippou, F. C., Popov, E. P., & Bertero, V. V. (1983). *Effects of bond deterioration on hysteretic behavior of reinforced concrete joints*. Earthquake Engineering Research Center, University of California.

Fiore, A., Netti, A., & Monaco, P. (2012). The influence of masonry infill on the seismic behaviour of RC frame buildings. *Engineering Structures*, *44*, 133–145. https://doi.org/https://doi.org/10.1016/j.engstruct.2012.05.023

Fiore, A., Porco, F., Raffaele, D., & Uva, G. (2012). About the influence of the infill panels over the collapse mechanisms actived under pushover analyses: Two case studies. *Soil Dynamics and Earthquake Engineering*, *39*, 11–22. https://doi.org/10.1016/j.soildyn.2012.02.004

Flanagan, R. D., & Bennett, R. M. (1999). Bidirectional behavior of structural clay tile infilled frames. *Journal of Structural Engineering*, *125*(3), 236–244. https://doi.org/10.1061/(ASCE)0733-9445(1999)125:3(236)

Foroushani, S. (2019). *Experimental Investigation of the In-Plane Behaviour of Concrete Masonry Infills Bounded by Reinforced Masonry Frames*. Dalhousie University.

Furtado, A., Rodrigues, H., & Arêde, A. (2015). Modelling of masonry infill walls participation in the seismic behaviour of RC buildings using OpenSees. *International Journal of Advanced Structural Engineering (IJASE)*, *7*(2), 117–127. https://doi.org/10.1007/s40091-015-0086-5

Gabor, A., Bennani, A., Jacquelin, E., & Lebon, F. (2006). Modelling approaches of the in-plane shear behaviour of unreinforced and FRP strengthened masonry panels. *Composite Structures*, *74*(3), 277–288. https://doi.org/https://doi.org/10.1016/j.compstruct.2005.04.012

Ghosh, A. K., & Amde, A. M. (2002). Finite Element Analysis of Infilled Frames. *Journal of Structural Engineering*, *128*(7), 881–889. https://doi.org/10.1061/(ASCE)0733-9445(2002)128:7(881)

Gouveia, J., & Lourenço, P. (2007). Masonry shear walls subjected to cyclic loading: influence of confinement and horizontal reinforcement. *10th North American Masonry Conference*.

Guerrero, N., Martínez, M., Picón, R., Marante, M. E., Hild, F., Roux, S., & Flórez-López, J. (2014). Experimental analysis of masonry infilled frames using digital image correlation. *Materials and Structures*, *47*(5), 873–884. https://doi.org/10.1617/s11527-013-0099-0

Haider, W., & Dhanasekar, M. (2004). Experimental study of monotonically loaded wide spaced reinforced masonry shear walls. *Australian Journal of Structural Engineering*, *5*(2), 101–118. https://doi.org/10.1080/13287982.2004.11464931

Hamid, A. A., & Drysdale, R. G. (1980). Concrete Masonry Under Combined Shear and Compression Along the Mortar Joints. *ACI Journal Proceedings*, *77*(5), 314–320. https://doi.org/10.14359/7008

Hansen, K. F. (1999). *Bending and shear tests with masonry*. SBI forlag.

Hashemi, A., & Mosalam, K. (2007). Seismic Evaluation of Reinforced Concrete Buildings Including Effects of Masonry Infill Walls, PEER 2007/100. In *Pacific Earthquake Engineering Research Center*. University of California.

Holmes, M. (1961). Steel frames with brickwork and concrete infilling. *Proceedings of the Institution of Civil Engineers*, *19*(4), 473–478. https://doi.org/10.1680/iicep.1961.11305

Hosseini, S. (2020). *Experimental Study of the In-Plane Behaviour of All-Masonry Infilled Frame Systems under Lateral Loading*. Dalhousie University.

Jäger, W., & Schöps, P. (2009). Confined masonry – a chance to improve the load bearing capacity. *11th Canadian Masonry Symposium*.

Jeon, J.-S., Park, J.-H., & DesRoches, R. (2015). Seismic fragility of lightly reinforced concrete frames with masonry infills. *Earthquake Engineering \& Structural Dynamics*, *44*(11), 1783–1803. https://doi.org/https://doi.org/10.1002/eqe.2555

Jiang, H., Liu, X., & Mao, J. (2015). Full-scale experimental study on masonry infilled RC moment-resisting frames under cyclic loads. *Engineering Structures*, *91*, 70–84. https://doi.org/10.1016/j.engstruct.2015.02.008

Kadysiewski, S., & Mosalam, K. M. (2008). Modeling of unreinforced masonry infill walls considering in-plane and out-of-plane interaction, PEER 2008/102. In *Pacific Earthquake Engineering Research Center*. University of California.

Kakaletsis, D. J., & Karayannis, C. G. (2008). Influence of Masonry Strength and Openings on Infilled R/C Frames Under Cycling Loading. *Journal of Earthquake Engineering*, *12*(2), 197–221. https://doi.org/10.1080/13632460701299138

Kaplan, H., Bilgin, H., Yilmaz, S., Binici, H., & Öztas, A. (2010). Structural damages of L'Aquila (Italy) earthquake. *Natural Hazards and Earth System Sciences*, *10*(3), 499–507. https://doi.org/10.5194/nhess-10-499-2010

Kareem, K. M., & Pantò, B. (2019). Simplified macro-modelling strategies for the seismic assessment of non-ductile infilled frames: a critical appraisal. *Journal of Building Engineering*, *22*, 397–414. https://doi.org/https://doi.org/10.1016/j.jobe.2018.12.010

Karsan, I. D., & James, O. J. (1969). Behavior of Concrete Under Compressive Loadings. *Journal of the Structural Division*, *95*(12), 2543–2564. https://doi.org/10.1061/JSDEAG.0002424

Kingsley, G., P., & Gangel, T. (2014). *NEHRP Seismic Design Technical Brief No. 9: Seismic Design of Special Reinforced Masonry Shear Walls*. Grant/Contract Reports (NISTGCR), National Institute of Standards and Technology, Gaithersburg, MD.

Klingner, R., & Bertero, V. (1977). *Infilled frames in earthquake-resistant construction*. University of California, Berkeley.

Klingner, R., Rubiano, N., Bashandy, T. R., & Sweeney, S. (1996). Evaluation and analytical verification of shaking table data from infilled frames. *Part*, *2*, 521–532.

Liberatore, L., & Decanini, L. D. (2011a). *Effect of infills on the seismic response of high-rise RC buildings designed as bare according to Eurocode 8*. *January 2011*.

Liberatore, L., Noto, F., Mollaioli, F., & Franchin, P. (2018). In-plane response of masonry infill walls: Comprehensive experimentally-based equivalent strut model for deterministic and probabilistic analysis. *Engineering Structures*, *167*, 533–548. https://doi.org/https://doi.org/10.1016/j.engstruct.2018.04.057

Liel, A. B., & Lynch, K. P. (2012). Vulnerability of Reinforced-Concrete-Frame Buildings and Their Occupants in the 2009 L'Aquila, Italy, Earthquake. *Natural Hazards Review*, *13*(1), 11–23. https://doi.org/10.1061/(ASCE)NH.1527-6996.0000047

Liu, Y., & Soon, S. (2012). *Experimental study of concrete masonry infills bounded by steel frames*. *190*(July 2011), 180–190. https://doi.org/10.1139/L11-122

Lotfi, H. R., & Shing, P. B. (1991). An appraisal of smeared crack models for masonry shear wall analysis. *Computers & Structures*, *41*(3), 413–425.

Lotfi, H. R., & Shing, P. B. (1994). Interface model applied to fracture of masonry structures. *Journal of Structural Engineering*, *120*(1), 63–80.

Lourenço, P. B., Milani, G., Tralli, A., & Zucchini, A. (2007). Analysis of masonry structures: review of and recent trends in homogenization techniquesThis article is

one of a selection of papers published in this Special Issue on Masonry. *Canadian Journal of Civil Engineering*, *34*(11), 1443–1457. https://doi.org/10.1139/L07-097

Lourenço, P., Barros, J., & Oliveira, J. (2004). Shear testing of stack bonded masonry. *Construction and Building Materials*, *18*(2), 125–132. https://doi.org/https://doi.org/10.1016/j.conbuildmat.2003.08.018

Lourenço, P., & Rots, J. (1997). Multisurface Interface Model for Analysis of Masonry Structures. *Journal of Engineering Mechanics*, *123*(7), 660–668. https://doi.org/10.1061/(ASCE)0733-9399(1997)123:7(660)

Mainstone, R. (1971). On the Stiffnesses and Strengths of Infilled Frames. *Proceedings of the Institute of Civil Engineers*, *4*, 57–90.

Mander, J., Nair, B., Wojtkowski, K., & Ma, J. (1993). *An experimental study on the seismic performance of brick-infilled steel frames with and without retrofit*. National Center for earthquake engineering research.

Manesh, P. B. (2013). *Experimental study of masonry-infilled steel frames subjected to combined axial and in-plane lateral loading.* Dalhousie University.

Martins, A., Vasconcelos, G., & Costa, A. C. (2017). Experimental assessment of the mechanical behaviour of ties on brick veneers anchored to brick masonry infills. *Construction and Building Materials*, *156*, 515–531. https://doi.org/https://doi.org/10.1016/j.conbuildmat.2017.09.013

Mazzoni, S., McKenna, F., Scott, M. H., & Fenves, G. L. (2006). Open System for Earthquake Engineering Simulation (OpenSEES) user command-language manual. *Pacific Earthquake Engineering Research Center*, 465.

Mehrabi, A., Shing, P. B., Schuller, M., & James, N. (1996). Experimental Evaluation of Masonry-Infilled RC Frames. *Journal of Structural Engineering*, *122*(3), 228–237. https://doi.org/10.1061/(ASCE)0733-9445(1996)122:3(228)

Minaie, E., Mota, M., Moon, F. L., & Hamid, A. A. (2010). *In-Plane Behavior of Partially Grouted Reinforced Concrete Masonry Shear Walls*. *136*(September), 1089–1097. https://doi.org/10.1061/(ASCE)ST.1943-541X.0000206

Miranda, E., Mosqueda, G., Retamales, R., & Pekcan, G. (2012). Performance of Nonstructural Components during the 27 February 2010 Chile Earthquake. *Earthquake Spectra*, *28*(1_suppl1), 453–471. https://doi.org/10.1193/1.4000032

Moghaddam, H. A. (2004). Lateral Load Behavior of Masonry Infilled Steel Frames with Repair and Retrofit. *Journal of Structural Engineering*, *130*(1), 56–63. https://doi.org/10.1061/(ASCE)0733-9445(2004)130:1(56)

Morandi, P., Hak, S., & Magenes, G. (2018). *Performance-based interpretation of in-plane cyclic tests on RC frames with strong masonry in fi lls*. *156*(March 2017), 503–521. https://doi.org/10.1016/j.engstruct.2017.11.058

Mosalam, K. (1996). *Experimental and computational strategies for the seismic behaviour evaluation of frames with infill walls*. Cornell University.

Mosalam, K., White, R., & Gergely, P. (1997). Static Response of Infilled Frames Using Quasi-Static Experimentation. *Journal of Structural Engineering*, *123*(11), 1462–4169. https://doi.org/10.1061/(ASCE)0733-9445(1997)123:11(1462)

Mwafy, A. M., & Elnashai, A. S. (2002). CALIBRATION OF FORCE REDUCTION FACTORS OF RC BUILDINGS. *Journal of Earthquake Engineering*, *6*(2), 239–273. https://doi.org/10.1080/13632460209350416

NBCC. (2015). *National Building Code of Canada*. National Research Council of Canada. Canadian Commission on Building and Fire Codes.

NIST. (2010). Evaluation of the FEMA P-695 methodology for quantification of building seismic performance factors. In *NIST GCR 10-917-8*.

Noh, N. M., Liberatore, L., Mollaioli, F., & Tesfamariam, S. (2017). Modelling of masonry infilled RC frames subjected to cyclic loads: State of the art review and modelling with OpenSees. *Engineering Structures*, *150*, 599–621. https://doi.org/https://doi.org/10.1016/j.engstruct.2017.07.002

Obaidat, A. T., Ahmed, A., & Khaled, G. (2018). Stress-Strain Behavior of C-Shaped Confined Concrete Masonry Boundary Elements of Reinforced Masonry Shear Walls. *Journal of Structural Engineering*, *144*(8), 4018119. https://doi.org/10.1061/(ASCE)ST.1943-541X.0002120

Panagiotakos, T. B., & Fardis, M. N. (1996). Seismic response of infilled RC frame structures. In *Proceedings of the 11th World Conference on Earthquake Engineering* (pp. 1–8).

Pantò, B., Caliò, I., & Lourenço, P. B. (2017). Seismic safety evaluation of reinforced concrete masonry infilled frames using macro modelling approach. *Bulletin of Earthquake Engineering*, *15*(9), 3871–3895. https://doi.org/10.1007/s10518-017-0120-z

Papia, M., Cavaleri, L., & Fossetti, M. (2003). Infilled frames: developments in the evaluation of the stiffening effect of infills. *Structural Engineering and Mechanics*, *16*(6), 675–693. https://doi.org/10.12989/SEM.2003.16.6.675

Paulay, T., & Priestley, M. J. N. (1992). *Seismic design of reinforced concrete and masonry buildings*. Wiley New York.

PEER. (2022). *Pacific Earthquake Engineering Research Center (PEER) Next-Generation Attenuation (NGA) database*.

Polyakov, S. V. (1956). *Masonry in Framed Buildings*. Gosudarstvennos Izdate'stvo Literatury Po Stroitel'stvu i Arkhitekture, Moscow. Translated from the Russian by G.L. Cairns.

Rahman, A., & Ueda, T. (2014). Experimental Investigation and Numerical Modeling of Peak Shear Stress of Brick Masonry Mortar Joint under Compression. *Journal of Materials in Civil Engineering*, *26*(9), 04014061. https://doi.org/10.1061/(asce)mt.1943-5533.0000958

Rashid, Y. R. (1968). Ultimate strength analysis of prestressed concrete pressure vessels. *Nuclear Engineering and Design*, *7*(4), 334–344. https://doi.org/https://doi.org/10.1016/0029-5493(68)90066-6

Rizaee, S., Lissel, S. S., & Shrive, N. G. (2020). The Effect of the Amount, Distribution and End Anchorage Conditions of Bond Beam Reinforcement on the Behaviour of Concrete Masonry Shear Walls. *Canadian Journal of Civil Engineering*. https://doi.org/10.1139/cjce-2020-0260

Roosta, S., & Liu, Y. (2021). Behavior of concrete masonry infills bounded by masonry frames subjected to in-plane lateral loading – Experimental study. *Engineering Structures*, *247*, 113153. https://doi.org/https://doi.org/10.1016/j.engstruct.2021.113153

Roosta, S., & Liu, Y. (2022). Development of a Macro-Model for concrete masonry infilled frames. *Engineering Structures*, *257*, 114075. https://doi.org/https://doi.org/10.1016/j.engstruct.2022.114075

Saneinejad, A., & Hobbs, B. (1995a). Inelastic Design of Infilled Frames. *Journal of Structural Engineering*, *121*(4), 634–650. https://doi.org/10.1061/(ASCE)0733-9445(1995)121:4(634)

Scott, B. D., Park, R., & Priestley, M. J. N. (1982). Stress-Strain Behavior of Concrete Confined by Overlapping Hoops at Low and High Strain Rates. *ACI Journal Proceedings*, *79*(1), 13–27. https://doi.org/10.14359/10875

Seah, C. K. (1998). *A universal approach for the analysis and design of masonry infilled frame structures*. University of New Brunswick, Fredericton, NB., Canada.

Sepasdar, R. (2017). *Experimental Investigation On The Out-Of-Plane Behaviour Of Concrete Masonry Infilled Rc Frames*. Dalhousie University.

Shames, I., & Cozzarelli, F. (1992). Elastic and Inelastic Stress Analysis. In *Inc. Englewood Cliffs, NJ*. Prentice Hall.

Shendkar, M. R., Kontoni, D.-P. N., Mandal, S., Maiti, P. R., & Gautam, D. (2021). Effect of Lintel Beam on Seismic Response of Reinforced Concrete Buildings with Semi-

Interlocked and Unreinforced Brick Masonry Infills. In *Infrastructures* (Vol. 6, Issue 1). https://doi.org/10.3390/infrastructures6010006

Shing, PB., Noland, JL., Klamerus, E., & Spaeh, H. (1989). Inelastic Behavior of Concrete Masonry Shear Walls. *Journal of Structural Engineering*, *115*(9), 2204–2225. https://doi.org/10.1061/(ASCE)0733-9445(1989)115:9(2204)

Soltanzadeh, G., Osman, H. Bin, Vafaei, M., & Vahed, Y. K. (2018). Seismic retrofit of masonry wall infilled RC frames through external post-tensioning. *Bulletin of Earthquake Engineering*, *16*(3), 1487–1510. https://doi.org/10.1007/s10518-017-0241-4

Sorrentino, L., Cattari, S., da Porto, F., Magenes, G., & Penna, A. (2019). Seismic behaviour of ordinary masonry buildings during the 2016 central Italy earthquakes. *Bulletin of Earthquake Engineering*, *17*(10), 5583–5607. https://doi.org/10.1007/s10518-018-0370-4

Stafford Smith, B., & Carter, C. (1969). A method of analysis for infilled frames. *Proceedings of the Institution of Civil Engineers*, *44*(1), 31–48. https://doi.org/10.1680/iicep.1969.7290

Stavridis, A., & Shing, P. B. (2010). Finite-Element Modeling of Nonlinear Behavior of Masonry-Infilled RC Frames. *Journal of Structural Engineering*, *136*(3), 285–296. https://doi.org/10.1061/(ASCE)ST.1943-541X.116

Steeves, R. (2017). *In-Plane Behaviour Of Masonry Infilled Rc Frames With Interfacial Gaps Subjected To Quasi-Static Loading* (Issue April). Dalhousie University.

Syrmakezis, C. A., & Vratsanou, V. Y. (1986). Influence of infill walls to RC frames response. *Proceedings of the Eighth European Conference on Earthquake Engineering*, *3*, 5–6.

Tarque, N., Leandro, C., Guido, G., & Enrico, S. (2015). Masonry infilled frame structures: state-of-the-art review of numerical modelling. *Earthquakes and Structures*, *8*(1), 225–251. https://doi.org/doi:10.12989/EAS.2015.8.1.225

Thiruvengadam, V. (1985). On the natural frequencies of infilled frames. *Earthquake Engineering \& Structural Dynamics*, *13*(3), 401–419. https://doi.org/https://doi.org/10.1002/eqe.4290130310

TMS 402/602. (2016). *Building Code Requirements and Specification for Masonry Structures*.

Tomaževič, M., Lutman, M., & Petković, L. (1996). Seismic Behavior of Masonry Walls: Experimental Simulation. *Journal of Structural Engineering*, *122*(9), 1040–1047. https://doi.org/10.1061/(ASCE)0733-9445(1996)122:9(1040)

Uva, G., Raffaele, D., Porco, F., & Fiore, A. (2012). On the role of equivalent strut models in the seismic assessment of infilled RC buildings. *Engineering Structures*, *42*, 83–94. https://doi.org/https://doi.org/10.1016/j.engstruct.2012.04.005

Vamvatsikos, D., & Cornell, A. C. (2002a). Incremental dynamic analysis. *Earthquake Engineering and Structural Dynamics*, *31*(3), 491–514. https://doi.org/10.1002/eqe.141

Vamvatsikos, D., & Cornell, A. C. (2002b). The Incremental Dynamic Analysis and Its Application To Performance-Based Earthquake Engineering. *European Conference on Earthquake Engineering*, *April*, 10.

Van der Pluijm, R. (1993). Shear behaviour of bed joints. In Drexel University (Ed.), *Proceedings of the 6th North American Masonry Conference* (pp. 125–136). Drexel University.

Vecchio, F. J. (2000). Disturbed stress field model for reinforced concrete: formulation. *Journal of Structural Engineering*, *126*(9), 1070–1077.

Vecchio, F. J. (2001). Disturbed stress field model for reinforced concrete: implementation. *Journal of Structural Engineering*, *127*(1), 12–20.

Voon, K. C., & Ingham, J. M. (2006). Experimental In-Plane Shear Strength Investigation of Reinforced Concrete Masonry Walls. *Journal of Structural Engineering*, *132*(3), 400–408. https://doi.org/10.1061/(ASCE)0733-9445(2006)132:3(400)

Wood, R. H. (1978). Plasticity, composite action and collapse design of unreinforced shear wall panels in frames. *Proceedings of the Institution of Civil Engineers*, *65*(2), 381–411. https://doi.org/10.1680/iicep.1978.2952

Yön, B., Onat, O., & Öncü, M. E. (2019). Earthquake Damage to Nonstructural Elements of Reinforced Concrete Buildings during 2011 Van Seismic Sequence. *Journal of Performance of Constructed Facilities*, *33*(6), 4019075. https://doi.org/10.1061/(ASCE)CF.1943-5509.0001341

APPENDIX A: COPYRIGHT PERMISSIONS

June 3rd, 2022

Engineering structures

I am preparing my Ph.D. thesis for submission to the Faculty of Graduate Studies at Dalhousie University, Halifax, Nova Scotia, Canada. I am seeking your permission to include a manuscript version of the following paper(s) as a chapter in the thesis:

[Behavior Of Concrete Masonry Infills Bounded By Masonry Frames Subjected To In-Plane Lateral Loading - Experimental Study, Soraya Roosta, Yi Liu, Engineering Structures Journal, Volume 247, 2021, 113153]

[Development of A Macro-Model for Concrete Masonry Infilled Frames, Soraya Roosta, Yi Liu, Engineering Structures Journal, Volume 257, 2022, 114075]

Canadian graduate theses are collected and stored online by the Library and Archives of Canada. I am also seeking your permission for the material described above to be stored online with the LAC. Further details about the LAC thesis program are available on the LAC website (www.bac-lac.gc.ca).

Full publication details and a copy of this permission letter will be included in the thesis.

Yours sincerely,

Soraya Roosta

Permission is granted for:

a) the inclusion of the material described above in your thesis.
b) for the material described above to be included in the copy of your thesis that is sent to the Library and Archives of Canada (formerly National Library of Canada) for online storage.

Name:	Soraya Roosta	Title:	
Signature:		Date:	June 3rd, 2022

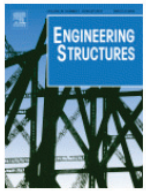

Behavior of concrete masonry infills bounded by masonry frames subjected to in-plane lateral loading – Experimental study

Author: Soraya Roosta,Yi Liu
Publication: Engineering Structures
Publisher: Elsevier
Date: 15 November 2021

Journal Author Rights

Please note that, as the author of this Elsevier article, you retain the right to include it in a thesis or dissertation, provided it is not published commercially. Permission is not required, but please ensure that you reference the journal as the original source. For more information on this and on your other retained rights, please visit: https://www.elsevier.com/about/our-business/policies/copyright#Author-rights

BACK CLOSE WINDOW

CCC Marketplace™

This is a License Agreement between Soraya Roosta ("User") and Copyright Clearance Center, Inc. ("CCC") on behalf of the Rightsholder identified in the order details below. The license consists of the order details, the CCC Terms and Conditions below, and any Rightsholder Terms and Conditions which are included below.

All payments must be made in full to CCC in accordance with the CCC Terms and Conditions below.

Order Date	03-Jun-2022	Type of Use	Republish in a thesis/dissertation
Order License ID	1228739-2	Publisher	PERGAMON
ISSN	0141-0296	Portion	Chapter/article

LICENSED CONTENT

Publication Title	Engineering structures	Rightsholder	Elsevier Science & Technology Journals
Article Title	Behavior of concrete masonry infills bounded by masonry frames subjected to in-plane lateral loading – Experimental study	Publication Type	Journal
		Start Page	113153
		Volume	247
Date	01/01/1978		
Language	English		
Country	United Kingdom of Great Britain and Northern Ireland		

REQUEST DETAILS

Portion Type	Chapter/article	Rights Requested	Main product
Page range(s)	1-16	Distribution	Worldwide
Total number of pages	16	Translation	Original language of publication
Format (select all that apply)	Electronic	Copies for the disabled?	No
Who will republish the content?	Academic institution	Minor editing privileges?	No
Duration of Use	Life of current edition	Incidental promotional use?	No

Development of a Macro-Model for concrete masonry infilled frames

Author: Soraya Roosta,Yi Liu
Publication: Engineering Structures
Publisher: Elsevier
Date: 15 April 2022

Journal Author Rights

Please note that, as the author of this Elsevier article, you retain the right to include it in a thesis or dissertation, provided it is not published commercially. Permission is not required, but please ensure that you reference the journal as the original source. For more information on this and on your other retained rights, please visit: https://www.elsevier.com/about/our-business/policies/copyright#Author-rights

BACK CLOSE WINDOW

CCC Marketplace™

This is a License Agreement between Soraya Roosta ("User") and Copyright Clearance Center, Inc. ("CCC") on behalf of the Rightsholder identified in the order details below. The license consists of the order details, the CCC Terms and Conditions below, and any Rightsholder Terms and Conditions which are included below.

All payments must be made in full to CCC in accordance with the CCC Terms and Conditions below.

Order Date	03-Jun-2022	**Type of Use**	Republish in a thesis/dissertation
Order License ID	1228745-1	**Publisher**	PERGAMON
ISSN	0141-0296	**Portion**	Chapter/article

LICENSED CONTENT

Publication Title	Engineering structures	**Rightsholder**	Elsevier Science & Technology Journals
Article Title	Development of a Macro-Model for concrete masonry infilled frames	**Publication Type**	Journal
		Start Page	114075
Date	01/01/1978	**Volume**	257
Language	English		
Country	United Kingdom of Great Britain and Northern Ireland		

REQUEST DETAILS

Portion Type	Chapter/article	**Rights Requested**	Main product
Page range(s)	1-12	**Distribution**	Worldwide
Total number of pages	12	**Translation**	Original language of publication
Format (select all that apply)	Electronic	**Copies for the disabled?**	No
Who will republish the content?	Academic institution	**Minor editing privileges?**	No
Duration of Use	Life of current edition	**Incidental promotional use?**	No
Lifetime Unit Quantity	Up to 499	**Currency**	CAD